



University of Kentucky  
UKnowledge

---

Theses and Dissertations--Molecular and Cellular Biochemistry

Molecular and Cellular Biochemistry

---


2023

## A CHARACTERIZATION OF KEY RESIDUES IN CLASS I VIRAL FUSION PROTEINS IMPORTANT FOR FUSOGENIC ACTIVITY

Hadley E. Neal

University of Kentucky, hadley.neal@uky.edu

Author ORCID Identifier:

 <https://orcid.org/0000-0001-8433-593X>

Digital Object Identifier: <https://doi.org/10.13023/etd.2023.278>

[Right click to open a feedback form in a new tab to let us know how this document benefits you.](#)

### Recommended Citation

Neal, Hadley E., "A CHARACTERIZATION OF KEY RESIDUES IN CLASS I VIRAL FUSION PROTEINS IMPORTANT FOR FUSOGENIC ACTIVITY" (2023). *Theses and Dissertations--Molecular and Cellular Biochemistry*. 67.

[https://uknowledge.uky.edu/biochem\\_etds/67](https://uknowledge.uky.edu/biochem_etds/67)

This Doctoral Dissertation is brought to you for free and open access by the Molecular and Cellular Biochemistry at UKnowledge. It has been accepted for inclusion in Theses and Dissertations--Molecular and Cellular Biochemistry by an authorized administrator of UKnowledge. For more information, please contact [UKnowledge@lsv.uky.edu](mailto:UKnowledge@lsv.uky.edu).

## **STUDENT AGREEMENT:**

I represent that my thesis or dissertation and abstract are my original work. Proper attribution has been given to all outside sources. I understand that I am solely responsible for obtaining any needed copyright permissions. I have obtained needed written permission statement(s) from the owner(s) of each third-party copyrighted matter to be included in my work, allowing electronic distribution (if such use is not permitted by the fair use doctrine) which will be submitted to UKnowledge as Additional File.

I hereby grant to The University of Kentucky and its agents the irrevocable, non-exclusive, and royalty-free license to archive and make accessible my work in whole or in part in all forms of media, now or hereafter known. I agree that the document mentioned above may be made available immediately for worldwide access unless an embargo applies.

I retain all other ownership rights to the copyright of my work. I also retain the right to use in future works (such as articles or books) all or part of my work. I understand that I am free to register the copyright to my work.

## **REVIEW, APPROVAL AND ACCEPTANCE**

The document mentioned above has been reviewed and accepted by the student's advisor, on behalf of the advisory committee, and by the Director of Graduate Studies (DGS), on behalf of the program; we verify that this is the final, approved version of the student's thesis including all changes required by the advisory committee. The undersigned agree to abide by the statements above.

Hadley E. Neal, Student

Dr. Rebecca Dutch, Major Professor

Dr. Trevor Creamer, Director of Graduate Studies

A CHARACTERIZATION OF KEY RESIDUES IN CLASS I VIRAL FUSION  
PROTEINS IMPORTANT FOR FUSOGENIC ACTIVITY

---

DISSERTATION

---

A dissertation submitted in partial fulfillment of the  
requirements for the degree of Doctor of Philosophy in the  
College of Medicine  
at the University of Kentucky

By

Hadley E. Neal

Lexington, Kentucky

Director: Dr Rebecca E. Dutch, Professor of Molecular and Cellular Biochemistry

Lexington, Kentucky

2023

Copyright © Hadley E. Neal 2023

## ABSTRACT OF DISSERTATION

### A CHARACTERIZATION OF KEY RESIDUES IN CLASS I VIRAL FUSION PROTEINS IMPORTANT FOR FUSOGENIC ACTIVITY

Viral fusion proteins are critical for viral entry and subsequent infection. Class I fusion proteins are characterized by synthesis as an inactive precursor requiring cleavage by a host cell protease to become fusion competent. Though vaccine and antiviral therapeutic developments often target the fusion protein, questions surrounding cleavage dynamics and protein stability remain. The work presented in this dissertation investigates specific regions of three class I viral fusion proteins in an effort to identify key residues involved in proteolytic processing and membrane fusion.

The trimeric severe acute respiratory syndrome coronavirus 2 (SARS-CoV-2) spike protein (S) mediates receptor binding, facilitates fusion needed for viral entry, and drives cell–cell fusion. We demonstrate that S must be proteolytically processed at the S1/S2 border and within the S2 subunit in order to become fusion competent. We also identify residues within the internal fusion peptide and the cytoplasmic tail that modulate S-mediated cell–cell fusion.

The transmembrane (TM) region of the HeV hendra virus fusion protein (F) has been shown to play a role in F protein stability and the overall trimeric association of F. Previous work classified  $\beta$ -branched residues within the C-terminal TM domain as important for F protein endocytosis, proteolytic processing, and protein stability. The work presented here completes the analysis of the HeV F TM and identifies specific residues that alter F protein function, suggesting a role for these residues in the fusion process.

The respiratory syncytial virus (RSV) fusion protein (F) requires cleavage at two sites, separated by 27 amino acids. Cleavage at both sites results in a 27 amino acid fragment, termed Pep27. Previous work has provided conflicting results

on the relative timing of when the two cleavage events occur. In addition, the fate of Pep27 is unclear. Examination of F cleavage kinetics in both infected and transfected systems over time determined that cleavage of both sites occurs within the secretory pathway as F is transported to the cell surface. We found that the deletion of Pep27 does not alter F function, but the mutation of N-linked glycosylation sites within Pep27 reduces both F surface expression and cell-cell fusion activity. This work clarifies the timing of RSV F proteolytic cleavage and offers insight into the crucial role the N-linked glycosylation sites within the Pep27 play in the biological function of F. The work presented in this dissertation identifies residues within distinct regions of class I viral fusion proteins critical for fusion protein cleavage and stability, therefore impacting infection.

Keywords: viral fusion, fusion protein, RSV, SARS-CoV-2, paramyxoviruses, pneumoviruses

---

Hadley E. Neal

---

04/13/2023

Date

A CHARACTERIZATION OF KEY RESIDUES IN CLASS I VIRAL FUSION  
PROTEINS IMPORTANT FOR FUSOGENIC ACTIVITY

By  
Hadley E. Neal

Dr. Rebecca E. Dutch  
\_\_\_\_\_  
Director of Dissertation

Dr. Trevor Creamer  
\_\_\_\_\_  
Director of Graduate Studies

04/13/2023  
\_\_\_\_\_  
Date

## TABLE OF CONTENTS

|   |    |
|---|----|
| LIST OF FIGURES .....                                     | vi |
| CHAPTER 1. BACKGROUND AND INTRODUCTION.....               | 1  |
| <i>Enveloped RNA Viruses</i> .....                        | 1  |
| 1.1.1 Class I viral fusion proteins.....                  | 1  |
| 1.1.2 Synthesis and posttranslational modifications ..... | 2  |
| 1.1.3 Fusion inhibitors.....                              | 2  |
| <i>SARS-CoV-2</i> .....                                   | 3  |
| 1.1.4 Known coronaviruses .....                           | 3  |
| 1.1.5 Fusion and entry.....                               | 4  |
| <i>HeV</i> .....  | 5  |
| 1.1.6 Fusion and entry .....                              | 5  |
| 1.1.7 TM-TM interactions.....                             | 6  |
| 1.1.8 $\beta$ -branched residues.....                     | 7  |
| <i>RSV</i> .....  | 8  |
| 1.1.9 RSV clades.....                                     | 8  |
| 1.1.10 F synthesis and cleavage .....                     | 9  |
| 1.1.11 N-linked glycosylation .....                       | 10 |
| 1.1.12 Mechanisms of entry.....                           | 12 |
| 1.1.13 Trimerization and stability .....                  | 14 |
| CHAPTER 2. METHODS.....                                   | 22 |
| <i>SARS-CoV-2 Spike Project</i> .....                     | 22 |
| 2.1.1 Cell lines and culture .....                        | 22 |
| 2.1.2 Plasmids, antibodies, and mutagenesis.....          | 22 |
| 2.1.3 Gel electrophoresis and western blotting.....       | 22 |
| 2.1.4 Syncytium assay.....                                | 23 |
| 2.1.5 Luciferase reporter gene assay .....                | 23 |
| 2.1.6 Surface biotinylation .....                         | 24 |
| 2.1.7 Time course immunoprecipitation .....               | 25 |
| 2.1.8 Immunofluorescence .....                            | 25 |
| 2.1.9 Statistical analysis .....                          | 26 |
| <i>HeV F Transmembrane Project</i> .....                  | 26 |
| 2.1.10 Cell lines and culture .....                       | 26 |
| 2.1.11 Plasmids and antibodies.....                       | 27 |
| 2.1.12 Syncytium assay.....                               | 27 |
| 2.1.13 Luciferase reporter gene assay .....               | 27 |
| 2.1.14 Surface biotinylation .....                        | 28 |
| 2.1.15 Immunoprecipitation .....                          | 29 |
| 2.1.16 Time course immunoprecipitation .....              | 29 |

|   |        |
|---|--------|
| <i>RSV Cleavage and P27 Project</i> .....   | 30     |
| 2.1.17 Cell lines, culture, and viruses .....   | 30     |
| 2.1.18 Antibodies .....   | 30     |
| 2.1.19 Syncytium assay and counts .....   | 30     |
| 2.1.20 Surface biotinylation .....  | 31     |
| 2.1.21 Radiolabel immunoprecipitation.....  | 32     |
| 2.1.22 Time course immunoprecipitation .....  | 32     |
| 2.1.23 Immunofluorescence .....   | 33     |
| 2.1.24 Flow cytometry.....  | 34     |
| 2.1.25 Statistical analysis .....   | 34     |
| <br>CHAPTER 3. EFFECT OF CLINICAL ISOLATE OR CLEAVAGE SITE<br>MUTATIONS IN THE SARS-COV-2 SPIKE PROTEIN ON PROTEIN STABILITY,<br>CLEAVAGE, AND CELL-CELL FUSION ..... | <br>35 |
| <i>Introduction</i> .....   | 35     |
| <i>Results</i> .....  | 38     |
| 3.1.1 Spike Mediated Cell-Cell Fusion.....  | 38     |
| 3.1.2 Importance of CoV-2 cleavage sites .....  | 39     |
| 3.1.3 Effect of Circulating S Mutations on Protein Stability, Cleavage, and<br>Fusion.....  | 41     |
| <i>Discussion</i> .....   | 42     |
| <br>CHAPTER 4. ANALYSIS OF HENDRA VIRUS FUSION PROTEIN N-<br>TERMINAL TRANSMEMBRANE RESIDUES .....  | <br>52 |
| <i>Introduction:</i> .....  | 52     |
| <i>Results</i> .....  | 53     |
| <i>Discussion:</i> .....  | 55     |
| <br>CHAPTER 5. CHARACTERIZING RSV FUSION PROTEIN CLEAVAGE<br>DYNAMICS AND THE POTENTIAL ROLE OF PEP27 .....   | <br>61 |
| <i>Introduction:</i> .....  | 61     |
| <i>Results:</i> .....   | 64     |
| 5.1.1 RSV F Cleavage is Nonsequential.....  | 65     |
| 5.1.2 Cleavage Dynamics are Consistent in Transfection and Infection<br>Models.....   | 67     |
| 5.1.3 Cell-cell fusion is abolished with the disruption of either cleavage site<br>67   |        |
| 5.1.4 The randomization of P27 decreases F <sub>1+</sub> product formation.....   | 68     |
| 5.1.5 P27 mutations impact cell-cell fusion differently in subtypes .....   | 70     |
| 5.1.6 Low levels of P27 but little uncleaved F <sub>0</sub> can be detected on the cell<br>surface.....   | 72     |
| <i>Discussion:</i> .....  | 73     |



|   |     |
|---|-----|
| CHAPTER 6. DISCUSSION AND FUTURE DIRECTIONS ..... | 90  |
| <i>Overview</i> .....                             | 90  |
| <i>SARS-CoV-2 spike protein mutations</i> .....   | 90  |
| <i>HeV F TM stability</i> .....                   | 91  |
| <i>RSV F cleavage dynamics</i> .....              | 92  |
| <i>P27 and conformational stability</i> .....     | 93  |
| <i>Pre-fusion F as a vaccine target</i> .....     | 95  |
| <i>Protein triggering</i> .....                   | 95  |
| <i>P27 potential biological functions</i> .....   | 96  |
| APPENDIX: Abbreviations.....                      | 98  |
| REFERENCES .....                                  | 99  |
| VITA .....  | 127 |

## LIST OF FIGURES

|  |    |
|--|----|
| Figure 1.1: Class I viral fusion mechanism. ....   | 16 |
| Figure 1.2: Viral entry and replication .....  | 17 |
| Figure 1.3: Cleavage products of enveloped virus fusion proteins .....   | 18 |
| Figure 1.4: Two proposed mechanisms of RSV entry .....   | 20 |
| Figure 3.1: CoV-2 spike alone mediates cell-cell fusion. ....  | 46 |
| Figure 3.2: Mutations at all three potential spike cleavage sites reduce cleavage at the S1/S2 subunit border. ....  | 47 |
| Figure 3.3: Mutations made at any of the three potential cleavage sites abolish syncytia formation. ....   | 49 |
| Figure 3.4: Spike S2 subunit mutations found in circulating variants variably affect spike mediated cell-cell fusion. ....                                     | 50 |
| Figure 3.5: Circulating mutations form large syncytia, similar to wt S. ....   | 50 |
| Figure 4.1: Several HeV F TM mutants have impaired protein expression and protein cleavage. ....   | 58 |
| Figure 4.2: HeV F TM mutations at residues SM and LY decrease protein cleavage levels. ....  | 59 |
| Figure 4.3: Mutations at residues IS, ML, SM, and LY in the HeV F TM reduce fusion. ....   | 60 |
| Figure 5.1: Mutations at the second cleavage site alter product formation in both surface and total populations. ....  | 79 |
| Figure 5.2: RSV F cleavage is nonsequential. ....  | 81 |
| Figure 5.3: Cleavage dynamics are consistent between transfection and infection models. ....   | 82 |
| Figure 5.4: Cell-cell fusion is abolished with the disruption of either cleavage site. ....  | 83 |
| Figure 5.5: Mutations within P27 targeting N-linked glycosylation and the deletion of P27 do not drastically impact protein expression in either subtype. .... | 84 |
| Figure 5.6: The randomization of P27 decreases F1+ product formation. ....   | 85 |
| Figure 5.7: Mutations within P27 impact cell-cell fusion. ....   | 87 |
| Figure 5.8: Low levels of P27 but little uncleaved F0 can be detected on the cell surface. ....  | 88 |

## CHAPTER 1. BACKGROUND AND INTRODUCTION

### Enveloped RNA Viruses

The virus order *Mononegavirales* is composed of 8 viral families, several of which are notable for their impact on human disease globally [1–4]. Structurally, these families share a lipid bilayer (termed the envelope) which is derived from the host cell and surrounds the viral genetic material. Studding this envelope are glycoproteins which facilitate the host cell attachment and fusion [2, 3].

#### 1.1.1 Class I viral fusion proteins

Though the *Mononegavirales* order is highly diverse, the basic mechanism of fusion remains consistent for members of this order. As shown in figure 1.1, the fusion glycoprotein (F) sits in a metastable prefusion state on the surface of a newly synthesized virion. Here, F is in a high energy state; stable enough to maintain the prefusion conformation, but prepared to change conformations upon a triggering event, initiating fusion [5, 6]. The triggering event is an environmental stimulus, often receptor binding, low pH, or both, that induces a conformational change allowing the heptad repeat A (HRA) to form a coiled-coil and project the hydrophobic fusion peptide (FP) into the target cell membrane. The protein folds back on itself bringing HRA to heptad repeat B (HRB). This facilitates the formation of the 6-helical bundle required for fusion merging the viral and host membrane, forming a fusion pore and allowing the viral genetic material into the target cell cytoplasm [7, 8]. The vital role the fusion glycoprotein plays in the viral life cycle makes it an excellent therapeutic target. Unfortunately, in the case of many viruses, a gap in knowledge remains around the details of the fusion protein and the mechanism of entry. The results reported in later chapters of this dissertation describe viruses from the *Mononegavirales* order, specifically the *Paramyxoviridae* and *Pneumoviridae* families. Fusion dynamics of another enveloped virus from the *Coronaviridae* family are also discussed.

### 1.1.2 Synthesis and posttranslational modifications

In the viral life cycle, these critical fusion proteins are initially synthesized in the endoplasmic reticulum (ER) in the inactive form. The protein trimerizes and moves through the secretory pathway to be post translationally modified and in some cases, proteolytically processed (Figure 1.2). The modifications made to F are important for stability intracellularly and to preserve the prefusion conformation on the cell surface and surface of the released viral particle. Specifically, glycosylation of the fusion protein has been shown to impact protein transport, expression, and surface stability [9–15]. The two primary forms of glycosylation seen in viral research are N-linked and O-linked. N-linked glycosylation is the addition of a glycan to the amine group of an asparagine residue, identified by the consensus sequence Asn-X-Ser/Thr where X is any amino acid except for proline. O-linked glycosylation modifies the oxygen atom of serine or threonine. Notably, N-linked glycosylation begins in the ER, making it a co-translational modification; while O-linked glycosylation does not occur until later in the secretory pathway. Intracellularly, N-linked glycosylation mediates interactions with ER chaperones, calnexin and calreticulin, which are critical for protein folding, and aids in the proper transport of the protein to the surface [12, 14, 16–18]. On the cell surface, glycans can shield the surface proteins from antibody recognition, evading the immune system. This shielding is seen across many enveloped viruses, including HIV-1 and influenza A virus [13, 17, 19]. Additionally, the glycosylation of the fusion protein can facilitate receptor binding and viral entry either by direct receptor interaction or through conformational stability [9, 13, 20].

### 1.1.3 Fusion inhibitors

The critical role of the fusion protein makes it an excellent therapeutic target. The formation of the six-helix bundle by HRA and HRB can be prevented using synthetic peptides to bind to these regions, blocking membrane fusion [21].

Synthetic peptides have been designed for many Class I fusion proteins and effectively prevent virus replication, cell-cell fusion, and in some cases virus infection [21–23]. The fluidity of the membrane is an important factor in viral fusion. Previous work has shown that cholesterol, which increases membrane fluidity, plays a direct role in viral entry by generating the membrane curvature necessary for endocytosis [24, 25]. This has been exploited using cholesterol-tagged peptide inhibitors to prevent infection [26, 27]. In viruses that have not been directly shown to enter through endocytosis, like respiratory syncytial virus, studies have shown that entry is sensitive to cholesterol depletion and regions rich in cholesterol were preferred sites of infection [24, 28]. Protease inhibitors have also been explored as a method to block viral fusion. The activation of the fusion protein through proteolytic processing is a requirement for viral entry. Blocking this priming event would effectively stop infection; however, the broad-spectrum inhibitors being explored target ubiquitous proteases and would likely impact other cellular functions [24, 29]. Although the fusion protein is a common target in antiviral therapeutics, gaps in the field remain regarding viral fusion and the specific residues that impact this mechanism.

## SARS-CoV-2

### 1.1.4 Known coronaviruses

The *Coronaviridae* family contains enveloped viruses composed of single stranded positive-sense RNA. Similar to viruses in the *Mononegavirales* order, a fusion event between the virus and the target cell membrane must occur for viral entry. In coronaviruses, the Spike protein (S) facilitates this event by mediating both receptor binding and membrane fusion. Several known coronaviruses can cause common colds in humans. As zoonotic viruses, infection can spread from animals to humans [30, 31]. Bats are the reservoir species for many coronaviruses, including severe acute respiratory syndrome (SARS) and middle eastern

respiratory syndrome (MERS) [30–33]. These two viruses are significant due to the outbreaks seen within the last two decades. In late 2002, the first case of SARS was detected in China. As a highly pathogenic virus, over 8,000 cases and 774 deaths were seen globally through 2004 [30, 31]. A decade later, MERS emerged after an infection in Saudi Arabia. Through 2016, there were nearly 2,000 cases worldwide with 624 deaths [30, 31]. Despite the threat of SARS or MERS re-emergence, no vaccines or antiviral treatments were developed.

#### 1.1.5 Fusion and entry

Severe acute respiratory syndrome coronavirus 2 (SARS-CoV-2) is the viral agent responsible for the COVID19 pandemic. As of February 14<sup>th</sup>, 2023, there have been over 6.8 million deaths worldwide due to SARS-CoV-2 infection [34]. As an enveloped virus, SARS-CoV-2 enters host cells through the fusion of viral and host cell membranes. Host cell attachment, fusion, and entry is facilitated by the S protein. S is composed of two distinct subunits: S1 which is responsible for host cell receptor binding, and S2 which promotes membrane fusion [7, 35, 36]. As shown in Figure 1.3a, within S1 there is a receptor binding domain (RBD), an N-terminal domain (NTD), and a signal peptide (SP). S2 contains the hydrophobic fusion peptide (FP), the internal fusion peptide (IFP), 2 heptad repeat domains (HR1 and HR2), a transmembrane domain (TM), and a cytoplasmic tail (CT).

After binding to the known host cell receptor, Angiotensin Converting Enzyme 2 (ACE2), cleavage by a host cell protease allows for the release of the S1 subunit [35–37]. The S2 subunit undergoes a conformational change to merge the viral and host cell membranes, allowing for the release of viral replication machinery into the host cell. The need for two sequential post-translational cleavage events for S activation is conserved among most coronaviruses. Typically, one event at the S1 and S2 subunit border, and a second within the S2 subunit, termed S2' [8, 35, 36, 38, 39].

SARS-CoV-2 S differs from the closely related SARS and MERS spike proteins in that it contains an insertion of 12 nucleotides upstream of the polybasic

furin recognition motif found at the S1/S2 border. It has been suggested that the addition of this sequence may provide increased transmission by further exposing the furin cleavage sequence [40]. Additionally, the SARS-CoV-2 S RBD is more stable than that of SARS and MERS [41]. Residues within the SARS-CoV-2 S RBD have been shown to increase interactions with the ACE2 receptor compared to SARS by increasing stability, thus increasing binding affinity [41, 42]. Compared to MERS which uses the dipeptidyl peptidase 4 receptor, the SARS-CoV-2 RBD secondary structure loops are more stable due to the position of crucial disulfide bonds [41–43]. This stability may contribute to the differences in pathogenesis seen in SARS-CoV-2 infection. Notably, the FDA gave emergency approval to Pfizer and Moderna for vaccines targeting SARS-CoV-2 composed of S mRNA, further demonstrating the importance of S as a therapeutic target [44, 45].

In Chapter 3, we aim to understand factors that are critical for S cell-cell fusion activity, including proteases involved, and cleavage events required. We demonstrate that S must be processed at the S1/S2 border in order to mediate cell-cell fusion, and that mutations at potential cleavage sites within the S2 subunit alter S processing at the S1/S2 border, thus preventing cell-cell fusion. We also identify residues within the internal fusion peptide and the cytoplasmic tail that modulate S cell-cell fusion. This work therefore offers insight into S stability, proteolytic processing, and factors that mediate S cell-cell fusion, all of which help give a more comprehensive understanding of this highly sought-after therapeutic target.

## HeV

### 1.1.6 Fusion and entry

All members of the paramyxovirus family express two surface glycoproteins, an attachment protein and the fusion protein (F), which promote viral entry. The attachment protein mediates the binding of the virus to a host cell surface receptor, while F facilitates the fusion of the two membranes [6, 46, 47]. F is a class I fusion

protein, meaning it requires proteolytic processing to become active and it remains a trimer in both the native and cleaved form [6]. As shown in figure 1.3b, HeV F is made up of a hydrophobic fusion peptide (FP), two heptad repeat domains (HRA and HRB), a single-pass transmembrane domain (TM), and a cytoplasmic tail (CT). F is synthesized as an inactive precursor ( $F_0$ ) and must undergo cleavage by a host cell protease to become active. These key regions of F are consistent among paramyxoviruses.

Unlike other paramyxoviruses, HeV F is furin-independent and proteolytic cleavage occurs following endocytosis [46–49]. After synthesis in the ER, F moves through the secretory pathway to the plasma membrane. Upon endocytosis, F re-enters the cell and is cleaved by the protease cathepsin L in an endosome. Cleaved F then traffics back to the plasma membrane to be incorporated into new virions [47, 49]. For infection, the HeV attachment protein (G) binds the host cell receptor, Ephrin B2 or B3, allowing F to initiate membrane fusion [50].

#### 1.1.7 TM-TM interactions

Work in the last two decades has challenged the idea of TM regions as simply protein anchors. Broadly, previous work has shown the importance of TM-TM interactions in protein stability [51, 52]. However, in viral fusion proteins TM regions play very specific roles that often reach beyond stabilization. Previous work on bovine papillomavirus and measles virus identified that the TM of their respective fusion proteins mediates and modulates receptor binding respectively [53–55]. In HIV-1, the TM of the fusion protein is important in intracellular trafficking [56]. Prefusion stability is required for viral entry, as the conformational change to the post-fusion form is kinetically essentially irreversible. Understanding what factors impact the stabilization of the fusion protein is crucial for the development of targeted antivirals and vaccines. In parainfluenza virus 5 (PIV5), the disruption of the fusion protein TM completely destabilized the pre-fusion conformation [57]. Interestingly, one study identified a leucine-isoleucine zipper motif spanning a



region of the HeV F TM [58]. Specific residues within the zipper were determined to have minor impacts on protein expression and fusion activity. In contrast, the disruption of the entire zipper motif resulted in premature triggering of HeV F, and therefore altered fusion activity [58].

### 1.1.8 $\beta$ -branched residues

An analysis of sequences from TM domains of 19 paramyxoviruses revealed a pattern of  $\beta$ -branched (leucine, isoleucine, and valine) repeats [58]. Alanine scanning mutagenesis of N-terminal  $\beta$ -branched residues in the PIV5 fusion protein identified residues whose loss significantly decreased fusion [59]. In a similar study, mutations made to HeV F C-terminal  $\beta$ -branched residues also resulted in a decrease in fusion activity [60]. This suggests that  $\beta$ -branched residues within the fusion protein TM may be impacting fusion activity across the paramyxovirus family.

To complete analysis of all residues within the HeV TM, alanine scanning mutagenesis was used to evaluate the remaining unexplored N-terminal residues. We discovered that changes to residues M491/L492 significantly reduce F fusion without drastically altering protein expression. Additionally, we show that residues S490, S493, and Y498 play important roles in protein processing, a critical step for fusion, consistent with previous work [61, 62]. Our studies in Chapter 4 demonstrate that targeted disruption of TM-TM interactions significantly impacts viral fusion protein stability and function, presenting these interactions as a novel target for antiviral development.

## RSV

### 1.1.9 RSV clades

RSV is an enveloped, single-stranded, negative sense RNA virus belonging to the *Pneumoviridae* family [63]. Similar to the closely related paramyxoviruses, pneumoviruses consists of a nucleocapsid protein (N) encapsidating the genetic material, with the polymerase (L) and polymerase co-factor, P (phosphoprotein), making up the functional replication complex. In addition, there is a matrix (M) protein layer linking the nucleocapsid protein complex with the phospholipid envelope, and three transmembrane glycoproteins [64]. Two of these glycoproteins, the fusion protein (F) and attachment (G) protein, are responsible for fusion and entry of newly synthesized virus. While the function of the small hydrophobic (SH) protein is not fully understood, functional and structural studies suggests that, similarly to its closely related human metapneumovirus (HMPV), the RSV SH protein is a pH-dependent viroporin that regulates membrane permeability, infectivity, and prevents host cell apoptosis [65–67].

RSV has two subgroups, A and B, differentiated by antigenic responses to monoclonal antibodies [68, 69]. Within subgroups, clades are determined by the sequence of a variable domain of G [68, 70]. RSV is seasonal, but A and B strains have been shown to co-circulate worldwide [71–73]. Although the prevalence of one strain over the other varies between RSV seasons, RSV A has been the primary focus of molecular studies. An RSV B strain that emerged in 1999 has become the dominant variant detected globally [73–76]. This strain includes a duplication in G that impacts viral-host cell attachment [75, 76], indicating that the molecular studies using RSV A are not universal to all strains of RSV.

### 1.1.10 F synthesis and cleavage

Broadly speaking, the F proteins of *pneumoviruses* and *paramyxoviruses* are class I fusion proteins, synthesized as inactive precursors ( $F_0$ ), and must undergo cleavage to become fusion competent. This cleavage is performed by a furin-like host cell protease, resulting in two disulfide-linked subunits termed  $F_1$  (50 kDa, AA 137 to 574) and  $F_2$  (20 kDa, AA 26 to 109) (Figure 1.3c) [77]. Fusion active F exists on the viral surface in a metastable “pre-fusion” state until a triggering event induces a conformational change, exposing the fusion peptide which undergoes transition to an alpha-helical coiled coil which inserts into the target membrane, followed by refolding to a six-helix bundle, and the energy released in this process is hypothesized to drive membrane fusion [64, 78]. This process is similar for all paramyxoviruses and pneumoviruses; however, there are several unique aspects to the RSV F protein that remain to be fully understood.

Collins et al. and Elango et al., in 1984 and 1985 respectively, were the first groups to sequence the RSV F protein [79, 80]. F is synthesized as a 574 amino acid, inactive precursor ( $F_0$ ) possessing a polybasic motif (KKRKRR<sup>136</sup>) corresponding to a consensus site for furin, a host cell protease. Unlike other paramyxoviruses, the polybasic sequence is six amino acids long, leading Bolt et al. to suggest that other proteases can cleave at the same motif (such as proprotein convertase 5 and 7) [81] and activate the RSV F protein [82]. However, RSV is unlike other paramyxoviruses because F requires cleavage at two sites, rather than one, to become fully active. It was not until 2001 that Gozáles-Reyes et al. and Zimmer et al. independently demonstrated that the RSV F protein is cleaved in two polybasic sites (RARR<sup>109</sup> and KKRKRR<sup>136</sup> [83, 84]), releasing an internal peptide of 27 amino acids, termed P27 (AA 110 to 136). The fate of this P27 fragment post-cleavage is still unknown.

Through site-directed mutagenesis of bovine respiratory syncytial virus (BRSV), Zimmer et al. determined that furin cleavage at site R109 is dispensable for fusion activity in vitro, although fusion efficiency was impaired. This highlighted

the importance of cleavage at site R136, which exposes the fusion peptide at the N-terminus of the F<sub>1</sub> subunit [85]. To identify how the presence of two polybasic cleavage sites impacts fusion, Rawling et al generated chimeric mutations of the Sendai virus (SeV) fusion protein including one, or both of the RSV furin recognition sites [86]. SeV is also part of the paramyxovirus family and contains a class I fusion protein; however, the fusion protein is only cleaved at one site. Additionally, for SeV fusion to occur, the HN attachment protein is required, unlike RSV which has demonstrated the ability to fuse in cell culture without the G protein [87]. Interestingly, all SeV chimeric mutants that contained both of the RSV cleavage sites formed syncytia in the absence of the HN protein. This suggests that the ability of RSV to fuse without the attachment protein is facilitated, at least in part, by the additional cleavage site.

#### 1.1.11 N-linked glycosylation

The F protein gene is generally well-conserved across RSV genotypes. Hause et al. compared the sequence variability of more than 1,000 RSV sequences of both subtypes A and B. They observed that compared to RSV/A Long, a popular strain in *in vitro* studies and vaccine development, amino acids in the P27 region of the RSV/B strains exhibited a greater number of non-synonymous amino acid changes than the RSV/A strains. However, entropy analysis, a measure of variability at each amino acid position, revealed that within the same subtype, several amino acid positions within the P27 sequence of RSV/As are more variable than in the P27 sequence of RSV/Bs [88].

Glycosylation is a key post-translational modification for viral proteins, as it impacts structure, function, stability, and translocation to the cell surface [89–91]. The RSV F protein is N-glycosylated on the asparagine (N) residue of the consensus sequences N-X-S/T [80, 83]. Five sites are well conserved among subtypes (N<sup>27</sup>, N<sup>70</sup>, N<sup>116</sup>, N<sup>126</sup>, and N<sup>500</sup>) [83], however certain RSV strains have

an additional N120 glycosylation site [92, 93]. Three of these sites are located within the P27 segment (N116, N120, and N126).

The presence of N-linked glycans on the F protein of prototypical RSV/A strains was assessed by Zimmer et al. in 2001 and by Leemans et al. in 2018 [83, 94]. Through systematic N to Q mutations, both groups showed that glycosylation in the P27 segment does not impact cleavage or transport of the F protein to the cell surface. Both groups transfected BSR T7/5 cells with F protein constructs containing the mutations N116Q or N126Q and did not observe molecular weight differences compared to the wild-type control. Therefore, Leemans et al. concluded that P27 would be missing in a mature F protein. Moreover, when evaluating the effect of glycosylation on the function of the F protein, both groups observed formation of larger syncytia in BSR T7/5 cells transfected with the mutant N116Q. Viral proteins can use glycosylation to shield antigenic sites, evading antibody recognition [95]; however, Leemans et al. demonstrated that glycosylation of P27 on sites N116 and N126 did not significantly compromise the binding of Palivizumab or other neutralizing antibodies targeting the pre-fusion conformation.

These findings were further supported by Leemans et al. in 2019 who explored the importance of F protein glycosylation in virus infectivity [96]. They incorporated the same aforementioned mutations into an RSV-BAC system to generate recombinant infectious viruses and performed infectivity studies in HEp-2 cells. Similar to what was previously observed using recombinant F proteins, the molecular weight of the F proteins expressed by viruses encoding mutations N116Q or N126Q was comparable to the molecular weight of the F protein from wild-type virus, again suggesting that P27 would be absent from the mature F protein. On the other hand, contrary to what was previously observed with transfecting HEp-2 cells with glycosylation-deficient recombinant F proteins, infection of HEp-2 cells with mutant virus RSV F N116Q led to a decrease in syncytium formation compared to wild-type RSV. Although the presence of glycosylated P27 was not confirmed, changes in syncytium formation *in vitro* and

*in vivo* indicates that glycosylation of at least one site on P27 might have an important role in RSV biology.

#### 1.1.12 Mechanisms of entry

RSV F protein detected on the cell surface has been shown to be cleaved and in the active state in several studies [83, 84]. One study in particular demonstrated that F<sub>0</sub> cannot be detected on the cell surface in an RSV infection model [82]. In contrast, a recent publication cited that P27 was found on the cell surface of infected cells, leading the authors to suggest that uncleaved or partially cleaved F<sub>0</sub> was present on the cell surface [97]. This finding would be consistent with the conclusions drawn by Krzyzaniak et al. in 2013, stating that F exists on the viral surface in a partially cleaved state [98]. In this study, the authors detected peptides corresponding to the P27 region on purified RSV/A particles through liquid chromatography coupled with mass spectrometry (LC/MS) analysis. Then, using western blot analysis of infected HeLa cells to examine F cleavage state, they concluded that cleavage of the second site to generate P27 did not occur until after viral macropinocytosis. In their model, the first of the two furin recognition sites (R109) is cleaved in the trans-Golgi after protein synthesis while trafficking to the cell surface, and a partially cleaved F is incorporated in RSV virions. Upon binding to the epidermal growth factor (EGF) receptor, RSV enters the host cell through macropinocytosis. In this model, it is not until the virus is within an endosome that the second furin recognition site (R136) is cleaved [98], indicating that F is present on the cell surface in a half-cleaved state and remains inactive until viral entry (Figure 1.4a). This work is particularly significant in the RSV field as it set the precedent for future studies on partially cleaved F protein. However, contrary to HMPV, RSV F protein-promoted fusion is pH independent, indicating that acidification of endosomes may not be required for cleavage of F protein, consequently, for RSV entry [99].

Endocytosis and acidification of endosomes to promote fusion protein cleavage and fusogenic function is a common mechanism of entry for many viruses. All known paramyxoviruses enter the host cell by direct fusion with the cell membrane, not utilizing endosomal routes [100]. Interestingly, in some strains of the most closely related human virus to RSV, human metapneumovirus (HMPV) requires endocytosis and pH-dependent enzymes to initiate fusion [101–103]. However, the cellular location of RSV fusion remains in debate. Early studies evaluated the mechanism of RSV entry through an R18 dequenching assay to monitor virion-cell fusion [99]. In infected HEP-2 cells, changing the environmental pH had no impact on fusion. Similarly, exposing cells to a lysosomotropic agent (known to inhibit viral endocytosis) after infection did not change the rate of cell-cell fusion or the production of new virus. This led the authors to conclude that entry primarily occurs through direct viral fusion with the plasma membrane. This claim was later supported by Khan et al., again using compounds that alter pH to determine that RSV fusion is pH independent (Figure 1.4b) [104].

However, later studies acknowledge that RSV is able to enter directly through the plasma membrane, but suggested that there may be an additional role played by endocytosis. Kolokoltsov et al. used siRNAs to knockdown genes associated with clathrin-mediated endocytosis, resulting in a significant decrease in infection [105]. The authors concluded that although RSV fusion is pH-independent, endocytosis is still used as a method of viral entry. Although the fusion location of RSV to host cells remains to be fully determined, future studies are needed to clarify if RSV may be able to use both, or either, direct fusion with the plasma membrane and endocytosis with an additional cleavage event in endosome as entry mechanisms in host cells.

### 1.1.13 Trimerization and stability

The fusion-competent RSV F is formed by non-covalent interactions between three disulfide-linked F<sub>1</sub> and F<sub>2</sub> protomers resulting from the enzymatic cleavage of F<sub>0</sub> [106–108]. A 2015 study from Gilman et al. characterized an RSV neutralizing antibody, AM14, that recognizes cleaved, trimeric, prefusion F [106]. AM14 binding proved to be dependent on furin cleavage and this was attributed to the potential interference of P27 on AM14 binding through steric inhibition, as well as the possibility that F is unable to fully trimerize prior to cleavage. Therefore, evidence suggests that P27 impacts trimer stability and therefore must be removed for proper stability of the cleaved trimer when it is incorporated into virions. In the same year, a study by Krarup et al. determined that the presence of P27 in F destabilizes the protein [107]. Using a single furin-site knockout recombinant protein, the authors were able to keep P27 associated with F<sub>2</sub>. This trimer containing P27 was subjected to denaturing conditions to evaluate stability compared to a trimer without P27. When incubating soluble F proteins in 0.1% SDS at room temperature, 97% of RSV F containing P27 were monomerized, while only 50% of RSV F without P27 were monomerized under these conditions [107], suggesting that P27 could in fact be negatively affecting the stability of trimerized F.

The stability of trimerized F was evaluated by Gilman et al. using an antibody specific for soluble, prefusion F trimers [109]. The authors determined that on the cell surface, the trimer of F<sub>1</sub>+F<sub>2</sub> heterodimers exist in a dynamic equilibrium between associated-dissociated trimers, suggesting a “breathing” mechanism for the trimerization of at least portions of F. Similar to the breathing motions described for the HIV-1 envelope protein [110–112], the authors indicate that trimerized F exhibits conformational flexibility and exists in at least two states on the cell surface, one more compact than the other. In the case of HIV-1, the more open trimeric state allows for the required conformational change to enable receptor binding, making this breathing mechanism an excellent therapeutic target [110–112].



In Chapter 5, we hypothesize that RSV F from different subtypes has different requirements for membrane fusion, including timing and proteolytic cleavage events. Our work, therefore, focused on characterizing differences in the RSV F proteins from both lab-adapted A and B subtypes. Through a series of mutations, we investigated the proteolytic processing, stability, protein trafficking kinetics, and fusion function of RSV F proteins from the difference subtypes. Additionally, the role of the P27 fragment has been evaluated in both subtypes. The fate of P27 after cleavage remains controversial in the field, given the conflicting nature of past studies. This work elucidated the impact of P27 and its sequence specificity on proteolytic processing, surface expression, and cell-cell fusion.

Collectively, the work presented here investigates the therapeutically relevant fusion proteins of several important human enveloped viruses. By specifically exploring proteolytic processing, surface expression, and cell-cell fusion we have further characterized the fusion dynamics of this critical protein.

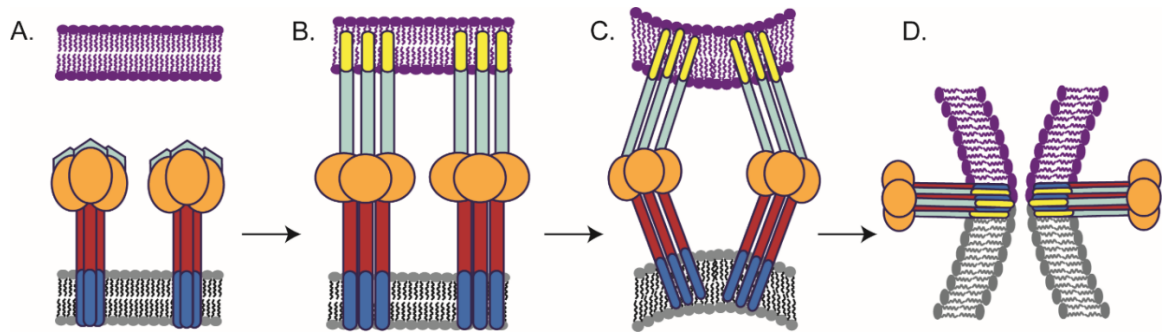


**Figure 1.1: Class I viral fusion mechanism.** A) After proteolytic processing, the fusion protein sits on the viral surface (grey) in a metastable, prefusion state. B) A triggering event induces a conformational change to form a pre-hairpin structure and insert the hydrophobic fusion peptide (yellow) into the target cell membrane (purple). C) The protein folds back on itself bringing N-terminal (light blue) and C-terminal (red) heptad repeats closer to form a 6-helical bundle. D) Lastly, the fusion peptide (yellow) and transmembrane domain (dark blue) are pulled together to merge the two membranes and open the fusion pore.

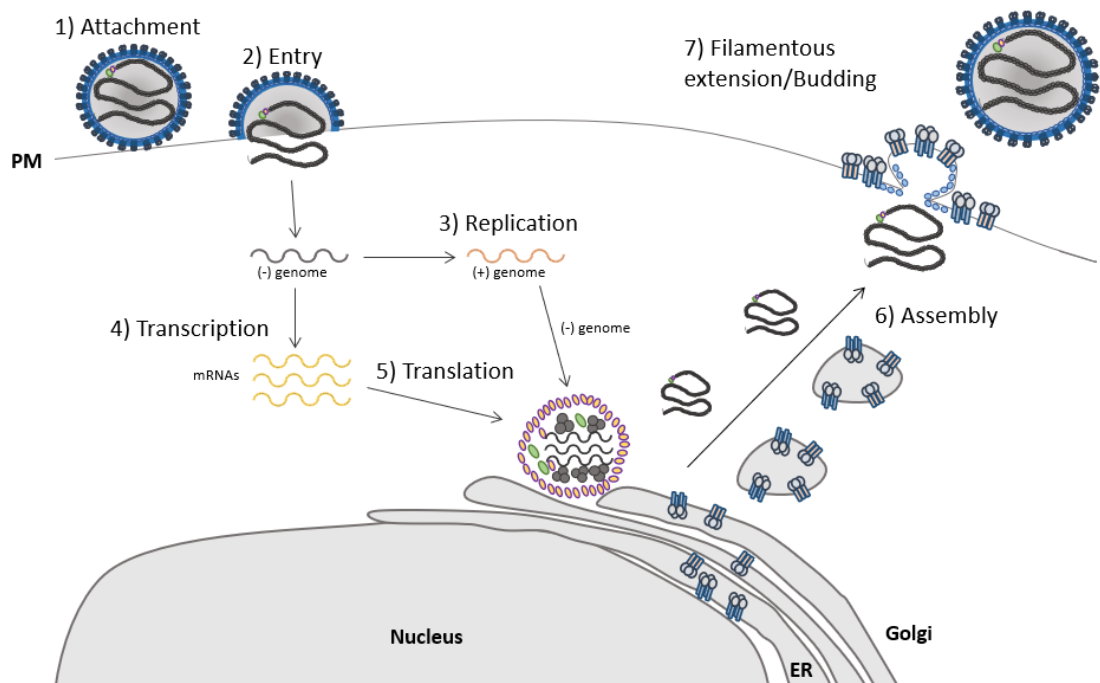


**Figure 1.2: Viral entry and replication.** 1) The attachment glycoprotein (G) on the viral surface mediate attachment to the host membrane. 2) Viral entry occurs through fusion with the host cell plasma membrane, facilitated by the fusion protein (F). 3) The viral genetic material is released into the cell, where the genome is replicated and 4) transcribed. 5) Encapsidated proteins are translated in the cytosol. Viral membrane proteins are translated in the ER and traffic through the trans-Golgi network, where they are proteolytically processed and posttranslationally modified before trafficking to the surface. 6) The newly synthesized virion is packaged and buds from the host cell membrane.

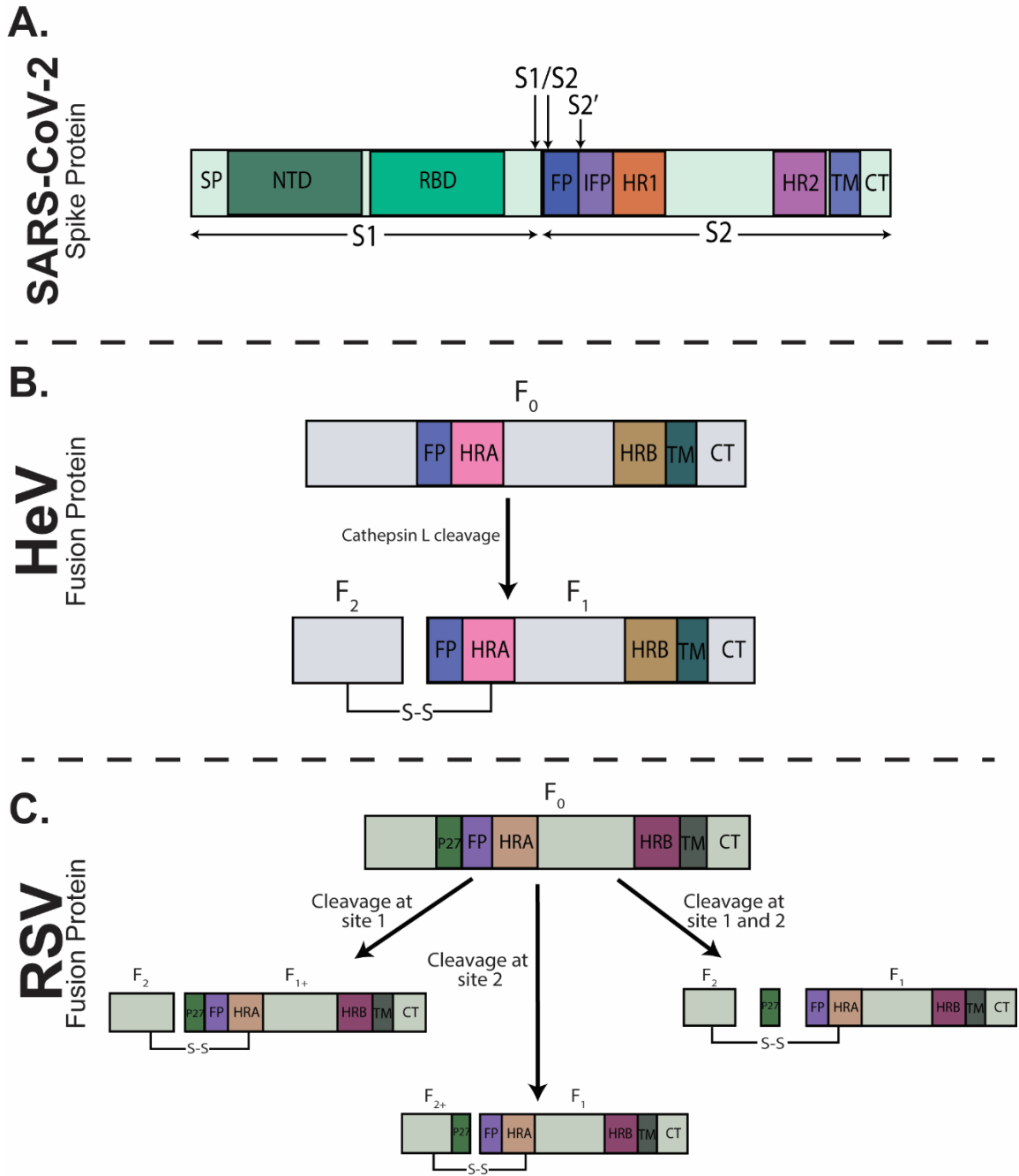


**Figure 1.3: Cleavage products of enveloped virus fusion proteins.** A) SARS-CoV-2 S is composed of two subunits: S1 and S2. S1 contains a signal peptide (SP), an N-terminal domain (NTD), and the receptor binding domain (RBD). The S2 subunit contains a fusion peptide (FP), an internal fusion peptide (IFP), two heptad repeat regions (HR1 and HR2), a transmembrane domain (TM), and a

cytoplasmic tail (CT). S is processed at the S1/S2 border during protein trafficking to the cell surface by furin or a member of the furin family. There are two other potential cleavage sites within the S2 subunit, one 10 amino acids downstream of the S1/S2 border, a conserved site used by SARS-CoV S, and one is 100 amino acids downstream of the border, termed the S2' site. B) HeV F is synthesized in an uncleaved form ( $F_0$ ) and trafficked to the cell surface. F is then endocytosed and cleaved by cathepsin L in endosomes to expose the hydrophobic fusion peptide (FP), creating a disulfide linked heterodimer ( $F_1$  and  $F_2$ ). The  $F_1$  subunit is made up of two heptad repeat regions (HRA and HRB), a transmembrane domain (TM), and a cytoplasmic tail (CT). C) RSV F is synthesized as an inactive precursor ( $F_0$ ) containing two heptad repeat regions (HRA and HRB), the hydrophobic fusion peptide (FP), a transmembrane domain (TM), and a cytoplasmic tail. Moving through the secretory pathway, F is cleaved by furin or a furin-like protease at two predicted sites. Cleavage at site 1 exposes the FP, while the function of cleavage at site 2 is unknown. If both sites are processed a small peptide (P27) is released from the resulting disulfide linked subunits.

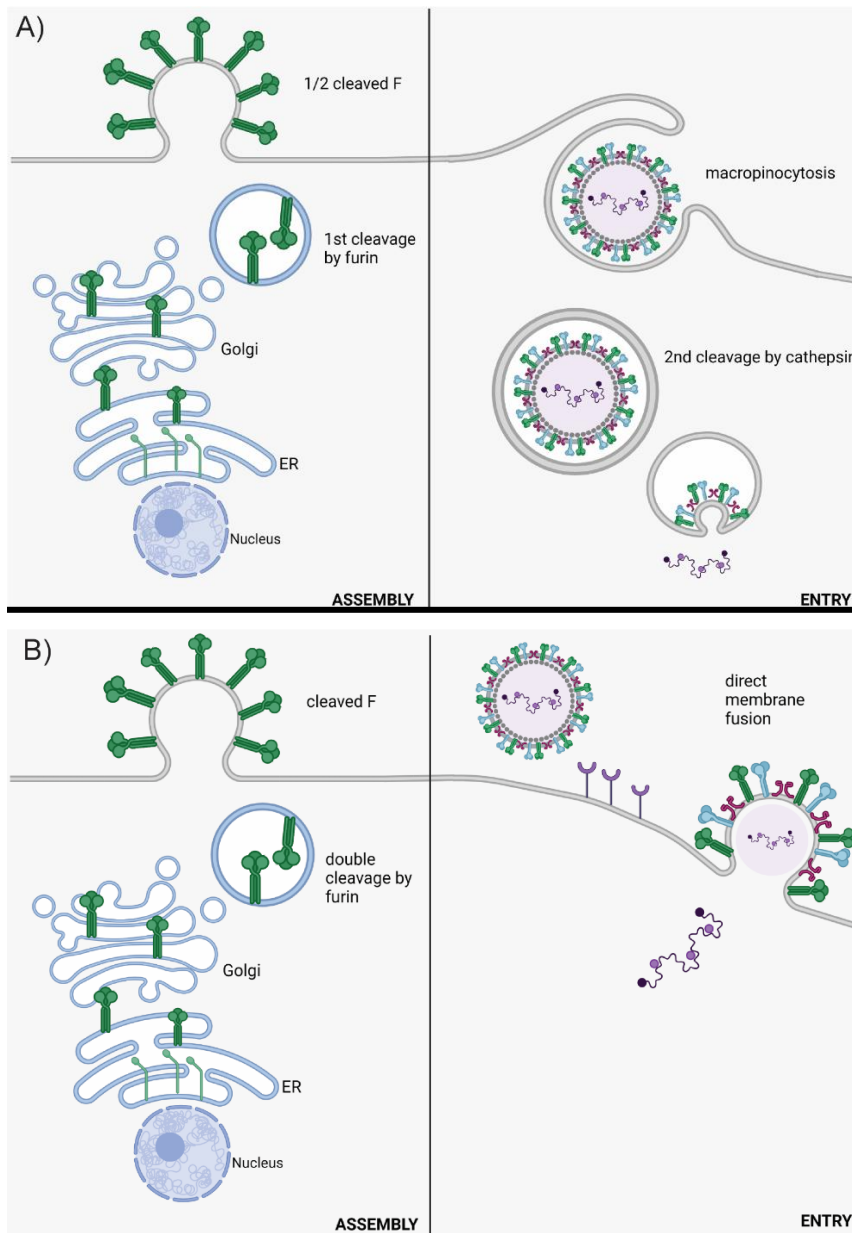


**Figure 1.4: Two proposed mechanisms of RSV entry.** A) In the macropinocytosis method of entry, F is only cleaved at FCS1 in the trans golgi, expressing on the viral surface in a half-cleaved state. Newly synthesized virus enters host cells through macropinocytosis, allowing for FCS2 to be cleaved by cathepsin L in an endosome. This activates F, facilitating fusion with the endosomal membrane and releasing the viral genetic material into the host cell cytoplasm. B) In the direct plasma membrane method of entry, F traffics through

the secretory pathway to be cleaved at both FCS1 and FCS2 by furin, expressing on the viral surface in a fully cleaved state. Entry occurs through receptor binding, resulting in the fusion of the viral and host cell membranes facilitated by F. Image was generated using BioRender.

## CHAPTER 2. METHODS

### SARS-CoV-2 Spike Project

#### 2.1.1 Cell lines and culture

Vero (ATCC), BSR T7/5 cells (provided by Karl-Klaus Conzelmann, Pettenkofer Institut), with 10% fetal bovine serum (FBS) and 1% penicillin/streptomycin. Every third passage, 0.5mg/ml of G-418 (Invitrogen) was added to the culture media of BSR T7/5 cells to select for the expression of the T7 polymerase. A549 cells (ATCC) were cultured in F12 Kaighns Modification media (GE Healthcare) with 10% FBS and 1% penicillin/streptomycin.

#### 2.1.2 Plasmids, antibodies, and mutagenesis

pCAGGS-SARS-CoV-2 spike was obtained from BEI Resources. SARS-CoV-2 S was subcloned into pUC57 and all S mutants were created in pUC57 using the QuikChange site-directed mutagenesis kit (Stratagene) with primers purchased from Eurofins. Constructs were then subcloned back into the pCAGGS expression vector. Other plasmids utilized include pSG5-Cathepsin L (from Terence Dermody, University of Pittsburgh), pCAGGS-furin (Promega), and T7 promoted-luciferase (Promega). Antibody anti-SARS spike glycoprotein (ab252690) was purchased from Abcam, and anti-TMPRSS2 (H-4) was purchased from Santa Cruz Biotechnology, Inc.

#### 2.1.3 Gel electrophoresis and western blotting

Proteins were separated on a 10% sodium dodecyl sulphate-polyacrylamide gel electrophoresis (SDS-PAGE). For western blot analysis, proteins were transferred to a polyvinylidene difluoride (PVDF) membrane (Fisher Scientific) at 60V for 100 minutes. After blocking with 5% milk in tris-buffered saline + Tween-20 (tTBS) for



1 hour, membranes were incubated with respective antibodies (anti-SARS S 1:5000 dilution, anti-TMPRSS2 1:1000 dilution, anti-hACE2 1:1000 dilution) at 4°C overnight. Membranes were then washed with tTBS and incubated with (Li-Cor) secondary antibodies at 1:10000 dilution in 5% milk solution for 1 hour. Membranes were washed again with tTBS and diH<sub>2</sub>O, before being imaged on the Odyssey Image Analyzer (Li-Cor).

#### 2.1.4 Syncytium assay

Cells (Vero or A549s) in 6 well plates were transiently transfected with 2µg of either wild-type or mutant SARS-CoV-2 S protein plasmid with Lipofectamine 3000 (Invitrogen) at a ratio of 1:2:2 DNA: P3000: Lipofectamine 3000. For experiments with the addition of proteases, the total DNA transfected was kept constant at 2µg, in those cases we used 1µg of S and 1µg of the indicated protease. Syncytia formation was imaged at 24 and 48 hours post transfection on a Nikon Ti2 at 20X magnification.

#### 2.1.5 Luciferase reporter gene assay

Effector cells (Vero or A549s) were plated in 12-well plates at 70-90% confluency and transfected with 1µg of total DNA (0.4µg of a T7 promoted luciferase plasmid, 0.6µg of wild-type (wt) or mutant S protein or S protein with additional proteases). At the same time BSR cells (constitutively expressing a T7 promoter) seeded in 6-well plates were transfected with 2µg either empty pCAGGS or pcDNA3.1(+)-hACE2. Eighteen to twenty-four hours post transfection BSR cells were lifted using trypsin, centrifuged for five minutes at 1500 rpm, resuspended in normal DMEM+10% FBS, and overlaid onto the S expressing cells at a ratio of 1:1. Overlaid samples were then incubated at 37°C for 9 hours (or as described in the text). Samples were lysed in 100µL of Reporter Gene Lysis buffer (Promega) and

frozen overnight. Plates were then scraped on ice, lysates were vortexed for 10 seconds, centrifuged at 13,000 rpm for 1 minute at 4°C, and 20µL of the supernatant was added to an opaque 96 well plate. Luciferase activity was measured on a SpectraMax iD3 (Molecular Devices) using a Luciferase Assay System (Promega). Background values were subtracted (empty pCAGGS in BSRs and effector cells) and luciferase activity was expressed as a percentage of wt S (effector cells) and hACE2 (BSR cells).

#### 2.1.6 Surface biotinylation

Two µg of wt or mutant S protein was transfected into Vero or A549 cells using the Lipofectamine 3000 system (Invitrogen; ratios described above). Eighteen to twenty-four hours post transfection, cells were starved in Cys-/Met- media (Gibco) for 45 minutes, and metabolically labelled for six hours using 50µCi of S35 (PerkinElmer) incorporated into Cys and Met (S35 Cys/Met). After the label, cells were washed once with PBS (pH 8) and incubated with 1 mg/ml of EZ-link Sulfo-NHS-biotin (Thermo Fisher) in PBS (pH 8) at 4°C for 35 minutes, and then at room temperature for 15 minutes. Next the cells were lysed in 500µl of RIPA buffer (100 mM Tris-HCl [pH 7.4], 0.1% SDS, 1% Triton X-100, 1% deoxycholic acid) containing 150 mM NaCl, protease inhibitors (1 U aprotinin, 1mM PMSF, [both from Sigma-Aldrich]), 5 mM iodoacetamide, and cOmplete EDTA-free Protease Inhibitor Cocktail Tablets (all from Sigma-Aldrich). Cell lysates were centrifuged at 55,000 rpm for 10 minutes, and the supernatant was incubated with anti-SARS S polyclonal antibody at 4°C for three hours. Following incubation, Protein A conjugated to Sepharose beads (Cytiva) were added to the samples, and incubated at 4°C for an additional 30 minutes. Post-incubation samples were washed two times with each RIPA Buffer+0.3M NaCl, RIPA Buffer+0.15M NaCl, and SDS-Wash II buffer (50mM Tris-HCl [pH 7.4], 150mM NaCl, and 2.5mM EDTA). After buffer aspiration and addition of 10% SDS, samples were boiled for 10 minutes. The supernatant was removed to a separate tube. 15µl of supernatant

was removed and added to an equal portion of 2X SDS loading buffer and labeled "TOTAL". Biotinylation buffer (20 mM Tris [pH 8], 150mM NaCl, 5mM EDTA, 1% Triton X-100, and 0.2% BSA) and Streptavidin conjugated beads were added to the remaining supernatant, and this was incubated at 4°C for one hour. Samples were again washed as described above and 2X SDS loading buffer was added following the washes. Samples were boiled for 15 minutes and run on a 10% SDS-PAGE gel. Gels were dried and exposed on a phosphoscreen for two to four days, then visualized using a Typhoon Imaging System (GE Healthcare). Bands were quantified using band densitometry using the ImageQuant software (GE Healthcare).

#### 2.1.7 Time course immunoprecipitation

Two µg of wt or mutant S was transfected into Vero or A549 cells using the Lipofectamine 3000 system (Invitrogen; ratios described above). Eighteen to twenty-four hours post transfection, cells were starved in Cys-/Met- media (Gibco) for 45 minutes, and metabolically label for one hour using 50µCi of S35 Cys/Met. After the one-hour label, cells were washed once with PBS and normal DMEM + 10% FBS was added for indicated times. Cells were then lysed in 500µl of RIPA lysis buffer. Anti-SARS S polyclonal antibodies were used to immunoprecipitate the CoV-2 S protein as previously described and the protein was analyzed on a 10% SDS-PAGE gel. Gels were dried and exposed on a phosphoscreen for 2-4 days and visualized using a Typhoon Imaging System (GE Healthcare). Bands were quantified using band densitometry using the ImageQuant software (GE Healthcare).

#### 2.1.8 Immunofluorescence

Sub-confluent cells on coverslips in 6 well plates were transfected with 2µg of DNA using the Lipofectamine 3000 transfection system (Invitrogen). Eighteen to twenty-four hours post transfection cells were fixed with 4% PFA for 15 minutes at room temperature. Cells were permeabilized in a solution of 1% Triton X-100 in

PBS+0.02% Sodium Azide (PBSN) for 15 minutes at 4°C. After permeabilization, coverslips were moved to a humidity chamber and blocked with 1% normal goat serum (NGS) in PBSN for 1 hour at 4°C. Cells were labeled with anti-SARS S antibody (1:2000 dilution) in blocking buffer overnight at 4°C or for three to five hours at room temperature. Samples were washed with PBSN+0.01% Tween-20 seven times and incubated for 1 hour at 4°C with goat anti-rabbit FITC (1:2000 dilution). Samples were again washed with PBSN+0.01% Tween seven times and mounted onto slides using Vectashield mounting media (Vector Laboratories). Slides were imaged on an Axiovert 200M (Zeiss) at 63x magnification using Metamorph to collect Z-stacks and processed using Nikon NIS Elements.

#### 2.1.9 Statistical analysis

Statistical analysis was performed using Prism 7 for Windows (GraphPad). A p value of <0.05 was considered statistically significant. Multiple comparison tests were generated using one-way or two-way analysis of variance (ANOVA) with Dunnett's multiple comparison test. \*: p<0.05, \*\*: p<0.01, \*\*\*: p<0.0005, \*\*\*\*: p<0.0001

### HeV F Transmembrane Project

#### 2.1.10 Cell lines and culture

Vero cells and BSR cell lines were maintained in Dulbecco's modified Eagle's medium (DMEM; Invitrogen) supplemented with 10% fetal bovine serum (FBS; Sigma) and 1% penicillin and streptomycin. For the BSR cell line, 0.5mg/ml G-418 sulfate (Invitrogen) was added to the medium every third passage to select for T7 polymerase expressing cells.

### 2.1.11 Plasmids and antibodies

Plasmids containing Hendra F or G provided by Dr. Lin-Fa Wang (Australian Animal Health Laboratory) were subcloned into pCAGGS either as described (Pager, Worth, Dutch (2004)), or using primers for PCR subcloning. pCAGGS plasmids were transiently transfected into Vero cells to express Hendra F or G. All Hendra F mutants were made in pGEM using the QuickChange site-directed mutagenesis kit (Stratagene) and subcloned into the eukaryotic expression vector pCAGGS. Polyclonal antibodies (Genemed Custom Peptide Antibody Service, San Francisco, CA) were generated to residues 516-529 of Hendra F.

### 2.1.12 Syncytium assay

Vero cells (70-90% confluent) in 6-well plates were transiently transfected with pCAGGS-Hendra F in combination with the attachment protein, pCAGGS-Hendra G. Transfections were performed at a ratio of 1:3 using Lipofectamine 3000 system (Invitrogen) according to the manufacturer's protocol. 24 h post transfection, syncytia formation was examined, and images were taken using a Nikon digital camera mounted atop a Nikon Ti2 microscope with a 20x objective.

### 2.1.13 Luciferase reporter gene assay

Vero cells (70-90% confluent) in 12-well plates were transiently transfected with 0.15ug of pCAGGS-Hendra F or one of the HeV F mutants, 0.45ug of pCAGGS-Hendra G, and 0.4ug of a T7 promoted Luciferase plasmid. Transfections were performed using Lipofectamine and Plus reagent (Invitrogen) according to the manufacturer's protocol. At 24 h post transfection, BSR cells were lifted with trypsin, resuspended in DMEM supplemented with 10% FBS were overlain on to Vero cells that were washed once with PBS. These were incubated for 4 h at 37C. Then, cells were lysed with reporter lysis buffer (Promega) and analyzed for Luciferase activity using the luciferase assay system (Promega) per

manufacturer's instructions. A SpectraMax iD3 plate reader (Molecular Devices; Sunnyvale, CA) was used to read the luminescence. Results were normalized to cells expressing WT Hendra F and G, after subtracting the background (HeV G only).

#### 2.1.14 Surface biotinylation

Vero cells were plated in 60mm dishes and transiently transfected using Lipofectamine 3000 reagent per the manufacturer's protocol with 2ug of WT pCAGGS-HeV F or one of the TMD mutants. At 24 h post-transfection, the cells were washed with PBS and starved for 45 min in DMEM deficient in cysteine and methionine (Cys-/Met- DMEM). The cells were radiolabeled for 3 h with Cys-/Met-DMEM containing Tran-35S. The cells were then washed twice with 1ml ice cold PBS (pH 8.8) and biotinylated for 35 min at 4°C with rocking using 1ml of 1mg/ml EZ-Link-Sulfo-NSH-Biotin (Pierce) in PBS (pH 8.8). This was followed by an incubation at room temperature for 15 min. Cells were washed twice with ice cold PBS (pH 8.8) and treated with 500 ul RIPA lysis buffer. The cell lysates were centrifuged at 136,500 X g for 15 min at 4°C. The supernatant was transferred to 1.5-ml tubes and incubated with 4µl of Hendra F antibody for 3 h at 4°C with rocking. Proteins were immunoprecipitated by incubating each sample with 30µl protein A-Sepharose beads (GE Healthcare) for 30 min at 4°C with rocking. The beads were washed twice with RIPA buffer plus 0.30 M NaCl, twice with RIPA buffer plus 0.15 M NaCl, and once with SDS wash II (150 mM NaCl, 50 mM Tris-HCl, pH 7.4, 2.5 mM EDTA). Following the washes, 60 µl of 10% SDS was added and the samples were boiled for 10 min, then transferred to a new tube, and repeated with 40 µl of 10% SDS for a total of 100 µl. Ten microliters of each sample was separated and resuspended in 2 X SDS loading buffer with 400 µl biotinylation dilution buffer (20 mM Tris [pH 8.0], 150 mM NaCl, 5 mM EDTA, 1% Triton X-100, 0.2% bovine serum albumin (US Biological Life Sciences)) and 30 µl streptavidin beads for 1 h at 4°C with rocking. The washes described previously were repeated and the samples were resuspended in 2 X loading buffer containing DTT. After the samples were boiled, analysis of HeV was conducted using 15%

SDS-PAGE and visualized using the Typhoon imaging system (GE Healthcare). Band densitometry using ImageQuant version 5.2 was performed for each experiment to quantitate the relative percent expression of F compared to WT HeV F. The quantification is the sum of F0 and F1 for each sample.

#### 2.1.15 Immunoprecipitation

Subconfluent Vero cells in six-well plates were transiently transfected using Lipofectamine Plus (Invitrogen) as previously described with pCAGGS-HeV F and one of the TMD mutants. At 24 h posttransfection, the cells were washed with PBS, starved for 45 min at 37°C in Cys-/Met- DMEM, and metabolically labeled for one h with Trans[<sup>35</sup>S] metabolic label (100 µCi/ml; MP Biomedicals). At appropriate time points, the cells were washed three times with PBS and lysed with RIPA buffer. Immunoprecipitation and imaging were performed as described for surface biotinylation.

#### 2.1.16 Time course immunoprecipitation

At 24 hr posttransfection, cells were washed twice with PBS and starved with Cys-/Met- DMEM for 45 min at 37°C. Cells were then metabolically labeled with Cys-/Met- DMEM containing Trans[<sup>35</sup>S] (100 µCi/ml; MP Biomedicals) for 2 h. Following the label, cells were washed twice with PBS, then chased with DMEM (10% FBS, 1% penicillin-streptomycin) for 1, 2, 4, 8, and 24 h. At the appropriate timepoints, chase media was aspirated and cells were washed three times with PBS. The cells were lysed with RIPA buffer and frozen at -20°C. The samples for the 0 h timepoint were immediately lysed with 500 µl of RIPA lysis buffer and frozen after the label. Cell lysate was immunoprecipitated and protein was visualized as described for surface biotinylation.

## RSV Cleavage and P27 Project

### 2.1.17 Cell lines, culture, and viruses

Vero cells (ATCC) and BSR T7/5 cells (provided by Karl-Klaus Conzelmann, Pettenkofer Institut), were maintained in Dulbecco's modified Eagle's medium (DMEM, GE Healthcare), with 10% fetal bovine serum (FBS;Sigma) and 1% penicillin/streptomycin. Every third passage, 0.5mg/ml of G-418 (Invitrogen) was added to the culture media of BSR T7/5 cells to select for the expression of the T7 polymerase. HEp-2 cells (ATCC) were grown in Opti-MEM (Gibco) supplemented with 2% FBS. A549 cells (ATCC) were cultured in F12 Kaighns Modification media (GE Healthcare) with 10% FBS and 1% penicillin/streptomycin. All cells were maintained at 37°C and 5% CO<sub>2</sub>. Recombinant respiratory syncytial virus A2 expressing green fluorescent protein (GFP, rgRSV-A2), was propagated in HEp-2 cells.

### 2.1.18 Antibodies

The mouse anti-human monoclonal antibody, mAb RSV7.10 was kindly provided by Dr. Gale Smith (Novavax, Gaithersburg, MD). The mouse anti-human monoclonal antibody, synagis, was a kind gift from MedImmune/Astrazeneca. RSV F lab adapted A2 and B9320 strains were kind gifts from MedImmune/Astrazeneca in the mammalian expression vector pVAX. All RSV F constructs were created in pVAX using the QuikChange site-directed mutagenesis kit (Stratagene) with primers purchased from Eurofins. The RSV F A2 and B9320 Randomized P27 mutants also use the pVAX expression vector, but were purchased from GenScript. Each mutant construct was fully sequenced through ACGT DNA sequencing services.

### 2.1.19 Syncytium assay and counts

Vero cells in 6 well plates were transiently transfected with 2µg of either wild-type (WT) or mutant RSV F protein plasmid with Lipofectamine 3000 (Invitrogen) at a



ratio of 1:2:2 DNA: P3000: Lipofectamine 3000. Syncytia formation was imaged at 24 and 48 hours post transfection on a Nikon Ti2 at 20X magnification. Nuclei were counted by defining the total syncytia area and dividing that by the area of the field. In some cases, nuclei were scored and counted as either nuclei in syncytia and total nuclei. The fusion index was expressed as  $1 - (\text{total nuclei} - \text{nuclei in syncytia} + \text{number of syncytia}) / \text{total nuclei}$ .

#### 2.1.20 Surface biotinylation

Two  $\mu\text{g}$  of WT or mutant F protein was transfected into Vero cells using the Lipofectamine 3000 system (Invitrogen; ratios described above). Twenty-four hours post transfection, cells were starved in Cys-/Met- media (Gibco) for 45 minutes, and metabolically labelled for three hours using  $50\mu\text{Ci}$  of  $^{35}\text{S}$  (PerkinElmer) incorporated into Cys and Met ( $^{35}\text{S}$  Cys/Met). After the label, cells were washed once with PBS (pH 8) and incubated with 1 mg/ml of EZ-link Sulfo-NHS-biotin (Thermo Fisher) in PBS (pH 8) at  $4^\circ\text{C}$  for 35 minutes, and again at room temperature for 15 minutes. After incubation, the cells were lysed in  $500\mu\text{l}$  of RIPA buffer (100 mM Tris-HCl [pH 7.4], 0.1% SDS, 1% Triton X-100, 1% deoxycholic acid) containing 150 mM NaCl, protease inhibitors (1 U aprotinin, 1mM PMSF, [both from Sigma-Aldrich]), 5 mM iodoacetamide, and cComplete EDTA-free Protease Inhibitor Cocktail Tablets (all from Sigma-Aldrich), and frozen overnight. Cell lysates were centrifuged at 55,000 rpm for 10 minutes, and the supernatant was incubated with Palivizumab at  $4^\circ\text{C}$  for three hours. Following incubation,  $30\mu\text{l}$  Protein A conjugated to Sepharose beads (Cytiva) were added to the samples and incubated at  $4^\circ\text{C}$  for an additional 30 minutes. Post-incubation, samples were washed twice with RIPA Buffer+0.3M NaCl, RIPA Buffer+0.15M NaCl, and once with SDS-Wash II buffer (50mM Tris-HCl [pH 7.4], 150mM NaCl, and 2.5mM EDTA). After buffer aspiration and addition of 10% SDS, samples were boiled for 10 minutes. The supernatant was removed to a separate tube.  $15\mu\text{l}$  of supernatant was removed and added to an equal portion of 2X SDS loading buffer and labeled

“TOTAL”. Biotinylation buffer (20 mM Tris [pH 8], 150mM NaCl, 5mM EDTA, 1% Triton X-100, and 0.2% BSA) and Streptavidin conjugated beads were added to the remaining supernatant, and incubated at 4°C for one hour. Samples were again washed as described above and 2X SDS loading buffer was added following the washes. Samples were boiled for 15 minutes and proteins were separated on a 10% sodium dodecyl sulphate-polyacrylamide gel electrophoresis (SDS-PAGE) gel. Gels were dried and exposed on a phosphoscreen for 2-4 days, then visualized using a Typhoon Imaging System (GE Healthcare). Bands were quantified using band densitometry using the ImageQuant software (GE Healthcare).

#### 2.1.21 Radiolabel immunoprecipitation

2µg of WT or mutant F was transfected into Vero or A549 cells using the Lipofectamine 3000 system (Invitrogen; ratios described above). Twenty-four hours post transfection, cells were starved in Cys-/Met- media (Gibco) for 45 minutes, and metabolically labeled for one hour using 50µCi of <sup>35</sup>S Cys/Met. After the one-hour label, cells were washed once with PBS, then lysed in 500µl of RIPA lysis buffer and frozen overnight. Palivizumab was used to immunoprecipitate the RSV F protein as described above and the protein was analyzed on a 10% SDS-PAGE gel. Gels were dried and exposed on a phosphoscreen for 2-4 days and visualized using a Typhoon Imaging System (GE Healthcare). Bands were quantified using band densitometry using the ImageQuant software (GE Healthcare).

#### 2.1.22 Time course immunoprecipitation

2µg of WT or mutant F was transfected into Vero or A549 cells using the Lipofectamine 3000 system (Invitrogen; ratios described above), or infected with rgRSV-A2 at MOI 0.3. Twenty-four hours post transfection or infection, cells were starved in Cys-/Met- media (Gibco) for 45 minutes, and metabolically labeled for

15 minutes using 50 $\mu$ Ci of  $^{35}$ S Cys/Met. After the label, cells were washed once with PBS and DMEM + 10% FBS was added for indicated times. The DMEM + 10% FBS was aspirated, then cells were washed once with PBS followed by lysis with 500 $\mu$ l of RIPA lysis buffer and frozen overnight. Palivizumab was used to immunoprecipitate the RSV F protein as described above, and the protein was analyzed on a 10% SDS-PAGE gel. Gels were dried and exposed on a phosphoscreen for 2-4 days and visualized using a Typhoon Imaging System (GE Healthcare). Bands were quantified using band densitometry using the ImageQuant software (GE Healthcare).

### 2.1.23 Immunofluorescence

Vero cells were split to have 4.9x10<sup>5</sup> on the day of infection, in 6-well plates with 12mm #1 coverslips (Fisher, NC1418755). Cells were infected with WT A2 RSV (ATCC VR-1540) at a MOI of 0.1. 24H post infection live cells were stained with wheat germ agglutinin 488 (Life Technologies, W11261) by diluting to 5 $\mu$ g/mL in HBSS. Samples were then fixed with 4% PFA at 4°C for 15 minutes, and washed with PBSN (0.02% NaN<sub>3</sub>), before being moved to a humidified chamber. Coverslips were blocked in PBSN with 1% natal goat serum (block buffer) for 1 hour, also at 4°C. Primary anti-pep27 antibody was adding at 1:1000 in block buffer, for 1 hour at room temperature. Samples were washed 7 times with PBSN + 0.05% tween prior to secondary goat anti-human 647 (prepared in block buffer), then incubated 1 hour at 4°C. Finally, PBSN + 0.05% tween washes were repeated, and coverslips were mounted to slides using 10 $\mu$ L of Everbrite hard-set mounting media (Biotium, 23002), and left covered overnight to solidify. Slides were imaged on the Axiovert 200M 63x, or 100x, oil objectives.

#### 2.1.24 Flow cytometry

A549 cells were infected with rgRSV-A2 at a multiplicity of infection (MOI) of 1.0 in OptiMEM (Fisher Scientific; CAS 31-985-088). At 24hpi, the cells were blocked with 5% Bovine Serum Albumin (BSA) (Cytiva; CAS: SH30574.02) in 1X PBS (pH 7.2) for 15 minutes at 4°C and lifted with 10mM EDTA (VWR; CAS: 60-00-4). The cell population was split in half and spun at 1,150 x g for 2 minutes. Each half of the cell population was rocked for 1 hour at 4°C with either human anti-Pep27 (1:250) or Palivizumab (1:1000) primary antibodies resuspended in 1% BSA in 1X PBS. Samples were subjected to two washes by centrifugation at 1,150 x g for 2 minutes and resuspension in 1X PBS, then resuspended in Alexa647 AffiniPure goat anti-human IgG (1:1000) (Jackson ImmunoResearch Laboratories; CAS: 109-605-003). After 1 hour of rocking at 4°C, the cells were washed twice as described, then resuspended in 1% Paraformaldehyde (VWR; CAS: 30525-89-4) in 1X PBS. After rocking at 4°C for 30 minutes, the samples were loaded onto Guava easyCyte HT benchtop flow cytometer (Millipore; Burlington, MA, USA) and ran until 7,000 events were acquired of cells gated by forward and side scatter parameters. A secondary gate was used to exclude debris fluorescence seen below the background control signal. The mean fluorescence intensity (MFI) was calculated using the Guava® InCyte software to quantify the mean 647 signal intensity of the debris-excluded cell events.

#### 2.1.25 Statistical analysis

Statistical analysis was performed using Prism 7 for Windows (GraphPad). A p value of <0.05 was considered statistically significant. Multiple comparison tests were generated using one-way or two-way analysis of variance (ANOVA) with Dunnett's multiple comparison test. \*: p<0.05, \*\*: p<0.01, \*\*\*: p<0.0005, \*\*\*\*: p<0.0001.

## CHAPTER 3. EFFECT OF CLINICAL ISOLATE OR CLEAVAGE SITE MUTATIONS IN THE SARS-COV-2 SPIKE PROTEIN ON PROTEIN STABILITY, CLEAVAGE, AND CELL-CELL FUSION

**\*Portions of this chapter were adapted and reprinted with permissions from the Journal of Biological Chemistry:** Barrett, C. T., Neal, H. E., Edmonds, K., Moncman, C. L., Thompson, R., Branttie, J. M., Boggs, K. B., Wu, C. Y., Leung, D. W., & Dutch, R. E. (2021). Effect of clinical isolate or cleavage site mutations in the SARS-CoV-2 spike protein on protein stability, cleavage, and cell-cell fusion. *The Journal of biological chemistry*, 297(1), 100902.

\*\*This work was completed in collaboration the help of several individuals, specifically Dr. Chelsea Barrett who contributed intellectually to this work. Myself, Dr. Rachel Thompson, and Dr. Cheng-Yu Wu generated all of the SARS-CoV-2 mutants used. Chelsea, Kearstin Edmonds, and I all performed the pulse chase and surface biotinylation experiments as well as the luciferase reporter gene assays. Chelsea and I performed all of the syncytia assays as well as compete the respective figure generation. All fluorescent images were taken and processed by Dr. Carole Moncman. This work was written by Chelsea, and myself as needed, as part of the manuscript listed above.

### Introduction

Severe acute respiratory syndrome coronavirus 2 (SARS-CoV-2) is the causative viral agent of the ongoing coronavirus disease of 2019 (COVID-19) global pandemic. As of February 14th, 2023, there have been over 6.8 million deaths worldwide due to SARS-CoV-2 infection [34]. Due to the widespread global impact of this pandemic, a concerted effort has been made to rapidly develop a vaccine or antiviral treatment.

The SARS-CoV-2 spike (S) protein is the major transmembrane glycoprotein studding the surface of the viral particle, and is exclusively responsible for viral attachment and cell entry, thus making it the major target of current vaccine strategies and antiviral therapeutics [113]. The S protein consists of two distinct subunits: the S1 subunit, which binds to the known host receptor, angiotensin converting enzyme 2 (ACE2) [114–122] and the S2 subunit that promotes the viral-to-host cell membrane fusion event needed for viral infection [39, 113, 118, 123–128]. Most known coronavirus (CoV) S proteins undergo two post-translational proteolytic cleavage events, one at the border of the S1 and S2 subunits, and one downstream within the S2 subunit (termed S2') [36, 38, 39, 113, 118, 123–125, 129].

Similar to several other CoVs, SARS-CoV-2 likely utilizes bats as a reservoir species, specifically *Rhinolophus affinis* or horseshoe bats [32, 121, 130–132]. SARS-CoV-2 has 96% sequence identity to a CoV found in this bat population, RaTG13, with limited differences between them [130]. One difference is the polybasic, PRRA, insertion at the S1/S2 border which gives this site the canonical sequence requirements for cleavage by the cellular proprotein convertase furin [40, 133–135]. This change may be a key factor in the zoonotic transmission of SARS-CoV-2. The presence of a furin consensus sequence at the cleavage site has been observed in other human infecting CoVs [40, 136–138], as well as in highly pathogenic forms of influenza [139, 140] and previous studies have demonstrated its functional significance. For SARS-CoV-2, the insertion is suggested to allow for expanded cellular tropism and infectivity [40, 125, 141, 142]. For most CoVs, cleavage at a downstream S2' site may be carried out by a number of cellular proteases, including serine proteases like transmembrane serine protease 2 (TMPRSS2), or endopeptidases, including members of the cathepsin family [36, 125, 127, 129, 143].

Following receptor binding by the S1 subunit and priming by proteolytic cleavage, the S2 subunit of S promotes the critical membrane fusion step of viral entry by undergoing dynamic conformational changes to promote merging of the

viral and host cell membranes [115, 142, 144]. For entry of SARS-CoV-2, cleavage at the S1/S2 border (by furin or a similar protease), is critical for TMPRSS2 cleavage and entry at the plasma membrane. However, when S1/S2 border cleavage is blocked, viral entry can be mediated through endosomal compartments with proteolytic cleavage carried out by a member of the cathepsin family, similar to the entry pathway of SARS-CoV [115, 142, 144–146]. In addition to promoting virus-cell fusion during viral particle entry, S can also promote cell-cell fusion, a pathogenic effect observed in the lungs of COVID-19 patients where neighboring cells fuse together to form large multi-nucleated cells, termed syncytia [147–152]. While the role of cellular proteases and S cleavage in viral entry is being extensively investigated, insight into the cleavage requirements for cell-cell fusion in SARS-CoV-2 remains more limited. Recent studies have suggested that S cleavage at the S1/S2 border is critical for cell-cell fusion, and TMPRSS2, while not required, appears to enhance this cell-cell fusion [115, 144, 147, 153, 154]. However, relatively little is known about the timing and efficiency of these cleavage events, and how mutations in S may affect the process.

Though CoVs mutate at a slower rate than most RNA viruses due to the presence of viral proofreading machinery, a meta-analysis of genomes of circulating SARS-CoV-2 found several mutations within S circulating in significant percentages of the analyzed populations [155, 156]. The most common mutation, now found in most of the global population, is an aspartate to glycine mutation at residue 614 (D614G) in the S1 subunit. Additional mutations throughout the S1 and S2 subunits of S have been found in a smaller percentage of the viral population. Since S2 contains the fusion machinery, mutations in this region may have an impact on overall protein stability and fusion. Understanding the effects of mutations in this region will allow for a more comprehensive understanding of the overall S function.

We tested wild-type (wt) SARS-CoV-2 S and variants in different host cell lines to analyze the effects on stability, proteolytic processing, and cell-cell fusion. Here we demonstrate that furin cleavage of S at the S1/S2 border is required for

efficient cell-cell fusion, and that the presence of TMPRSS2 in target cells enhances S mediated cell-cell fusion, consistent with previous studies [115, 144, 153]. We also show that mutations of the cleavage sites at the S1/S2 border, S2' site, or a cathepsin L (cath L) cleavage site, conserved from SARS-CoV S, all reduce initial cleavage at the S1/S2 border during viral protein synthesis, suggesting that mutations downstream of the S1/S2 border likely alter the overall conformation of the protein. Additionally, we identify two S2 subunit residues, one in the internal fusion peptide and another in the cytoplasmic tail, that alter protein fusion function when mutated without changing overall protein expression and cleavage, providing more insight into regions of the protein important for the regulation of the fusion process. Finally, we demonstrate protein turnover and cleavage kinetics in a range of host cells, as well as in the presence of several exogenous proteases, providing a more comprehensive picture of the S protein.

## Results

### 3.1.1 Spike Mediated Cell-Cell Fusion

The S2 subunit of S mediates both viral-cell fusion and cell-cell fusion [147, 148, 150], with cell-cell fusion readily observed both in a laboratory setting and in the lungs of SARS-CoV-2 infected patients [147–152]. To better understand the requirements and contribution of cellular proteases to S2 mediated cell-cell fusion, we performed syncytia and reporter gene assays. For syncytia analysis, a small number of syncytia, were observed at 24 hpt in all samples (Fig. 3.1a). At 48 hpt, similar numbers of large syncytia were observed with S alone or S co-expressed with TMPRSS2 or cath L (Fig. 3.1b). However, co-expression of S with furin resulted in increased syncytia formation. The cells exhibited nearly complete fusion, suggesting that the presence of exogenous furin further increases S mediated cell-cell fusion (Fig. 3.1b, panel 3).



To characterize the role of cellular proteases in the hACE2 expressing target cells, S-expressing effector cells were overlaid with target cells containing hACE2 alone or hACE2 with TMPRSS2, furin, or cath L. The amount of plasmid transfected was kept constant by supplementing with a plasmid encoding an empty expression vector (EV). When Vero cells were used as the S-expressing effector cell and TMPRSS2 was present in the target cells, a significant increase in fusion was observed. This is consistent with the concept that TMPRSS2 plays a role in fusion after or during the hACE2 (receptor) binding step in the fusion cascade (Fig. 3.1c) [115, 126, 138, 144, 153], although the presence of TMPRSS2 in these target cells also appeared to process hACE2. In samples with cath L or furin in the target cells, fusion levels were similar to hACE2+EV (Fig. 3.1c). When A549 cells were used as the S-expressing effector cell, none of the conditions produced statistically significant differences from background levels (Fig. 3.1c), so Vero cells were used as the effector cells for the remainder of the experiments performed.

Having analyzed the function of proteases in the target cells, we were also interested in the role of proteases present in the S-expressing effector cells. To test this, EV, TMPRSS2, cath L, or furin were co-expressed with S and samples were overlaid with target cells expressing hACE2 (Fig. 3.1d). Similar to what we observed in syncytia assays, only co-expression of S and furin produced a statistically significant increase in fusion (Fig. 3.1d).

### 3.1.2 Importance of CoV-2 cleavage sites

Early protein sequence analysis of CoV-2 S protein demonstrated the presence of three potential cleavage sites [40]: a putative furin cleavage site at the S1/S2 border; a conserved site 10 residues downstream from the S1/S2 border, shown to be cleaved by cath L in SARS-CoV; and the S2' site which is potentially cleaved by TMPRSS2 [40]. To functionally understand the role of each cleavage site in S cell-cell fusion, a series of mutants were made. Alanine mutations of all the residues within each potential cleavage site (S1/S2 AAAAA, Cath L AAAA, S2'

AA), and single alanine mutations at the terminal arginine of the S1/S2 border and S2' site (S1/S2 PRRAA, S2' KA) were created. Finally, a mutant with residues (PRRA) upstream of the S1/S2 border deleted (del. PRRA), leaving a single R residue at this site, was made, creating an S1/S2 border similar to SARS-CoV S (Fig. 3.2a). Pulse-chase analysis (Fig. 3.2b) showed that all mutants exhibited similar protein degradation compared to wt S in Vero cells. However, in A549s several mutants demonstrated more rapid protein turnover than wt S at later chase time points. Surprisingly, mutations at all three sites led to either a complete loss or significant delay in the proteolytic processing of the S protein at the S1/S2 border, indicated by the lack of a band corresponding to the S2 subunit. This suggests that mutations at distal sites can strongly influence cleavage at S1/S2. After an eight-hour chase, no cleavage at the S1/S2 border was observed for the mutants del. PRRA and S1/S2 AAAAA, confirming that deletion or mutation of the furin consensus prevents cleavage at this site. For all other mutants, cleavage at the S1/S2 border reached 30-50% of wt levels in both Vero and A549 cells the eight-hour time point (Fig. 3.2c and 3.2d). Finally, surface biotinylation showed that both total and cell surface expression of all mutants were not significantly different from wt S levels (Fig. 3.2e, f, and g). Similar to the results discussed previously, a band corresponding to cleavage at the cath L site or the S2' site was not observed in any condition tested.

To assess the effects of the mutations on cell-cell fusion, syncytia formation assays in Vero cells were performed. While syncytia were readily observed in all samples containing wt S, none of the mutants exhibited syncytia formation at 24 or 48 hpt when expressed alone (Fig. 3.3, panel 2). Addition of TMPRSS2 did not recover syncytia formation in any mutant (Fig. 3.3, panel 3), and the addition of furin only recovered syncytia formation in the S1/S2 PRRAA mutant (Fig. 3.3, panel 4, syncytia denoted with black arrows). To analyze this result, cells were lysed following the 48-hour imaging and protein levels examined by western blot. Results showed that co-expression of furin with the S1/S2 PRRAA mutant restored cleavage at the S1/S2 border, while all other mutants did not show cleavage at this site (data not shown). This suggests that cleavage at the S1/S2 border is critical

for cell-cell fusion, and that the double R motif in the PRRAA mutant can be cleaved by over-expressed furin.

### 3.1.3 Effect of Circulating S Mutations on Protein Stability, Cleavage, and Fusion

An early examination revealed several mutations in the S protein gene in circulating viral variants [155, 156], including the D614G substitution now found in most of the global SARS-CoV-2 [156–163]. The D614G mutation lies in the S1 subunit of the protein, just downstream of the receptor binding domain, and is proposed to play a critical role in receptor binding by alteration of the positioning of the receptor binding domain. Other mutations in circulating variants were found throughout the S2 subunit [155, 156]. To assess the effect(s) of these mutations, we created the mutants D614G, A831V, D839Y/N/E, S943P, and P1263L (Fig. 3.4a). Pulse-chase analysis in Vero and A549 cells (Fig. 3.4b) demonstrated that all circulating mutants tested exhibited protein turnover (Fig. 3.4f) and protein cleavage (Fig. 3.4c) at similar rates as wt S in both cell lines. Surface biotinylation confirmed that all tested mutants displayed total protein and surface protein levels comparable to wt S, suggesting that none of the mutants caused major defects or enhancement of protein trafficking to the cell surface (Fig. 3.4d, e). Syncytia formation and evaluation of protein location by immunofluorescence were similar between all mutants and wt S (Fig. 3.5). Interestingly, cellular extensions containing the S protein were observed for the wt and each of the mutants (Fig. 5, white arrows) [164]. While most of the mutants displayed fusion levels similar to wt S, three mutants exhibited significant changes (Fig. 3.5). D839Y and D839N displayed reduced levels of cell-cell fusion compared to wt, while P1263L cell-cell fusion increased. These changes in fusion are unlikely to be due to significant differences in cell surface protein expression or cleavage levels, although it is worth noting that D839Y and D839N demonstrated a lower percent cleavage than other mutations tested, though this decrease was not statistically significant. This data may suggest that residues near the internal fusion peptide, where D839 is

located, and residues in the cytoplasmic tail, where P1263 is located, may play an important role in controlling the fusion cascade.

## Discussion

In this study, we present a detailed characterization of the cleavage patterns, protein stability, and cell-cell fusion function of the SARS-CoV-2 S protein, as well as analysis of mutations within the S2 subunit that may affect these important protein properties. Consistent with recently published work [40, 142, 154, 165–167], our analysis confirms that S is readily cleaved at the S1/S2 border in a variety of mammalian cell lines. While cleavage appears to be primarily carried about by the cellular protease furin, the sequence at this border does have the ability to be cleaved by other members of the pro-protein convertase family when furin is not present [154].

Additionally, we carefully assessed the role different proteases play in cell-cell fusion, finding that furin increases cell-cell fusion when present in the same cell as S, and TMPRSS2 increases cell-cell fusion when present in a target cell, consistent with previous studies [115, 144, 153]. Interestingly, when cell-cell fusion assays were performed using A549 cells as the effector cell (Fig. 3.1c), high background fusion levels were observed. High TMPRSS2 expression or exogenous treatment with trypsin has been shown to restore cell-cell fusion in low ACE2 receptor expression environments for SARS-CoV S [168, 169]. It is also worth noting that co-expressing TMPRSS2 and hACE2 in the target cells (BSR/T7) leads to a double banding pattern for hACE2, suggesting that TMPRSS2 may be cleaving hACE2 (Fig. S2c, [147]). Therefore, we cannot exclude the possibility that the increase in fusion observed when TMPRSS2 is present in these cells is due to an effect on hACE2.

The viral entry and cell-cell fusion pathways of SARS-CoV, MERS-CoV, and SARS-CoV-2 have several noteworthy commonalities, but do have marked differences. They all share the ability to facilitate entry through endosomal

pathways, with S proteolytic activation mediated by endosomal/lysosomal proteases [36, 115, 142, 144–146, 152, 170–173]. Additionally, they all can utilize cell surface (such as TMPRSS2) or extracellular proteases (trypsin) for S activation and subsequent viral entry [115, 144, 146, 154, 168, 173–178]. SARS-CoV-2 and MERS-CoV S differ from SARS-CoV S in that their S1/S2 border harbors a canonical furin cleavage motif [40, 134, 138], resulting in S pre-activation by furin during synthesis and cellular trafficking, prior to reaching the cell surface or being incorporated into viral particles [36, 115, 142, 144, 145, 177]. This pre-activation by furin likely enhances the ability of SARS-CoV-2 and MERS-CoV S to participate in cell-cell mediated fusion without over-expression of cell surface or extracellular proteases [115, 144, 153]. Addition of this cleavage sequence in SARS-CoV S allows SARS-S to facilitate cell-cell fusion without exogenous proteases [115, 179]. We show an increase in both syncytia formation and luciferase reporter gene assay fusion when cleavage at the S1/S2 border is enhanced by overexpression of furin (Fig. 3.1b and c), confirming that furin cleavage of SARS-CoV-2 S plays a critical role in cell-cell fusion. Interestingly, furin cleavage is not required for SARS-CoV-2 infection [115, 142, 144, 154], although removal of the site or inhibition of furin does appear to attenuate the virus [142, 145, 154] and reduce cellular tropism [153].

Two other potential cleavage sites have been identified in work with other CoVs. The S2' site is essential for both SARS and MERS infection [126, 138, 180–182] while a cath L activated site play a critical role for SARS-CoV S [125, 143, 183, 184]. Interestingly, mutations made at the S2' site of SARS-CoV-2 S significantly reduce S1/S2 border cleavage, both in our study and others (Fig. 3.2b-d, [153, 185]), even though the sites are distal from each other. A similar reduction in cleavage is observed when the conserved cathepsin site is mutated (Fig. 3.2 b-d). Our analysis of the published structures [116, 119, 186, 187] indicates that a full alanine mutation of this site may simply collapse the exposed S1/S2 loop, rendering it inaccessible. However, these mutants are still synthesized and trafficked to the surface despite not being cleaved (Fig. 3.2 e-g), thus this change in conformation is unlikely to have drastically misfolded the protein. These results

suggest that there may be a dynamic interaction between the S1/S2 border and S2' cleavage sites in SARS-CoV-2 S needed to facilitate viral entry and cell-cell fusion. This dynamic control could also be regulated by S receptor binding exposing cryptic protease sites, although studies analyzing this in SARS and MERS S conflict on this topic [36, 171, 176, 188, 189].

We also assessed the effect on protein stability, cleavage, and cell-cell fusion function of a series of mutations in other regions of S. The D614G mutation emerged during 2020, and is now found in most circulating variants globally [156]. D614G has been shown to increase S incorporation into viral particles [190], increase receptor binding [191, 192], and reduce S1 subunit shedding and particle infectivity [193]. Importantly, the D614G mutant shifts S to favor a “heads up” conformation of the receptor binding domain [192, 194, 195]. In our study, the D614G mutation did not impact the cell-cell fusion function (Fig. 3.5), expression, or stability of the protein (Fig. 3.4 c-f), consistent with one previous study [185]. Our fusion results however conflict with two previous studies that demonstrated D614G increases cell-cell fusion, measured by cell depletion in flow cytometry [191], and syncytia formation in 293T and Hela cells stably expressing hACE2 [196]. These discrepancies may be due to differences in experimental conditions or cell types utilized. We are, however, the first to date to utilize a luciferase reporter gene assay to quantitate cell-cell fusion of a D614G S mutant. Using this assay, we also show that mutations found at two other residues (discovered in small, non-dominant population subsets [155]) alter the cell-cell fusion activity of S (Fig. 3.5) without changing the overall protein expression or stability levels (Fig. 3.4d-f). Mutations at D839, a residue within the internal fusion peptide, to the polar amino acids, tyrosine or asparagine, significantly reduce fusion. Interestingly, a mutation at this residue that conserves the negative charge, D839E, has no effect on fusion activity. The negative charge at this residue may play a role in the regulation of S mediated fusion due to its location in the internal fusion peptide. Alternatively, this residue is in close proximity to C840, which may participate in a disulfide bond, so mutations at D839 may disrupt this disulfide bond, destabilizing the protein and changing fusion activity. Additionally, mutation of residue P1263 to

a leucine significantly increases S mediated cell-cell fusion, suggesting that residues in the cytoplasmic tail may play a role in the S-promoted cell-cell fusion process. Notably, a study that removed the entire S cytoplasmic tail still observed syncytia formation at levels similar to wt S [185], indicating that regulation by the cytoplasmic tail may be complex or that the role of the cytoplasmic tail in fusion is not regulation, but interaction with cellular host factors [197].

In this work, we also provide critical insight into the kinetics of protein cleavage and overall stability of CoV-2 S. S protein processing at the S1/S2 border occurs within two hours of synthesis and continues to increase over time, reaching 60-80% protein cleavage by eight hours of chase time, depending on the cell type. It is likely that an overexpression of furin increases the efficiency of S1/S2 border cleavage, and which may account for the increase in cell-cell fusion observed when furin is co-expressed with S (Fig. 3.1a-c, [144, 153]). This protein turnover is similar to turnover rates seen in PIV5 fusion protein, also activated by cellular furin [198], and slightly slower turnover than Hendra fusion protein, activated by cellular cathepsins [199, 200]. Over-expression of cellular proteases that may process S did not affect these protein turnover rates. Protein oligomers with differential proteolytic processing may also account for the small population of un-cleaved protein we observed at the cell surface in our experiments (Fig. 3.2e, Fig. 3.4d).

Through biochemical and cell biological analysis of the SARS-CoV-2 S protein, we have provided important observations about the stability, proteolytic processing, and requirements for cell-cell fusion of this highly sought-after therapeutic target. This information may be helpful in directing treatments that inhibit S protein fusion, or for discerning methods to stabilize CoV-2 S in therapeutic development. Additional studies are needed to understand the potential interplay between S cleavage sites and how that may contribute to S protein function, as well as to further investigate spike S2 subunit regions that are critical for protein function.

## Figures

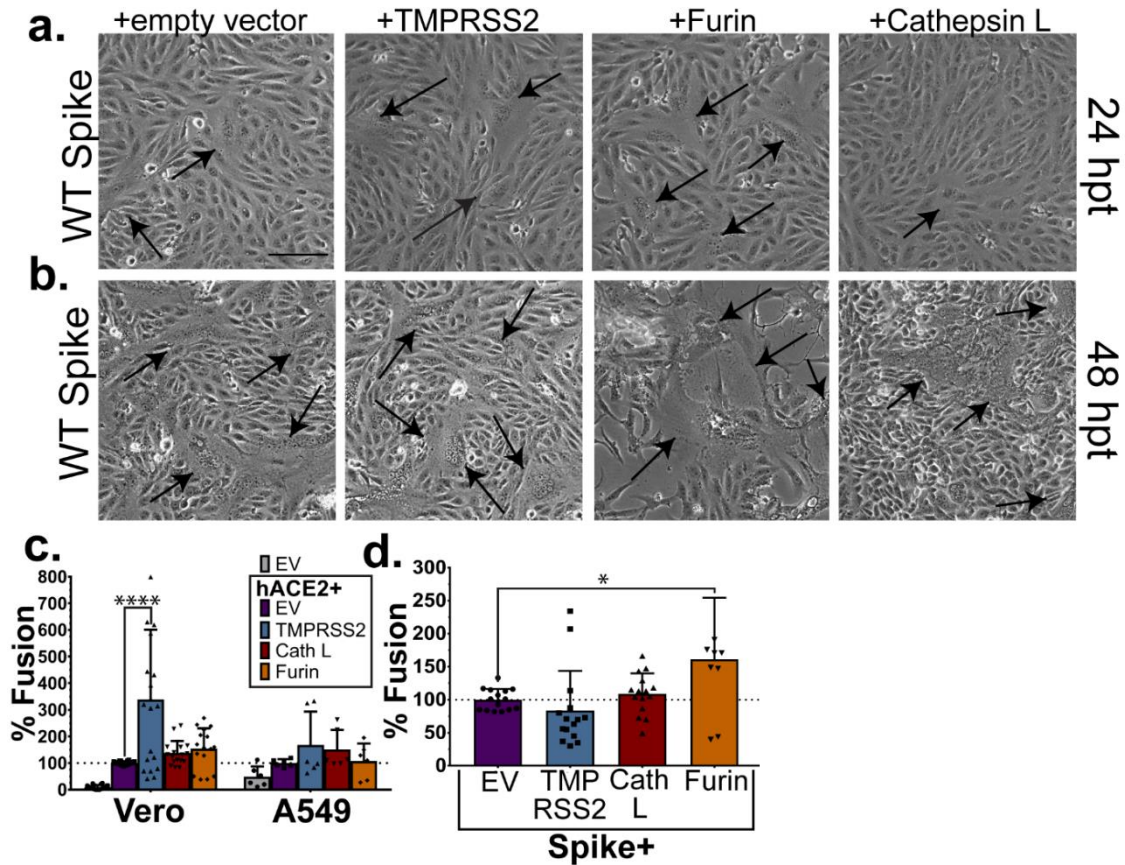


**Figure 3.1: CoV-2 spike alone mediates cell-cell fusion.** Vero cells expressing S and TMPRSS2, furin, or cathepsin L were imaged at 24 (a) and 48 (b) hpt for syncytia formation (black arrows). Magnification bar is 100 $\mu$ M. c) A luciferase reporter gene assay was performed with target cells (BSR/T7 cells expressing hACE2 and additional proteases) overlaid onto effector cells (Vero or A549 cells expressing S) for 9 hours. d) Luciferase reporter gene experiment was performed with additional proteases co-expressed with S in Vero cells and overlaid with target cells expressing hACE2. Results expressed as the percent fusion normalized to samples with S in the effector cells, and hACE2 only in the target cells (c-e are average  $\pm$  SD for 3 independent experiments, performed in duplicate). Significance was determined by two-way ANOVA. \*:  $p < 0.05$ , \*\*\*\*:  $p < 0.0001$  Chelsea Barrett, Kearstin Edmonds, and I completed the luciferase reporter gene assays. Chelsea Barrett and I performed all of the syncytia assays.



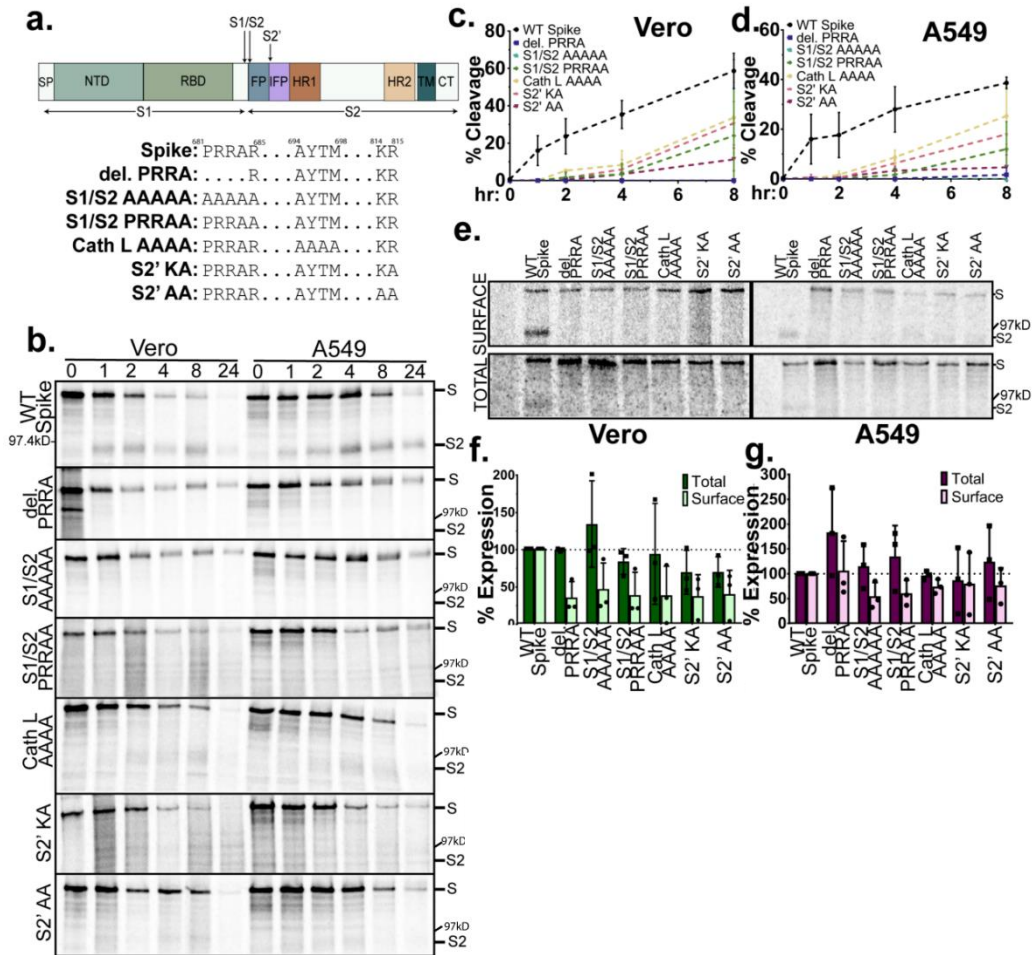


**Figure 3.2: Mutations at all three potential spike cleavage sites reduce cleavage at the S1/S2 subunit border.** a) Full or partial alanine substitution mutations were made at each of the three potential cleavage sites. b) Plasmids expressing wt S or mutants were transfected into Vero and A549 cells, cells were metabolically labeled for one hour, and chased for the times indicated. Percent cleavage was determined in (c) Vero cells and (d) A549 cells (average  $\pm$  SD for 3 independent experiments) e) Surface biotinylation was performed on cells expressing wt S and each mutant. Cells were radiolabeled for 6 hours. Protein expression in (f) Vero and (g) A549 cells, results are normalized to wt S, and error bars represent the standard deviation (average  $\pm$  SD for 3 independent experiments). Myself, Rachel, and Cheng-Yu generated all of the SARS-CoV-2 mutants used. Chelsea Barrett, Kearstin Edmonds, and I all performed the pulse chase and surface biotinylation experiments.

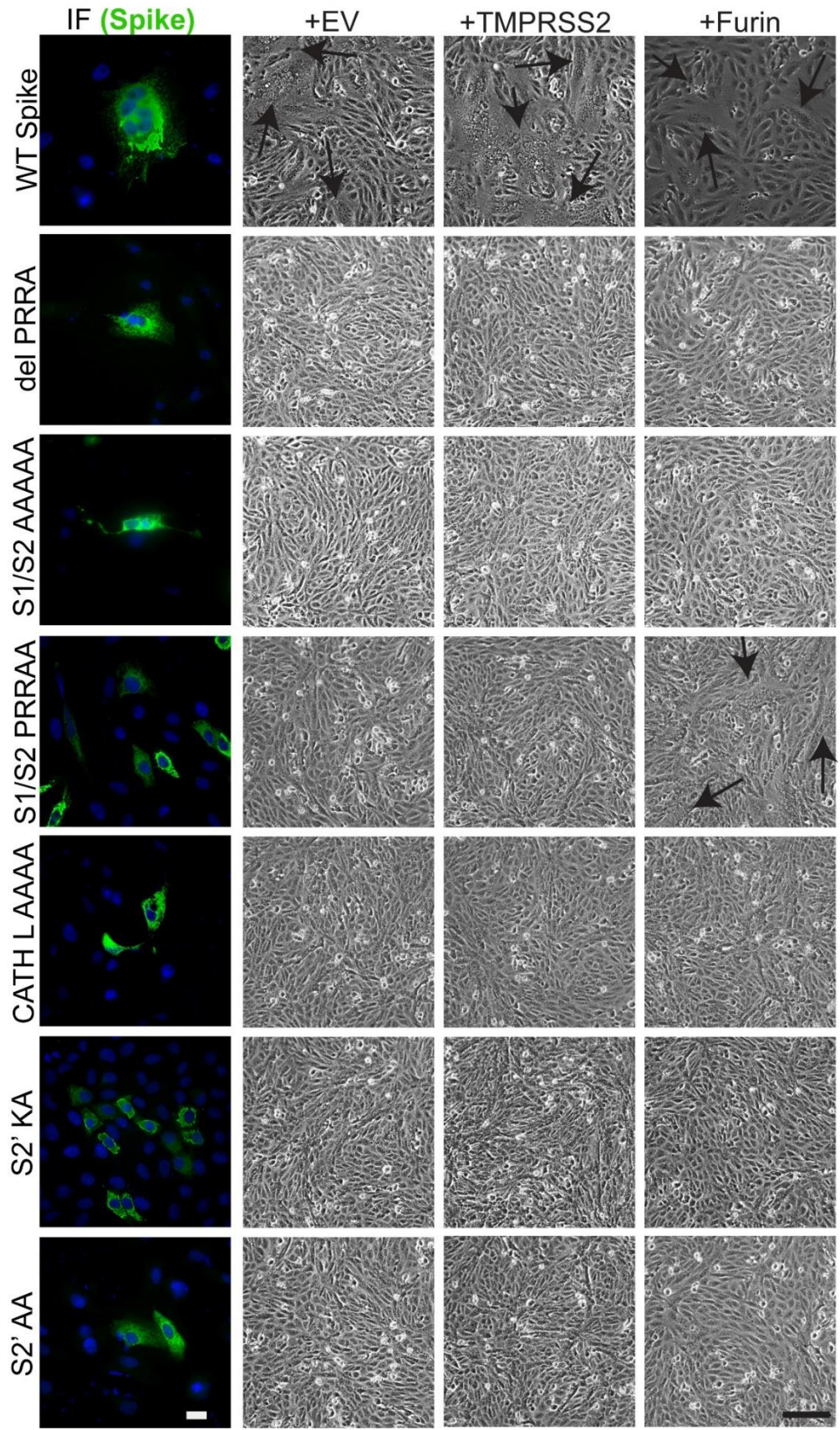




**Figure 3.3: Mutations made at any of the three potential cleavage sites abolish syncytia formation.** Vero cells were transfected with wt S or each of the cleavage mutants. The first panel shows immunofluorescence of wt S or S cleavage mutants (green, magnification bar is 20 $\mu$ m). The remaining panels show syncytia formation at 24 hours post transfection with S or mutants co-expressed with EV, TMPRSS2, or furin. Syncytia are indicated by the black arrows, magnification bar is 100 $\mu$ m. Chelsea Barrett and I performed all of the syncytia assays. All fluorescent images were taken and processed by Carole Moncman.

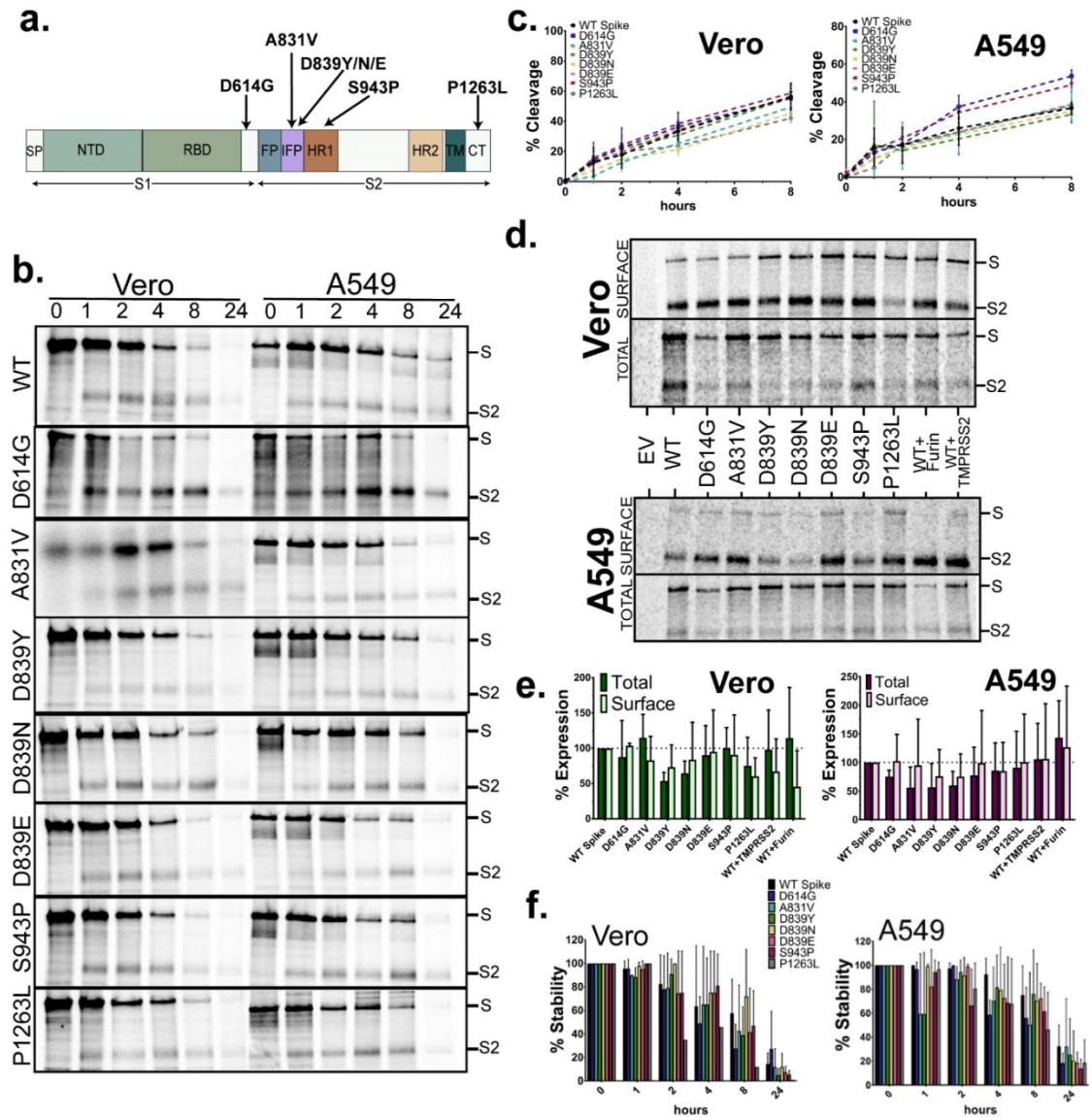


**Figure 3.4: Spike S2 subunit mutations found in circulating variants variably affect spike mediated cell-cell fusion.** a) Mutations in the S2 subunit of S identified in circulating SARS-CoV-2 variants, b) WT S or the mutants were transfected into Veros and A549 cells, metabolically labeled for one hour, and chased for the times indicated. Percent cleavage was determined in (c) Veros and A549 cells (average  $\pm$  SD for 3 independent experiments). d) Surface biotinylation on cells expressing wt S or each mutant. e) Total and surface protein expression normalized to wt S (average  $\pm$  SD for 3 independent experiments). f) Overall protein stability normalized to wt S (average  $\pm$  SD for 3 independent experiments). Significance was determined by two-way ANOVA, \*:  $p < 0.05$ , \*\*:  $p < 0.01$ . Myself, Rachel Thompson, and Cheng-Yu Wu generated all of the SARS-CoV-2 mutants used. Chelsea Barrett, Kearstin Edmonds, and I all performed the pulse chase and surface biotinylation experiments.

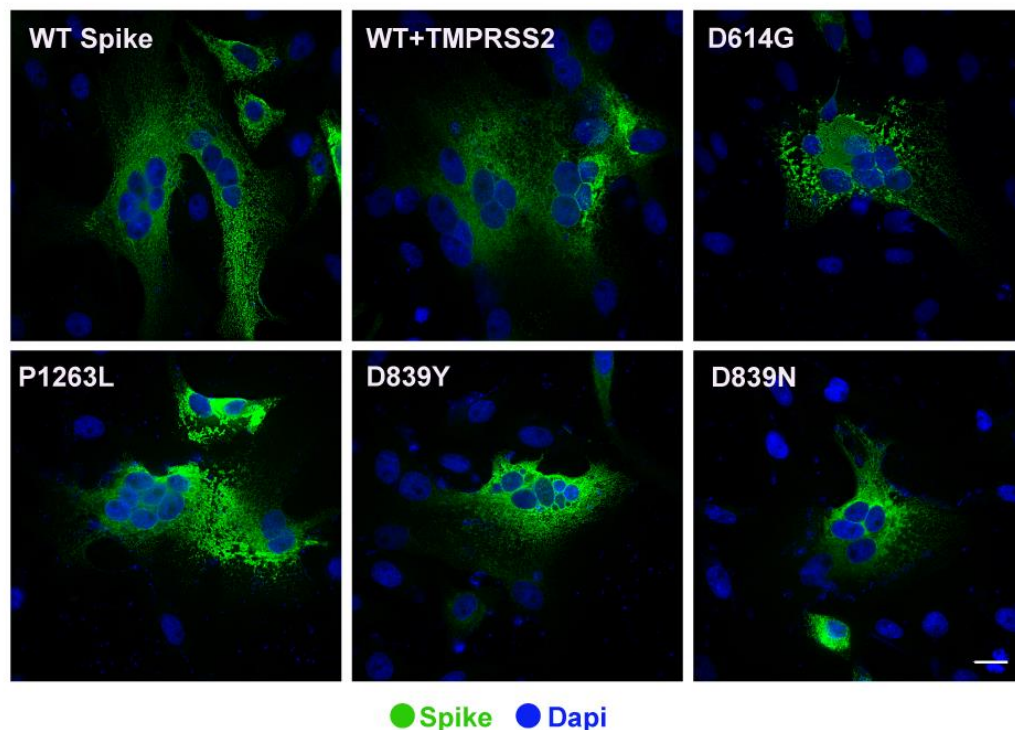


**Figure 3.5: Circulating mutations form large syncytia, similar to wt S.** Immunofluorescence of wt S or the circulating mutants (S stained in green) transiently expressed in Vero cells. White arrows indicated S positive cellular

extensions. The magnification bar is 20 $\mu$ M All fluorescent images were taken and processed by Carole Moncman.

## CHAPTER 4. ANALYSIS OF HENDRA VIRUS FUSION PROTEIN N-TERMINAL TRANSMEMBRANE RESIDUES

**\*Portions of this chapter were adapted and reprinted with permissions from Viruses:** Barrett CT, Neal HE, Edmonds K, Zamora JLR, Moncman CL, Popa A, Smith EC, Webb SR, Dutch RE. Analysis of Hendra Virus Fusion Protein N-Terminal Transmembrane Residues. *Viruses*. 2021 Nov 24;13(12):2353.

\*\*This work completed was completed in collaboration with Dr. Chelsea Barrett, Dr. Juana Reyes-Zamora, and Kearstin Edmonds. Chelsea, Juana, Kearstin, and I all completed independent replicates of syncytia assays and reporter gene assays (Fig. 4.4a and 4.4b). Chelsea, Kearstin, and I completed independent replicates of the surface biotinylation assay and pulse chase experiments (Fig. 4.1b/c/d and Fig. 4.3b/c/d). All other experiments, as well as figure generation was completed by me and Chelsea. This work was co-written as part of the manuscript listed above.

### Introduction:

Hendra virus (HeV) is a zoonotic, enveloped virus within the viral family *Paramyxoviridae*. HeV, similar to all enveloped viruses, uses surface glycoproteins to promote binding to a host cell and fusion with host cell membranes to facilitate viral entry [201–204]. In HeV, these proteins are termed the attachment protein (G), responsible for binding the host cell, and the fusion protein (F), responsible for merging the viral and host cell membranes. F is a trimeric transmembrane protein [205]. Following proteolytic cleavage, receptor binding, and receipt of a triggering signal, HeV F undergoes a large, dynamic conformational change enabling the viral and host cell membranes to merge [47, 202, 205]. In order to be cleaved by cellular cathepsins, HeV, and the closely related Nipah virus, F proteins undergo a unique trafficking pattern. They are initially synthesized, trafficked through the secretory pathway to the cellular surface, then are endocytosed to be

cleaved by cathepsin L in recycling endosomes before being trafficked back to the cell surface [49, 61, 206–208]. Throughout this trafficking, the F protein remains associated as a trimer [57, 62, 201, 202]. Interactions within the transmembrane (TM) regions of F trimers have been implicated in protein stability and fusion function [58, 60–62, 209]. Additionally, residues S490 and Y498, have been demonstrated to be involved in the endocytosis of F [61]. Previously, alanine scanning mutagenesis of the C-terminal end of the HeV F TM region has been performed [60]; however, this has not been completed for the N-terminal end of the TM region.

Here we performed double-alanine scanning mutagenesis of the first 20 amino acids of the TM region of HeV F and assessed the effect on protein stability, expression, proteolytic processing, and fusion. Mutants altering residues S490 and Y498 show defects in protein cleavage, surface expression and fusion, consistent with previous work showing these residues are important in protein endocytosis [61]. Additionally, a mutant altering S493 had lower protein surface expression, slightly lower cleavage, and significantly reduced fusion, again consistent with previous work [62]. Interestingly, we found that the alanine mutation of residues M491 and L492 significantly reduced fusion without altering protein expression, newly implicating these residues in the fusion process. Additionally, we demonstrate that alanine mutation of the remaining residues does not have an effect on protein expression, stability or fusion function. The work presented here, when considered with previously published work [58, 60–62, 208], provides a comprehensive analysis of the entire HeV F TM region and identifies the critical residues within it.

## Results

To assess the potential role of residues at the N-terminus of the HeV F protein TM region, double alanine scanning mutants were created (Fig. 4.1a). Surface biotinylation was then performed to determine the surface and total protein population of transiently transfected wild-type (WT) HeV F or mutant F (Fig. 4.1b).

WT HeV F and most TM mutants were detected after immunoprecipitation as two bands, corresponding to F<sub>0</sub> (un-cleaved F) and F<sub>1</sub> (cleaved F) (Fig. 4.1b). Using band densitometry, percent expression (Fig. 4.1c) and percent cleavage (Fig. 4.1d) were calculated for both surface and total protein populations and normalized to WT HeV F. Mutants IS, SM, and LY all showed reduced surface expression compared to WT F. SM also demonstrated lower total protein expression. Additionally, mutants IS, SM, and LY all had a significant reduction in protein cleavage in both surface and protein populations. Interestingly, the ML mutant had a slight, but significant reduction in cleavage in the surface protein population, while showing no cleavage differences in the total protein or overall protein expression. This suggests, consistent with previous studies, that mutant IS, SM, and LY have defects in the endocytosis process needed for proteolytic processing.

Pulse-chase analysis was utilized to examine WT F or mutant protein cleavage kinetics and protein stability (Fig. 4.2a). Most TM mutants displayed no change in protein cleavage compared to WT F; however, two showed lower cleavage at later chase time points (Fig. 4.2b). At four and eight hours of chase, the SM mutant demonstrated a significant reduction in cleavage compared to WT F ( $p < 0.01$  at four hours and  $p < 0.0001$  at eight hours). Additionally, the LY mutant exhibited a reduction in cleavage at eight hours of chase ( $p < 0.01$ ). Despite these two differences in cleavage, all TM mutants had similar protein turnover kinetics compared to WT F, with protein remaining stably expressed through 2 hours of chase. After four and eight hours of chase, only about 40-50% of protein remains, and only about 10-15% remains after twenty-four hours (Fig. 4.2b). This suggests that even mutations that alter F protein cleavage do not disrupt protein stability.

To understand how the mutations created effected the overall fusion function of HeV F syncytia formation analysis and a luciferase reporter gene fusion assay were performed. For the syncytia assay, WT HeV F or the TM mutants were transiently co-expressed with HeV G and imaged at 48 hours (Fig. 4.3a). The formation of large syncytia was observed in WT samples, as well as mutants SL, II, VL, SI, and LC. Very few syncytia were observed in samples IS and ML, and



no syncytia were found in samples with mutant SM or LY (Fig. 4.3a). To quantitate fusion, a luciferase reporter gene assay was employed by transiently co-expressing WT HeV F or each TM mutant with HeV G in Vero cells, and overlaying them with BSR/T7 cells. All samples were normalized to samples expressing WT HeV F and G. Similar to the syncytia results, samples SL, II, VL, SI, and LC demonstrated fusion levels similar to WT (Fig. 4.3b). Samples SM and LY did not exhibit any fusion about background levels ( $p < 0.0001$ ), and mutants IS and ML exhibited significantly reduced fusion levels (20% [ $p < 0.01$ ] and 50% [ $p < 0.05$ ], respectively) compared to WT. The reduction in cleavage observed for mutants IS, SM, and LY is consistent with the significantly reduced protein expression and cleavage observed for these mutations (Fig. 4.1c and 4.1d). However, the slight reduction in cleavage observed for the surface population of ML is not enough to account for the 50% reduction in fusion since previous work has shown that the amount of cleaved protein at the cell surface directly correlates to the amount of fusion [203].

#### Discussion:

The role of several residues within the N-terminus of the TM of HeV F has previously been explored. Residues L488 (mutant SL), I495 (mutant II), and I502 (mutant SI) were determined to be part of a Leucine-Isoleucine zipper (LI Zipper) motif that ran through the TM region [58]. Single mutations of each of these residues resulted in only minor protein expression, cleavage, and fusion activity change [58] consistent with our study. However, mutation of the entire LI zipper resulted in a significantly destabilized pre-fusion conformation protein, thus abolishing the fusion activity [58]. Interestingly, including the neighboring residues (S, I, S) with mutations to the LI Zipper had no appreciable effect on protein expression, stability, or fusion function suggesting that these serine residues and isoleucine residue are dispensable for HeV F function (Fig. 4.1, 4.2, 4.3). Residues S490 (mutant IS) and Y498 (mutant LY) were demonstrated to play a role in protein endocytosis and subsequent recycling, with the hydroxyl group and aromatic nature being critical in each residue, respectively [61]. Efficient endocytosis and

recycling of the HeV F protein was also shown to be critical for proper virus-like particle assembly, as endosomes are the likely location of HeV F association with HeV matrix protein during particle assembly [208]. Remarkably, inclusion of the neighboring residues methionine and leucine seemed to allow for slightly more protein cleavage and slightly enhanced stability compared to previous work on the single point mutations [61]. This suggest that mutation of the two neighboring residues may have compensatory effect, potentially restoring some of the protein endocytic recycling. Residue S493 (mutant SM) has been demonstrated to have slightly reduced cell surface expression and fusion levels reduced by about 80% in a previous study [62]. Interestingly, when we including the neighboring methionine residue in the mutation, cell surface expression was further reduced and fusion activity was abolished, indicating a compounding effect when both the S and M are mutated. This may indicate both of these residues play critical roles in fusion, protein conformation, and stability.

Residues M492 and L493 (mutant ML) had not previously been explored in the context of HeV F. Residue M492 is predicted to lie on the contact interface between the protomers in the trimeric protein [61], suggesting it may have a role in TM-TM associations of this protein. While this mutant is still able to form protein oligomers (Fig. 4.2d), it does exhibit a significant reduction in protein fusion (Fig. 4.3b). The mutation of the large methionine and  $\beta$ -branched leucine residues to alanines may cause the protein trimer to pack together too tightly disrupting the TM-TM dissociation needed to carry out fusion [209]. Alternatively, this mutation could increase the flexibility of the protein in this region, loosening TM-TM associations, causing the TM regions to dissociate too much during the fusion process, thus destabilizing protomer association during intermediate steps of fusion or these mutations disrupt interactions with the fusion peptides that are needed for fusion pore expansion.

In addition to mutation of residues M492 and L493, this work also represents the first-time residues V499/L500 and L505/C506 were investigated. When the C-terminal end of the HeV F TM region was studied, mutations of  $\beta$ -

branched residues appeared to play a critical role. Interestingly, both mutant VL and LC, which lie in the middle of the predicted HeV F TM and contain  $\beta$ -branched residues, demonstrate no change to protein expression or fusion activity, indicating these residues are not critical. This suggests that these residues play a larger role in the C-terminus of the HeV F TM, potentially contributing to an increase in flexibility needed by that end [60]. This work, when partnered with previous studies [58, 60–62, 208], completes characterization of the entire HeV F TM region. While this work has investigated HeV F protein stability, expression, and cell-cell fusion function, understanding the interactions of HeV F TM residues with viral proteins other than HeV G, or host proteins and membrane lipids remains to be explored.

## Figures

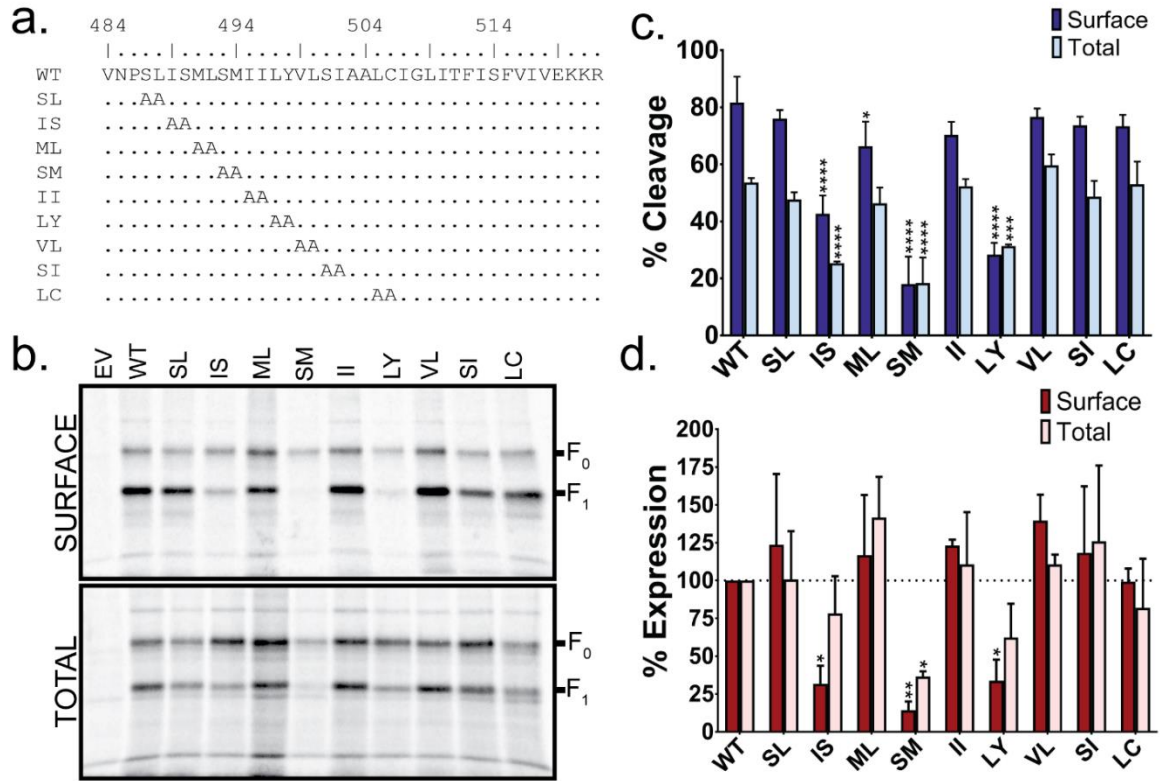


**Figure 4.1: Several HeV F TM mutants have impaired protein expression and protein cleavage.** (a) Alanine scanning mutations at the N-terminus of the HeV F TM were generated to assess the importance of these residues. (b) Surface biotinylation was performed to analyze the surface and total population of HeV F for WT and each of the mutants created. Cells were radiolabeled for 3 hours. Using band densitometry, percent expression (c) and percent cleavage (d) was measured for the total and surface protein. All measurements represent the average of three independent experiments  $\pm$  SD, and all samples were normalized to WT. Significance was determined by two-way ANOVA \* =  $p < 0.05$ , \*\* =  $p < 0.01$ , \*\*\* =  $p < 0.005$ , \*\*\*\* =  $p < 0.001$ . Chelsea Barrett, Kearstin Edmonds, and I completed independent replicates of the surface biotinylation assay.

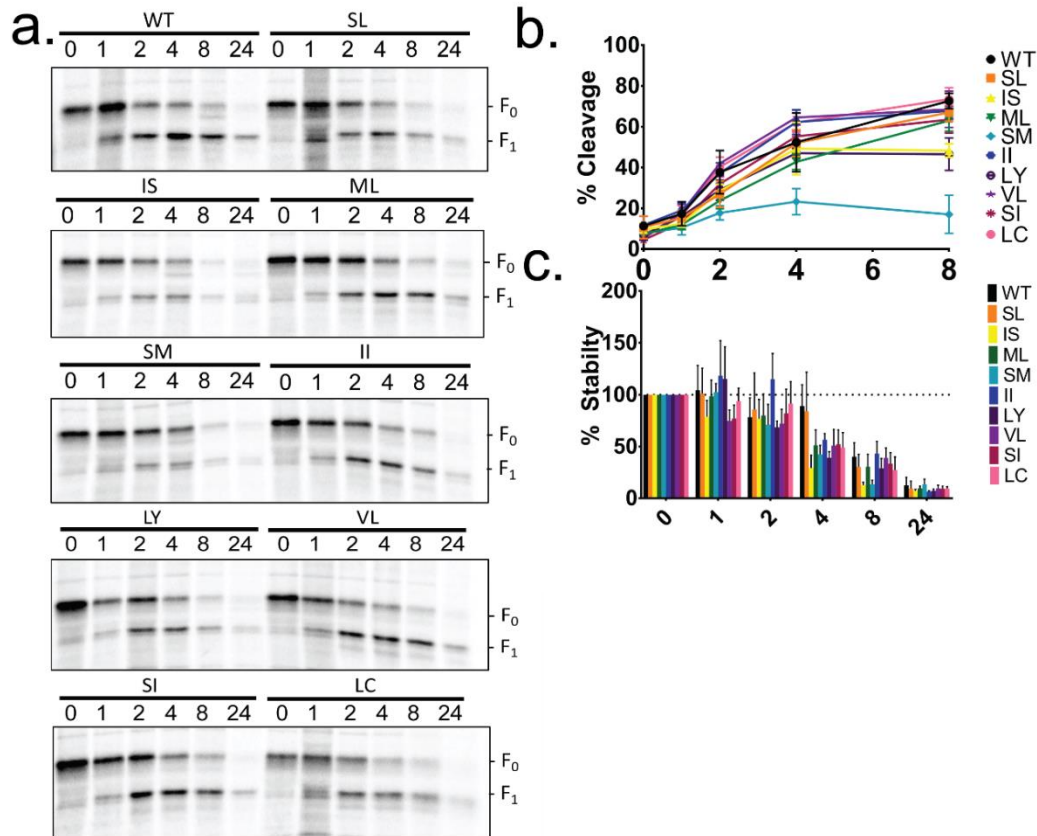


**Figure 4.2: HeV F TM mutations at residues SM and LY decrease protein cleavage levels.** (a) Vero cells were transfected with WT HeV F or the TMD mutant DNA, metabolically labeled for one hour, and chased for times indicated (hours). Using band densitometry (b) percent cleavage and (c) percent stability were calculated. Graphs are shown as the average of three independent experiments  $\pm$  SEM. Chelsea Barrett, Kearstin Edmonds, and I completed independent replicates of the pulse chase experiments.

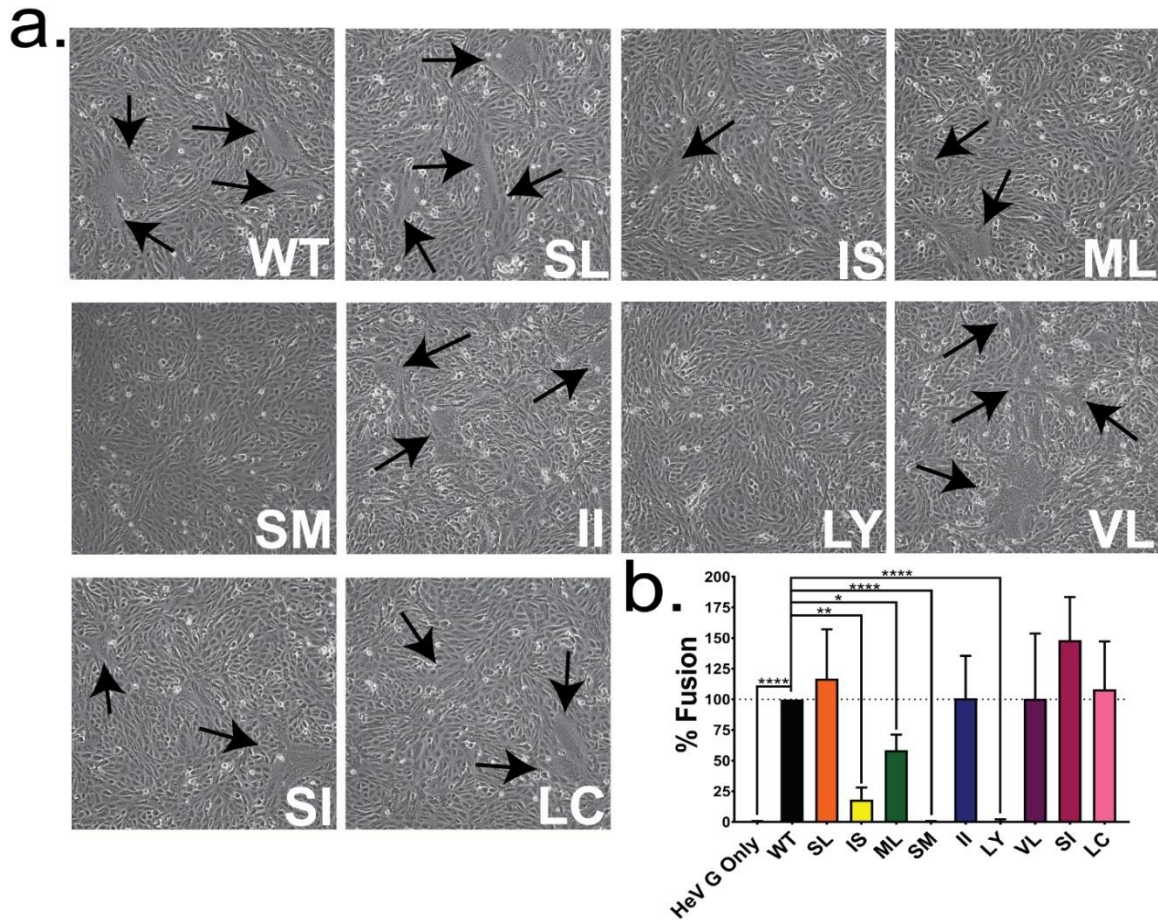


**Figure 4.3: Mutations at residues IS, ML, SM, and LY in the HeV F TM reduce fusion.** (a) Vero cells were transfected with the HeV attachment protein (G), and WT HeV F or one of the TMD mutants. Syncytia formation was analyzed at 48 hpt. Black arrows indicate syncytia formation. Images are representative of 4 independent experiments. (b) A luciferase reporter gene assay was performed using BSR/T7 cells overlaid onto Vero cells transfected with HeV G and WT HeV F or each of the TMD mutants at 24 hpt. Results are normalized to samples with WT HeV F and G and representative of 3 independent experiments, performed in duplicate. Significance was determined by one-way ANOVA. \* =  $p < 0.05$ , \*\* =  $p < 0.01$ , \*\*\* =  $p < 0.005$ . Chelsea Barrett, Juana Reyes-Zamora, Kearstin Edmonds, and I all completed independent replicates of syncytia assays and reporter gene assays.

## CHAPTER 5. CHARACTERIZING RSV FUSION PROTEIN CLEAVAGE DYNAMICS AND THE POTENTIAL ROLE OF PEP27

\*This work was completed with the help of Dr. Chelsea Barrett. Chelsea performed pulse chase and surface biotinylation replicates (Fig. 5.1 and 5.2) and took syncytia images (Fig. 5.4). Syncytia counts were done by Dr. Carole Moncman (Fig. 5.4b and 5.7b). Chase Heim performed the flow cytometry experiment (Fig. 5.8E). Kearstin Edmonds performed the immunofluorescence experiment and took fluorescent images (Fig. 5.8F). All other experiments, figure generation, and writing were completed by me.

### Introduction:

Respiratory syncytial virus (RSV) is an important cause of hospitalizations and death worldwide for young children, the immunocompromised, and adults over the age of 65 [210, 211]. This global burden has led to significant research on this virus and a concerted effort to develop an RSV vaccine for over 60 years [212]. The ongoing RSV research has resulted in countless discoveries; however, several aspects of the mechanisms of entry, triggering, and fusion remain unclear. The two RSV clades, A and B, co-circulate worldwide [71–73]. Although the dominance of one strain over the other varies between RSV seasons, RSV A has been the primary focus of molecular studies.

The RSV fusion glycoprotein (F) facilitates fusion between viral and host cell membranes. RSV F is a class I fusion protein synthesized as an inactive precursor (F<sub>0</sub>) in the endoplasmic reticulum (ER) and must undergo cleavage by a host cell protease to become fusion competent [213–216]. RSV F differs from other paramyxovirus/pneumovirus class I fusion proteins in that cleavage must occur at

two sites, rather than one, to be active. These two sites both contain a canonical furin recognition motif (R-X-K/R-R), and are separated by a 27 amino acid fragment termed Pep27 (P27) [77, 83, 213]. Furin cleavage site 1 (FCS1) is located between residues 105-109 with furin cleavage site 2 (FCS2) between residues 130-136. During infection, the timing of cleavage at each site remains controversial among the field.

Because P27 is not covalently attached through disulfide bonds to the rest of RSV F, it has been widely assumed that after proteolytic processing in the trans golgi, P27 separates from the rest of F, playing no further role in fusion or infection. However, recent studies have found that after RSV infection, children and young adults display a strong immune response to the P27 region of F [217, 218]. Because P27 is not thought to be present with the rest of F on the cellular or viral surface, it has been concluded that the p27 immune response is likely due to exposure to immature virions or dying infected cells [217]. Interestingly, a very recent study detected P27 on the surface of infected A549 cells and lung tissue samples from infected mice [97]. The authors suggested that this was due to a large proportion of unprocessed F<sub>0</sub> on the cell surface, which would be consistent with a model where part of F proteolytic processing occurs after viral entry [98].

In the RSV A2 subtype, there are five putative N-linked glycosylation sites within the F protein. A large body of previous work in many different viruses has shown a vital role for the glycosylation of viral proteins in proper folding and transport [219–225], though little is known about the impact of RSV F glycosylation on folding and glycosylation. Two of these five N-linked glycosylation sites are highly



conserved among RSV A2 and RSV B9320 subtypes. Early studies indicated that the removal of RSV F N-linked glycosylation sites had no effect on surface protein expression [226]. However, the authors did note that in the mature F protein P27 is not present, leading them to exclude the two N-linked glycosylation sites within P27 from surface expression experiments. In a more recent study, an attempt to generate replication competent recombinant virus failed when all five glycosylation sites were mutated simultaneously. The inability to produce viable virus suggests a crucial role in infection for at least one of these N-linked glycosylation sites [96], and combined with the earlier data suggests that these vital sites are within P27. Recent work has shown that immunizing mice with a plasmid encoding a mutation to block N-glycosylation at site 116 led to an increased immune response [94]. This further suggests that the P27 region may be important in entry, infection, or immune evasion.

We evaluated the timing of RSV F cleavage at both recognition sites using mutagenesis to disrupt the furin recognition motifs, followed by time course experiments. We confirm that F surface expression remains similar to WT levels when either cleavage site is disrupted. We also show that both RSV A2 and RSV F B9320 require both furin recognition sites to be fusogenically active, a finding that confirms previous work for RSV F A2 [83, 213], but is novel for RSV F B9320. In both subtypes, the presence and the glycosylation of P27 was evaluated. We conclude that in the absence of P27, F remains stably expressed on the cell surface, but cell-cell fusion is reduced. The glycosylation of P27 impacts cell-cell fusion differently in RSV F A2 and RSV F B9320. Importantly, we also demonstrate

that cleavage at FCS1 and FCS2 occur within the same timeframe, suggesting that RSV F cleavage is nonsequential, in contrast to a currently existing model [98].

### Results:

RSV F has two predicted furin cleavage sites, FCS1 (RARR109) and FCS2 (KKRKRR136) (Figure 5.1A). Mutants were created to alter these motifs for both RSV F A-2 and RSV F B9320 to assess the role of each cleavage site, and to allow comparison between F proteins from the A and B clades, as the one previous study had examined only RSV A [83]. These mutations (Figure 5.1a) remove the furin cleavage motif at either FCS1 or FCS2. Cleavage at only FCS1 generates F<sub>1+</sub> (the F<sub>1</sub> subunit with P27) disulfide linked to the F<sub>2</sub> subunit, while cleavage at only FCS2 generates F<sub>1</sub> disulfide linked to F<sub>2+</sub> (the F<sub>2</sub> subunit with P27) (Figure 5.1b). Radiolabeling combined with surface biotinylation was used to evaluate how cleavage at primarily one site impacts protein total and surface expression. As shown in Figure 5.1c, F proteins containing the mutation altering FCS1 (RARA) generated a band corresponding to the F<sub>1</sub> cleavage product in the surface and total protein populations for both the RSV F A2 and B9320 subtypes. This indicates that cleavage still occurs at FCS2 in the absence of cleavage at FCS1, and verifies that P27 remains attached to the F<sub>2</sub> subunit. The F protein mutants with altered FCS2 showed a band corresponding to F<sub>1+</sub> product formation for both RSV F A2 and B9320 in both surface and total protein populations. Although the FCS2 mutations introduced are not consistent with the canonical furin recognition motif, furin or an alternative protease did inefficiently cleave at these sequences, as a small amount of F<sub>1</sub> product formation was observed. These F protein mutants

showed varying levels of protein expression in surface and total populations. In both RSV F subtypes, the KKKKKK mutant had the highest level of protein observed while effectively generating the F<sub>1+</sub> cleavage product, potentially because this mutant was more stable than the other FCS2 mutants. In subsequent experiments, the F proteins with the RARA and KKKKKK mutations were exclusively used. Bands for surface and total protein populations were quantified and indicated that altering FCS1 did not significantly change the ratio of F<sub>1</sub> or F<sub>1+</sub> product formation compared to what was observed for the WT F protein for either surface and total protein for either subtype (Figure 5.1d and e). Additionally, in the FCS2 mutants there was a significant decrease in F<sub>1</sub> product formation (Figure 5.1d) and a significant increase in F<sub>1+</sub> product formation (Figure 5.1e) compared to WT. The F<sub>2</sub> and F<sub>2+</sub> products are too small to accurately be measured through this assay.

### 5.1.1 RSV F Cleavage is Nonsequential

The relative timing of cleavage at the two sites has proven to be controversial. While the earliest examinations of RSV F indicated cleavage of both sites in the cell [83, 213], a 2013 study presented data that suggested that RSV F was cleaved at FCS1 in the trans-golgi after initial protein synthesis, with cleavage at FCS2 occurring later after viral entry. If this is the case, F<sub>1</sub> and F<sub>1+</sub> cleavage products would appear at different timepoints during F protein processing.

Using the FCS1 and FCS2 mutants for both RSV F A2 and RSV F B9320, the timing of cleavage at each site was evaluated through a pulse-chase time course. Vero cells were transfected with plasmids expressing WT, the FCS1

mutant (RARA), or the (FCS2) mutant KKKKKK, for either subtype. For both the WT RSV F A2 and WT RSV F B9320, bands corresponding to F<sub>1+</sub> and F<sub>1</sub> were present beginning at the 0.5-hour chase mark, becoming more prevalent at the 1-hour chase mark (Figure 5.2a). This indicates that cleavage at FCS1 and FCS2 occurs within the same timeframe, suggesting cleavage is nonsequential. F proteins with the RARA mutations (altering FCS1) produced bands corresponding to F<sub>1</sub> at the 0.5-hour chase mark, again becoming more prevalent at the 1-hour chase mark, while F proteins with the KKKKKK mutations (altering FCS2) produced bands corresponding to F<sub>1+</sub> at the same timeframe. This supports the independent nature of cleavage at either site, as the timing of cleavage was similar in F proteins with both cleavage sites or F proteins with only one.

When bands were quantified, there were no significant differences in F<sub>1</sub> or F<sub>1+</sub> product formation between WT A2 and WT B9320 at any timepoint (Figure 5.2b and e), indicating that cleavage timing is similar in F proteins from the two clades. There was a significant decrease in F<sub>1</sub> product formation in the FCS2 mutant (KKKKKK) compared to WT of either respective subtype starting at 0.5-hours, as predicted from the mutation of the cleavage site needed to generate F<sub>1</sub>. However, a significant increase in F<sub>1+</sub> product formation was seen in the FCS2 mutant (KKKKKK) compared to WT at the same timepoint (Figure 5.2f and g). These results suggest that cleavage at FCS1 and FCS2 occur independently and within the same timeframe. Figure 5.2c and d again show that although inefficient, cleavage can occur at the FCS2 site in the KKKKKK mutants, likely either due to inefficient furin processing or due to cleavage by other cellular proteases.

### 5.1.2 Cleavage Dynamics are Consistent in Transfection and Infection Models

The model proposing cleavage of the second site after viral internalization into target cells was based on data from an infection with RSV A2 [98]. To determine if cleavage is nonsequential in both transfection and infection systems, a time course immunoprecipitation experiment was performed using rgRSV A2 Long infected A549 or Vero cells, and this was direction compared to transfected cells expressing WT A2 F. As shown in Figure 5.3a, in both transfected and infected Vero cells, bands corresponding to the F<sub>1</sub> and F<sub>1+</sub> products began at the 0.5-hour timepoint, becoming more prominent at the 1-hour timepoint. These bands were quantified and showed no significant differences in F<sub>1</sub> or F<sub>1+</sub> product formation (Figure 5.3c and e). In A549 cells, the same pattern was seen (Figure 5.3d and f). Thus, for both RSV infected cells and transfected cells expressing RSV F, products of cleavage at both sites are detectable within the first hour after protein synthesis. These findings strongly support a model where furin cleavage of both sites occurs at similar times during transport through the secretory pathway.

### 5.1.3 Cell-cell fusion is abolished with the disruption of either cleavage site

Previous studies have indicated that cleavage at both FCS1 and FCS2 is necessary for cell-cell fusion activity [83, 213]. However, this has exclusively been shown for a clade A virus. To evaluate the impact of cleavage site alterations in both clades, Vero cells were transfected with plasmids expressing WT F or a cleavage site mutation, and cells were imaged at 48-hours post transfection.

Syncytia formation was used as an indicator for cell-cell fusion. In either subtype, mutants with a mutation in either FCS1 or FCS2 could not promote detectable syncytia formation (Figure 5.4a). Images were analyzed and syncytia were counted, as displayed in Figure 5.4b. Thus, in either subtype, processing at both cleavage sites is required for cell-cell fusion competency.

#### 5.1.4 The randomization of P27 decreases F<sub>1+</sub> product formation.

The necessity of cleavage at both FCS1 and FCS2 raises questions regarding the role of P27, which is between these two sites, and which would not be covalently attached to the rest of RSV F after cleavage at both sites occurs. It has generally been assumed that P27 separates from F and does not serve a further role in viral infection. However, recent studies indicate an immunogenic response to the P27 region in children and young adults, suggesting it may play a larger role in the infection process or immune evasion [217]. Within the P27 fragment, two N-linked glycosylation sites are conserved among subtypes. The glycosylation of these specific sites has also recently been defined as immunogenic, further indicating that P27 is more important for RSV than previously thought [94, 96].

To evaluate how N-linked glycosylation at these sites impacts protein expression, cleavage, surface expression, and cell-cell fusion, mutants were created to remove the glycosylation site at either site 116 or 126, in both RSV F A2 and RSV F B9320 (Figure 5.5a). Additionally, a mutant was made to randomize

the residues within P27, with the exception of the N-linked glycosylation sites, to explore the sequence specificity of P27 on its potential functions. A P27 deletion mutation was also generated, keeping both FCS1 and FCS2 intact (Figure 5.5a).

The stability and expression of these mutations was tested using a metabolic radiolabel (Figure 5.5b). Vero cells were transfected with plasmids expressing each of the designed mutations, then labeled with  $^{35}\text{S}$  for 1 hour, and immunoprecipitated. All mutations were properly expressed in Vero cells (Figure 5.5b), though some decrease was observed in the overall protein expression levels for some of the mutants compared to the WT F proteins indicating that none of the mutations drastically disrupted the stability of the F protein.

A time course immunoprecipitation experiment was performed to identify how these mutations impact F cleavage and stability over time (Figure 5.6a). In Vero cells transfected with plasmids expressing a P27 deletion, bands corresponding to  $F_1$  appeared at 0.5-hours, similar to what was observed in the WT F protein of each respective subtype, suggesting that the timing and efficiency of cleavage is not impacted by the deletion of P27. Additionally, the protein expression over time was similar to that of WT, indicating that the deletion of P27 does not drastically change stability in either subtype. As expected, there was no formation of the  $F_{1+}$  cleavage product as P27 has been deleted. In the N116Q and N126Q mutations, stability over time, cleavage timing, and cleavage efficiency were similar to that of WT F (Figure 5.6a). Interestingly, compared to WT F for either subtype, the P27 random mutant showed less  $F_{1+}$  product formation (Figure 5.6a), indicating that cleavage at FCS1 prior to FCS2 does not occur as frequently

in this mutant. In addition, in both subtypes, an upward shift was seen in  $F_0$  starting at the 1-hour timepoint potentially indicating changes in post-translational modifications

Bands corresponding to  $F_1$  were quantified for both subtypes (Figure 5.6b and d). In RSV F A2 (Figure 5.6b), there was a small but statistically significant increase in  $F_1$  product formation for the P27 deletion mutation compared to WT at 0.5 and 1-hour timepoints. However, in RSV F B9320 (Figure 5.6d), this significant increase was seen at 0.25 and 0.5-hour timepoints. This slight increase in proportion of  $F_1$  product formation compared to WT can be attributed to the absence of P27, and therefore the lack of  $F_{1+}$  formation. The  $F_{1+}$  cleavage products were quantified for both subtypes as shown in Figure 5.6c and e. As expected, no  $F_{1+}$  was formed in the P27 deletion mutant for either subtype. Interestingly, in the RSV F A2 randomized P27 mutant, there was a significant decrease in  $F_{1+}$  formation compared to WT at hours 1 and 2 (Figure 5.6c). This suggests that the formation of  $F_{1+}$  as an intermediate product may be P27 sequence specific.

#### 5.1.5 P27 mutations impact cell-cell fusion differently in subtypes

Previous work with bovine RSV (BRSV) concluded that the deletion or randomization of residues within P27 results in reduced cell-cell fusion [227]. This indicates that in the case of BRSV, P27 is sequence specific. To understand how similar mutations impact cell-cell fusion in human RSV, Vero cells were transfected



with the P27 mutations designed in Figure 5.5a, and syncytia formation imaged at 48-hours post transfection. As shown in Figure 5.7a, in RSV F A2 the disruption of either N-linked glycosylation site reduced syncytia formation compared to WT. The deletion of P27 also reduced the size and frequency of syncytia (Figure 5.7a). Interestingly, in the randomized P27 construct, the level of syncytia detected was similar to that of WT A2 (Figure 5.7a). Given that in the randomized P27 mutant both N-linked glycosylation sites are conserved, this suggests that either the asparagine residues at sites 116 and 126, or the glycosylation at these sites, is important for cell-cell fusion efficiency in RSV F A2. The reduction in syncytia formation in the P27 deletion mutant indicates that the presence of this fragment is not vital to cell-cell fusion, but does aid in efficiency. The same is not true for RSV F B930. As shown in Figure 5.7a, WT B9320 did not form syncytia as efficiently as WT A2. In the N116Q and N126Q mutants, syncytia detection was similar to that of WT B9320. In contrast to what was seen in A2, in both the RSV F B9320 P27 deletion and randomized constructs, very little syncytia formation was detected (Figure 5.7a). This indicates that glycosylation within P27 may impact cell-cell fusion differently between subtypes. Syncytia formation was quantified as shown in Figure 5.7b. In the cells transfected with plasmids containing the RSV F A2 mutant constructs, there was a significant decrease in cell-cell fusion compared to WT RSV F A2. There was no significant difference in cell-cell fusion between cells transfected with plasmids containing RSV F B9320 mutant constructs and cells transfected with WT RSV F B9320.

### 5.1.6 Low levels of P27 but little uncleaved F<sub>0</sub> can be detected on the cell surface

In a recent study, P27 was detected on the cell surface of infected A549 cells [97]. The authors attributed this detection to immature, uncleaved F<sub>0</sub> on the cell surface; however, other studies have concluded that F<sub>0</sub> is inefficient in reaching, or unable to reach the surface [77, 82, 228]. To determine the proportion of F<sub>0</sub>, F<sub>1</sub>, and F<sub>1+</sub> on the cell surface, a surface biotinylation experiment was performed. Vero cells were transfected with plasmids expressing WT RSV F, the FCS2 mutation KKKKKK (Figure 5.1a) or the P27 mutations (Figure 5.5a). Bands corresponding to F<sub>0</sub>, F<sub>1+</sub>, and F<sub>1</sub> were quantified for both total and surface levels (Figure 5.8b-d). Very little F<sub>0</sub> was detected in the surface or total protein populations, indicating that during the 3-hour label period, most of the F protein was cleaved (Figure 5.8b). As anticipated, the FCS2 mutants KKKKKK formed significantly less F<sub>1</sub> and significantly more F<sub>1+</sub> than WT for either subtype (Figure 5.8c and d), and this form was expressed on the cell surface, indicating that lack of cleavage at FCS2 did not prevent cellular transport. In WT F and the remaining mutants, nearly 80% of surface and total protein was detected as F<sub>1</sub> (Figure 5.8c). As shown in Figure 5.8d, there was a significant decrease in A2-N116Q F<sub>1+</sub> surface expression compared to WT A2. A significant decrease in total F<sub>1+</sub> expression for A2-Random compared to WT A2 was also observed. In both subtypes, there was no F<sub>1+</sub> formation detected in the P27 deletion mutation (Figure 5.8d). These results indicate that in WT RSV F A2 and B9320, uncleaved F accounts for less than 10% of F expressed on the cell surface in a transfection model. To examine for the presence of uncleaved F in infected cells, A549 cells were infected with rgRSV-

A2. The infected cell population was split into two groups to be labeled with palivizumab, which detects F in either the pre-fusion or post-fusion state, or a P27 monoclonal antibody, both used under saturating conditions. Flow cytometry was used to determine the mean fluorescence intensity (MFI) of each group and measurements were normalized to palivizumab. As shown in figure 5.8E, P27 can be detected on the surface of infected cells at a level 20-fold less than palivuzumab, though both are well characterized human monoclonal antibodies. The P27 monoclonal antibody was used to detect P27 on the cell surface through immunofluorescence (Figure 5.8F). Vero cells were transfected with plasmids expressing the cleavage site mutation A2-KKKKKK as a control because P27 would remain within the F<sub>1</sub> subunit, forcing the fragment to the surface to be detected by the antibody. Vero cells transfected with plasmids expressing WT RSV F A2 also demonstrated strong P27 surface expression (Figure 8F).

#### Discussion:

In this study, we present a detailed evaluation of RSV F cleavage timing and kinetics, as well as a functional characterization of the role of P27 in RSV F-mediated cell-cell fusion, F surface expression, and F stability over time. Consistent with previous work, we show that cleavage at both furin cleavage sites is necessary for cell-cell fusion in RSV-A2 [83, 213]. Importantly, we confirmed that both the A and B subtypes require cleavage at FCS1 and FCS2 for cell-cell fusion by evaluation of the strain RSV-B9320. Our study also evaluated the timing of

cleavage at either site using mutations to alter the furin recognition motif at one site or the other, combined with time course radiolabel experiments. We determined that cleavage at both sites occurs within the same time frame and is consistent with both sites undergoing cleavage during initial transport through the secretory pathway, in contrast to the model of a previous report [98]. Analysis of cleavage timing was also performed using an infection model, and again showed that cleavage consistently occurs within the same timeframe (Figure 5.4).

The requirement for cleavage at both sites raises questions about the role of the P27 fragment between them. P27 has recently been shown to play a significant role in immune recognition in children and young adults [94, 96, 217], though the mechanism by which P27 is available for B cell recognition is not known. A recent study detected P27 on the surface of infected A549 cells and lung tissue of infected mice [97], which the authors attributed to the presence of the uncleaved  $F_0$  form on the cell surface. This conclusion was in contrast to previous research which concluded that very little, if any,  $F_0$  was displayed on the cell surface [82, 228]. Our studies found that less than 10% of the F surface population is in the uncleaved,  $F_0$  form (Figure 5.8b). In infected A549 cells, P27 is detected on the surface at levels 20-fold lower than that of palivizumab under saturating conditions, consistent with the majority of F no longer containing P27 because it has been fully cleaved (Figure 5.8E). However, in transfected cells, P27 can be detected through immunofluorescence (Figure 5.8F). This suggests that P27 is either reaching the cell surface independently of uncleaved F, or that the small amount of uncleaved  $F_0$  is sufficient for significant antibody recognition.

No closely related viruses require cleavage at two sites, though cleavage at two sites is needed for other viral fusion proteins including the coronavirus spike protein (S). Similar to RSV F, S is cleaved by a furin-like host cell protease to generate two disulfide linked subunits, and when one cleavage site is rendered inactive, fusion competency suffers [40, 229, 230]. Interestingly, in the unenveloped human adenovirus capsid protein, cleavage at two sites produces a 33 amino acid peptide [231]. The capsid protein, synthesized as pVI, is cleaved at both termini. The resulting C-terminal fragment is an important protease cofactor. Only recently, the N-terminal cleavage product, termed pVIn, has been shown to remain non-covalently associated with mature adenovirus, aiding in the release of the newly synthesized virus from the endosome [232]. The pVIn fragment remains in a cavity created by hexon trimers until fusion with the endosomal membrane [231, 233–235]. It is plausible that P27 could similarly remain non-covalently associated with either F subunit, leading to surface detection of P27 with little F<sub>0</sub> present, as seen in this study. Ultimately, the structural plasticity of RSV F has made structural studies or many of its conformations difficult. Currently, only structures for uncleaved F are available [236]. A cleaved, post fusion conformational structure of F might illuminate the complex interactions between F and P27.

P27 contains two of the five N-linked glycosylation sites within RSV A2 F. These two sites are conserved in the B9320 F subtype as well. Posttranslational modifications to viral fusion proteins of viruses can impact protein expression, intracellular transport, proteolytic cleavage, receptor binding, and biological activity

[237–240]. Studies evaluating the glycosylation of P27 have revealed that disrupting the N-linked glycosylation motif at site 116 increases the level of F protein immune recognition in an RSV infection [94, 96]. To better understand how glycosylation at either site impacts the RSV F protein, we generated mutations to disrupt the P27 glycosylation sites in both RSV A and B. The P27-Random mutation was used to determine if the processing of P27 was sequence specific, or if the presence of any combination of residues induces the same impact. When previously evaluated in BRSV F, a randomized P27 mutant and a P27 deletion mutant both led to a reduction in cell-cell fusion compared to WT [227], but in these mutants, the N-linked glycosylation sites were not preserved. Here, the A2-Random P27 mutation maintained the two P27 glycosylation sites, and did not alter cell-cell fusion compared to WT A2 F. In contrast, a reduction in cell-cell fusion was seen in the A2-P27 deletion mutant, which lacked both the P27 region and its glycosylation sites. Combined with the significant decrease in syncytia formation seen in A2 N116Q and N126Q compared to WT, glycosylation at these sites does impact cell-cell fusion in RSV F A2. There were no significant changes to F surface expression or stability seen in these mutations, so the decrease in syncytia formation suggests that N-linked glycosylation is important for cell-cell fusion activity by some mechanism beyond overall protein stability. It is possible that P27 is used as a placeholder to maintain conformational stability. Similarly, when infecting cells with recombinant RSV A2 expressing disruptions to N-linked glycosylation motifs within the F protein, Leemans et al. saw a decrease in syncytia formation [96]. In combination with the data shown here, it can be predicted that

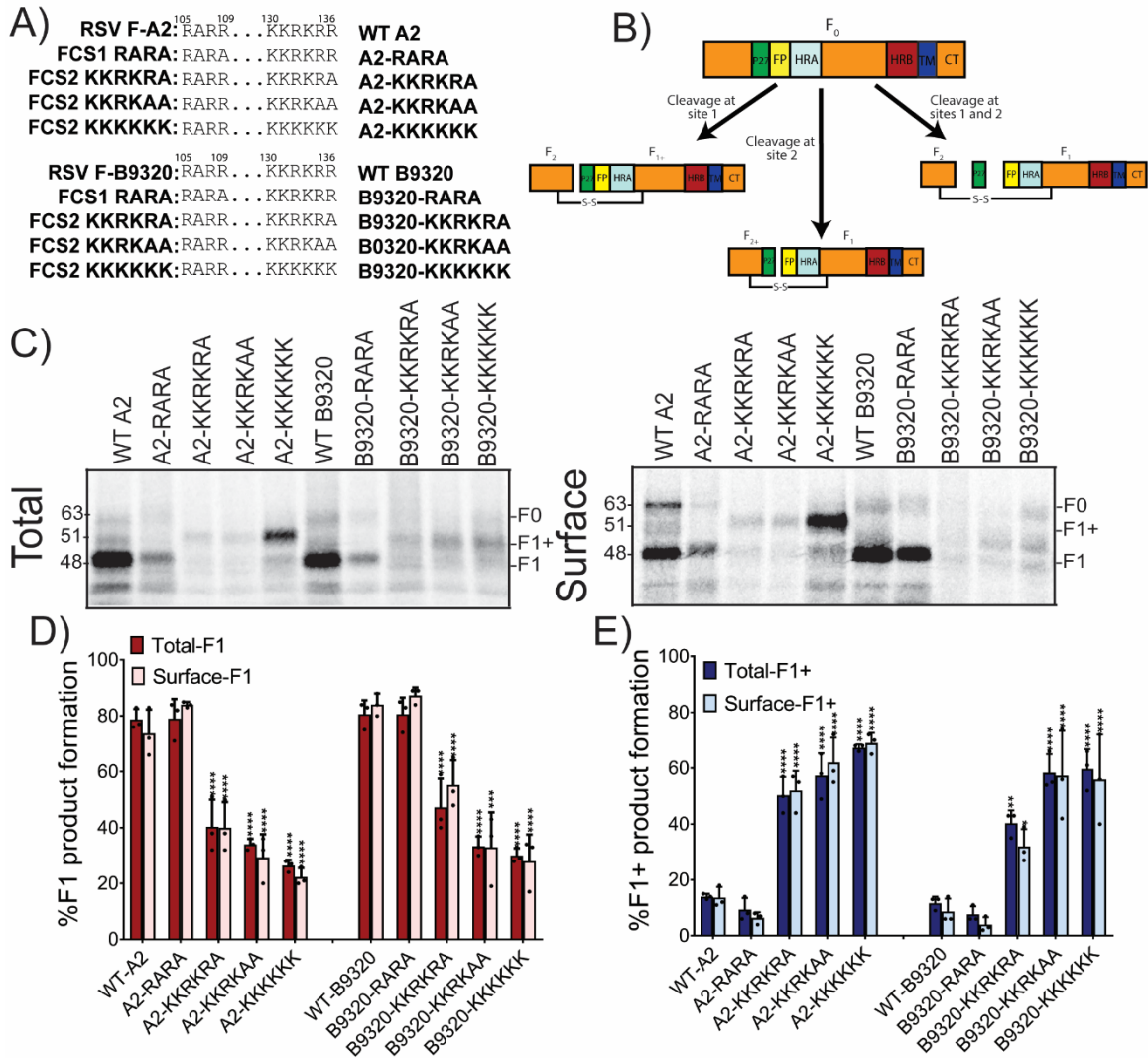
N-linked glycans within P27 are important for proper folding and conformational stability to facilitate cell-cell fusion.

The same impact for N-linked glycans in P27 was not seen in RSV B9320 F. There was a slight increase in syncytia formation seen the N116Q construct and a slight decrease in syncytia formation seen for N126Q Compared to WT B9320 F. Consistent in both subtypes, cells transfected with the N116Q construct showed an increase in cell-cell fusion compared to cells transfected with the N126Q construct. Interestingly, there was very little cell-cell fusion detected in cells transfected with plasmids containing the B9320 F P27-Random construct. This may indicate a striking difference in cell-cell fusion requirements between clades. However, this also may be attributed to sequence specificity that remains unaccounted for. As the WT P27 fragments were randomized, the residues remained consistent, only the order changed. The sequence used in the A2 P27 randomized mutant may have retained conformational stability that was not seen in the B9320 P27-Random construct, disrupting cell-cell fusion. Further studies are needed to ascertain whether cell-cell fusion relies on the N-linked glycosylation of P27 for conformational stability.

The work presented here provides a biochemical characterization of RSV F cleavage and explores the fate of the P27 fragment in both RSV A2 and RSV B9320. We have made important observations regarding role of P27 in F stability and surface expression, while the biological function remains to be determined. In the closely related BRSV, after F protein cleavage, P27 is further processed and secreted by cells as virokinin, a peptide hormone in the tachykinin family. The

constant secretion of virokinin was shown to desensitize the G-protein coupled receptor tachykinin receptor 1 (TACR1) [241]. Given that tachykinin receptors are prominently expressed in immune cells, desensitization by virokinin could attenuate immune responses to BRSV infection. Though human RSV does not contain a tachykinin motif, there may be different downstream modifications made to P27 to generate an alternative biologically active peptide. Additional studies are needed to fully understand the fate of the P27 fragment.





Figures

**Figure 5.1: Mutations at the second cleavage site alter product formation in both surface and total populations.** A) Alanine or Lysine mutations were made at each of the RSV cleavage sites in both subtypes, disrupting the furin recognition motif. B) This diagram outlines the products formed according to which cleavage site is active. C) Vero cells transfected with plasmids expressing WT RSV F or the RSV F cleavage mutants were metabolically labeled for 3 hours and surface proteins were biotinylated to analyze the surface and total populations. Using band densitometry, percent F<sub>1</sub> (D) and F<sub>1+</sub> (E) cleavage product formation was

measured for both surface and total populations. All measurements represent the average of three independent experiments  $\pm$  SD. Significance was determined by two-way ANOVA \* =  $p < 0.05$ , \*\* =  $p < 0.01$ , \*\*\*\* =  $p < 0.001$ . Surface biotinylation was done in collaboration with Chelsea Barrett.

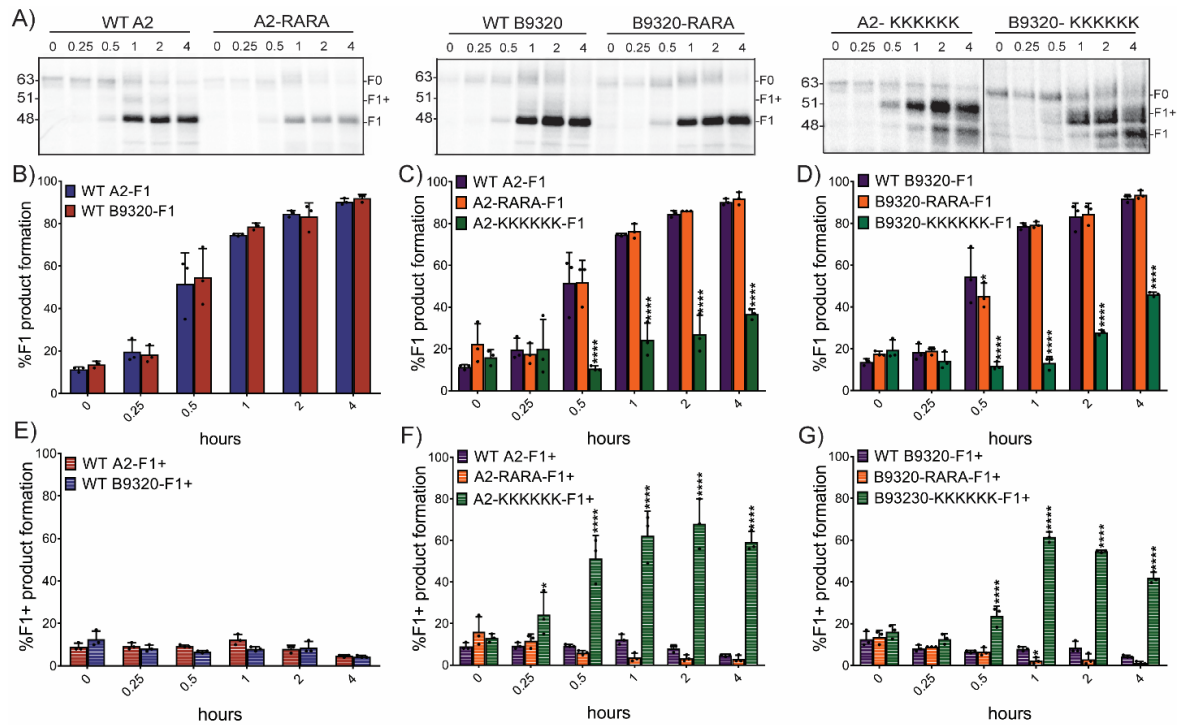


**Figure 5.2: RSV F cleavage is nonsequential.** A) Vero cells transfected with plasmids expressing WT RSV F or the RSV F cleavage mutants were metabolically labeled for 15 minutes and chased for the times indicated (hours). Using band densitometry, percent F<sub>1</sub> (B, C, and D) and F<sub>1+</sub> (E, F, and G) cleavage product formation was measured. All measurements represent the average of three independent experiments  $\pm$  SD. Significance was determined by two-way ANOVA \* =  $p < 0.05$ , \*\* =  $p < 0.01$ , \*\*\*\* =  $p < 0.001$ . Pulse chase was done in collaboration with Chelsea Barrett.

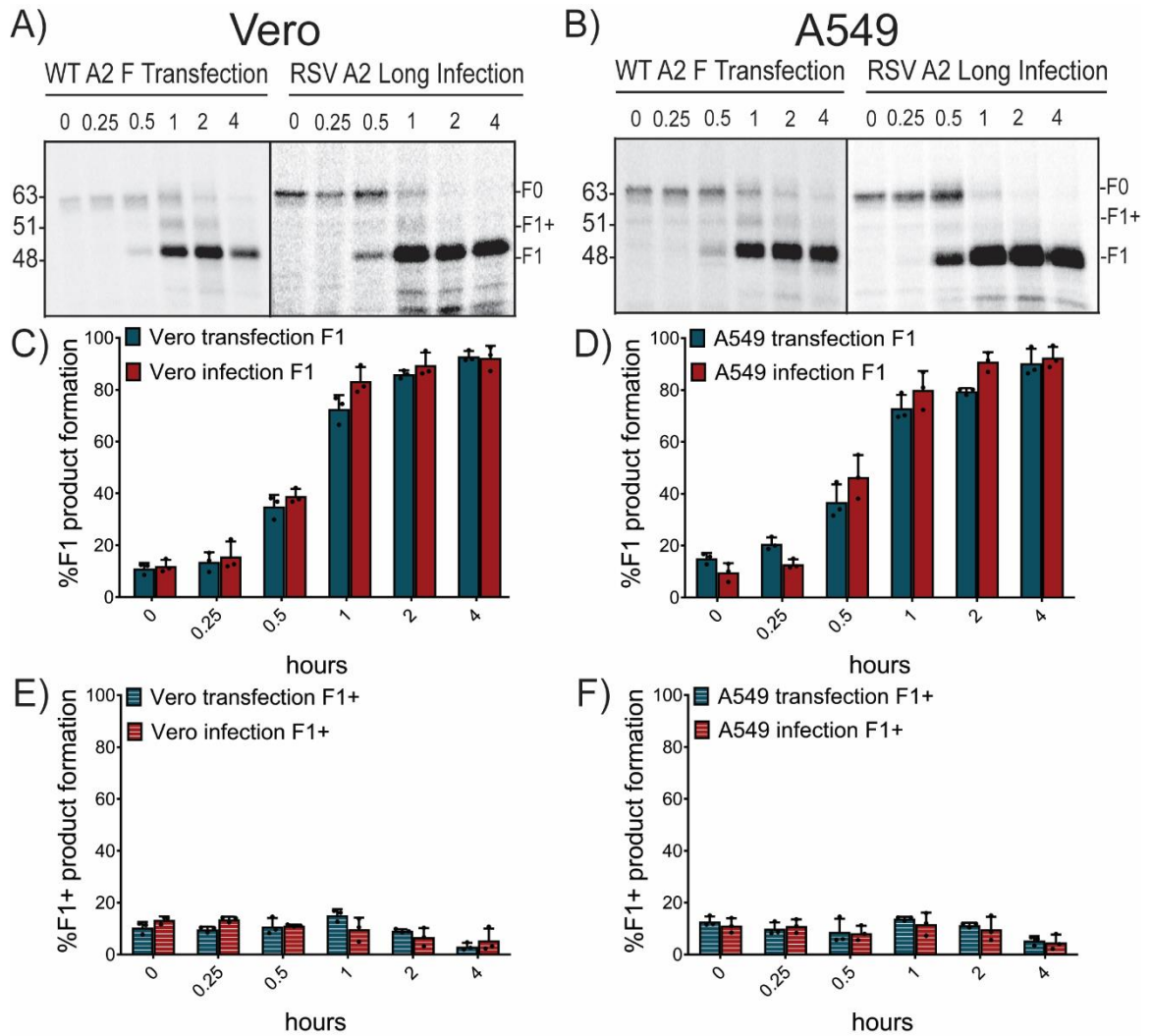


**Figure 5.3: Cleavage dynamics are consistent between transfection and infection models.** Vero cells (A) and A549 cells (B) were transfected with plasmids expressing WT RSV A2 F or infected with RSV A2 Long were metabolically labeled for 15 minutes and chased for the times indicated (hours). Using band densitometry, percent F<sub>1</sub> (C and D) and F<sub>1+</sub> (E and F) cleavage product formation was measured for both cell types. All measurements represent the average of three independent experiments ± SD. Significance was determined by two-way ANOVA \* = p < 0.05, \*\* = p < 0.01, \*\*\*\* = p < 0.001.

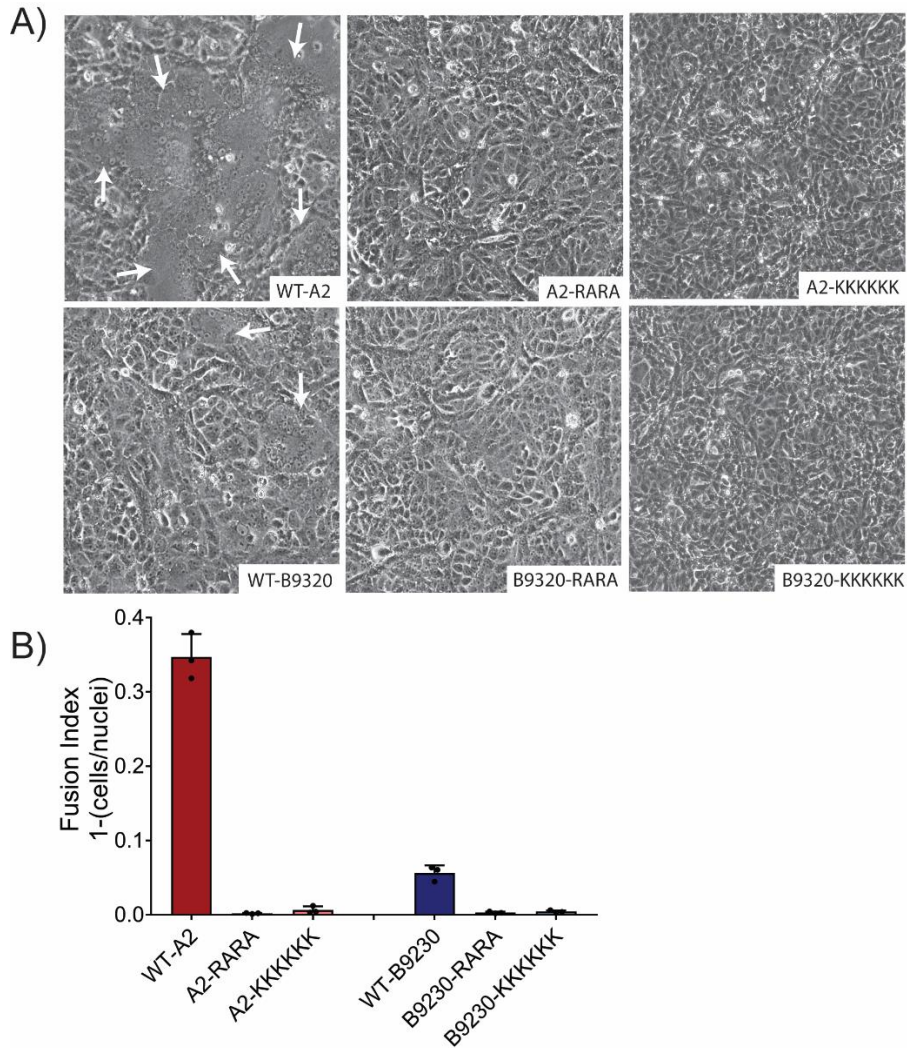


**Figure 5.4: Cell-cell fusion is abolished with the disruption of either cleavage site.** A) Vero cells were transfected with plasmids expressing WT F or a cleavage site mutation and imaged at 48 hours post-transfection on a Nikon Ti2 for the presence of syncytia formation (denoted by white arrows). Images are representative. B) Nuclei were counted by defining the total syncytia area and dividing that by the area of the field. In some cases, nuclei were scored and counted as either nuclei in syncytia or total nuclei. The fusion index was expressed as  $1 - (\text{total nuclei} - \text{nuclei in syncytia} + \text{number of syncytia}) / \text{total nuclei}$ . All measurements represent the average of three independent experiments  $\pm$  SD. Syncytia images were taken in collaboration with Chelsea Barrett. Syncytia counts were done by Carole Moncman.

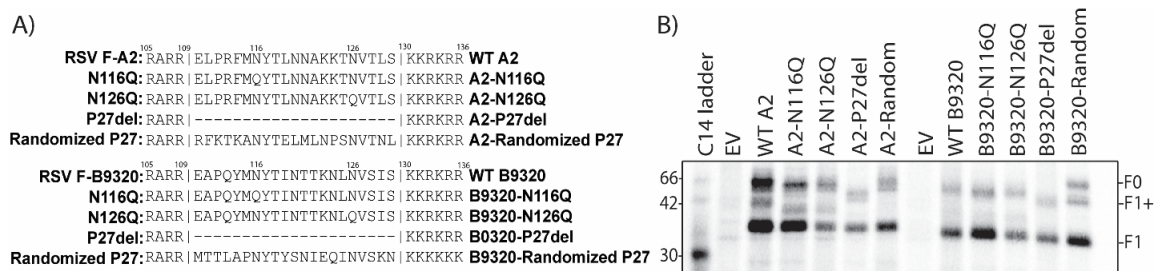


**Figure 5.5: Mutations within P27 targeting N-linked glycosylation and the deletion of P27 do not drastically impact protein expression in either subtype.** A) Mutations were made in both subtypes to delete P27, randomize the P27 sequence while preserving N-linked glycosylation sites, and to disrupt either N-linked glycosylation site. B) Vero cells were transfected with plasmids expressing WT F or the mutant constructs. An <sup>35</sup>S metabolic label was performed to determine if the mutant constructs impact protein expression.



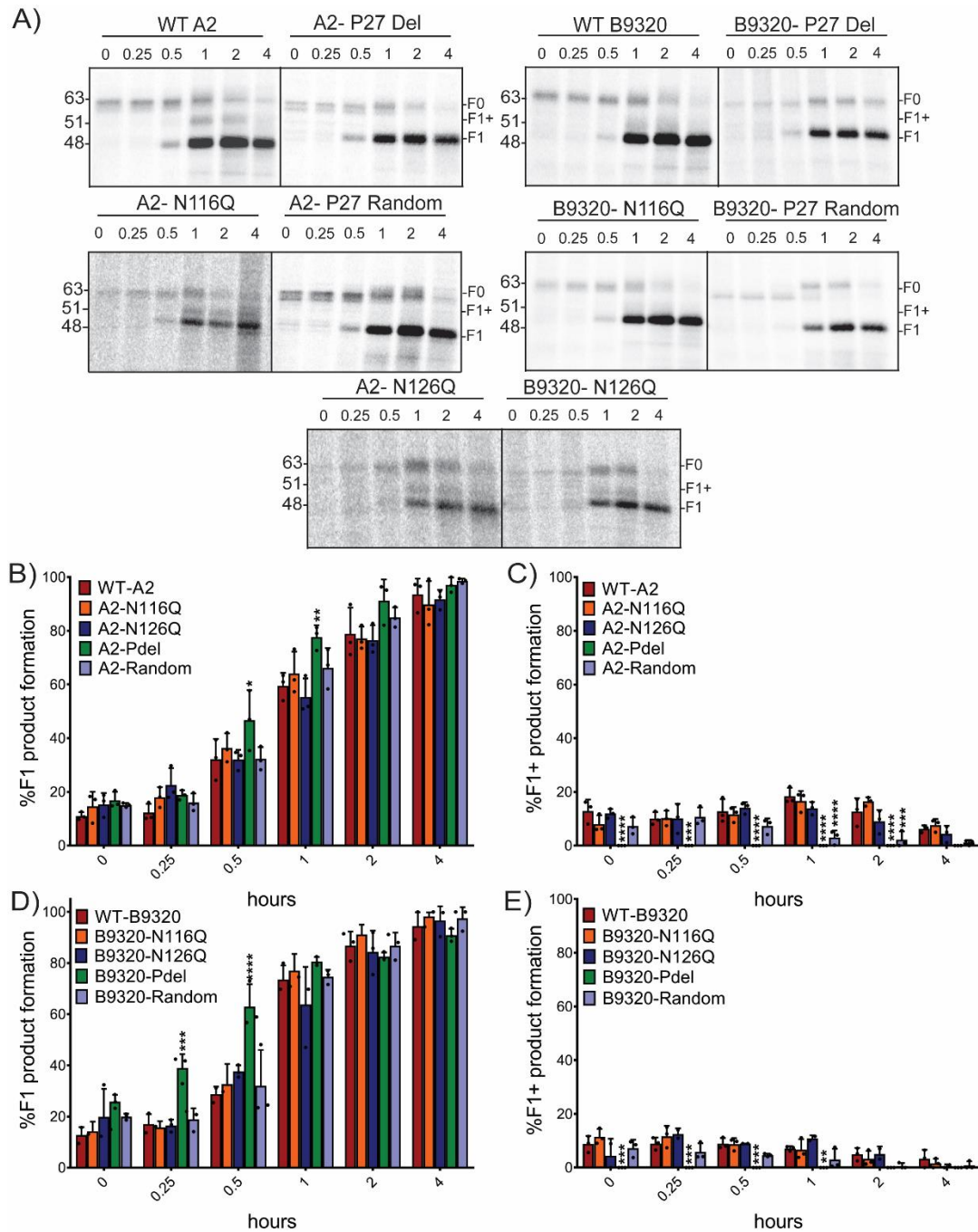


**Figure 5.6: The randomization of P27 decreases F1+ product formation.** A)

Vero cells transfected with plasmids expressing WT RSV F or the RSV F P27 mutants were metabolically labeled for 15 minutes and chased for the times indicated (hours). Using band densitometry, percent F<sub>1</sub> (B and D) and F<sub>1+</sub> (D and E) cleavage product formation was measured. All measurements represent the

average of three independent experiments  $\pm$  SD. Significance was determined by two-way ANOVA \* =  $p < 0.05$ , \*\* =  $p < 0.01$ , \*\*\*\* =  $p < 0.001$ .



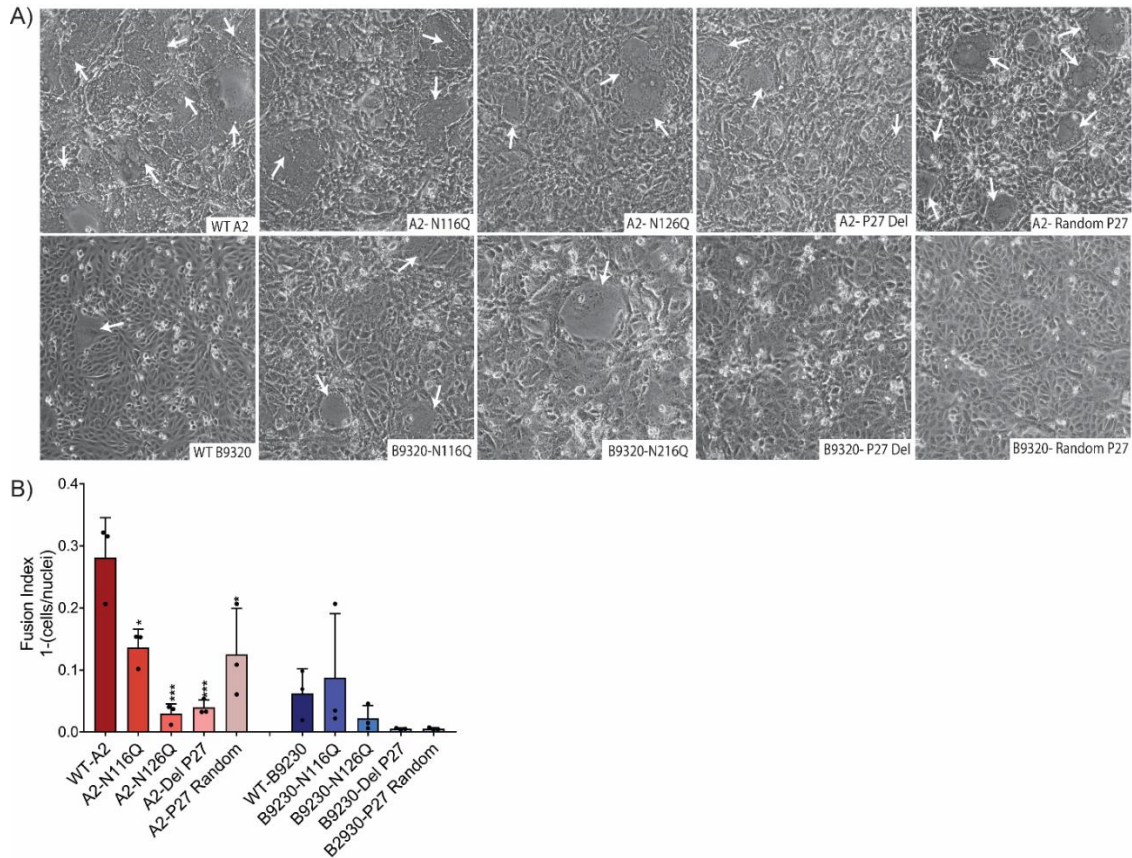


**Figure 5.7: Mutations within P27 impact cell-cell fusion.** A) Vero cells were transfected with plasmids expressing WT F or a P27 mutation and imaged at 48 hours post-transfection on a Nikon Ti2 for the presence of syncytia formation (denoted by white arrows). Images are representative. Nuclei were counted by defining the total syncytia area and dividing that by the area of the field. In some cases, nuclei were scored and counted as either nuclei in syncytia or total nuclei. The fusion index was expressed as  $1 - (\text{total nuclei} - \text{nuclei in syncytia} + \text{number of syncytia}) / \text{total nuclei}$ . All measurements represent the average of three independent experiments  $\pm$  SD. Syncytia counts were done by Carole Moncman.

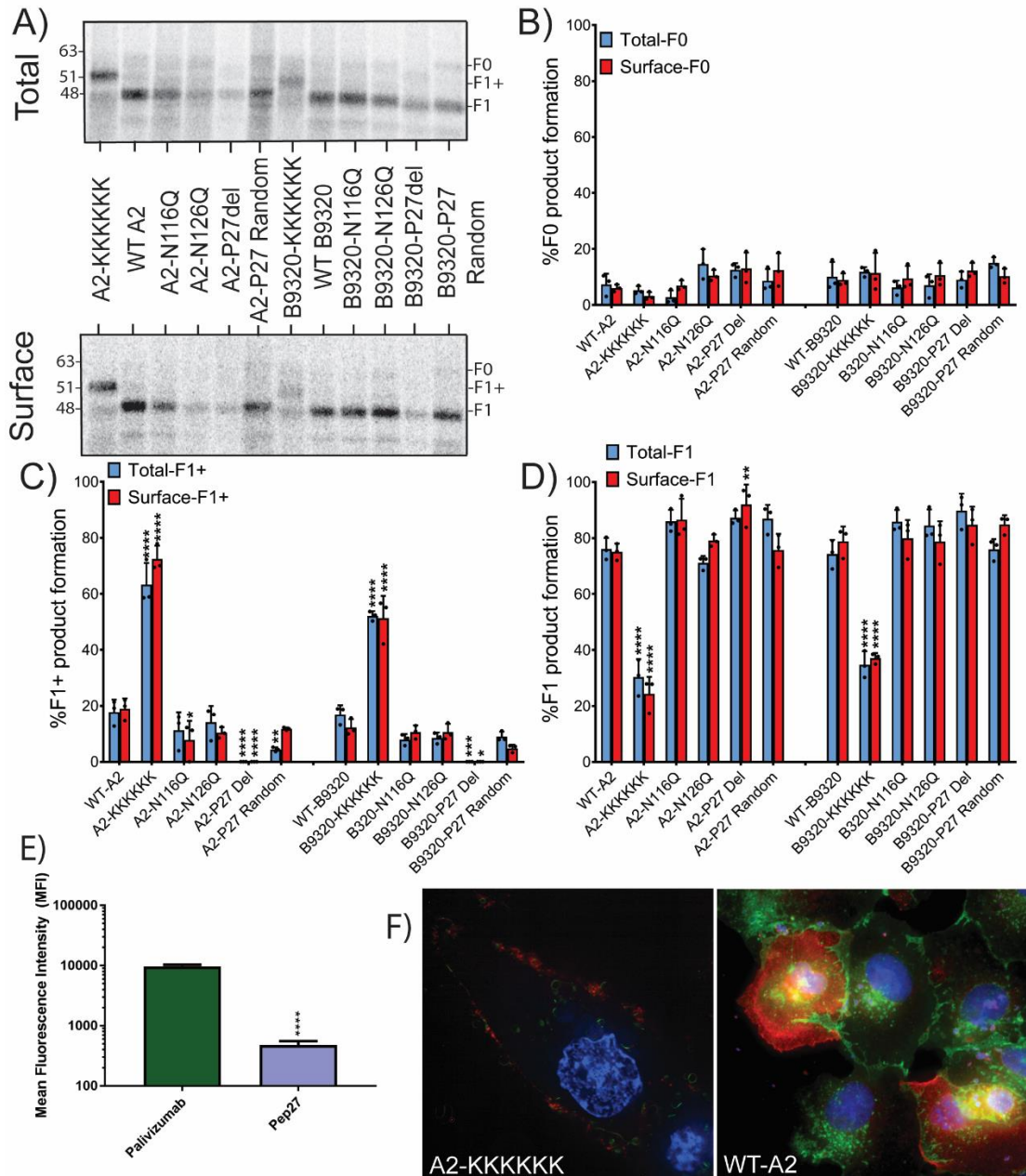


**Figure 5.8: Low levels of P27 but little uncleaved F0 can be detected on the cell surface.** A) Vero cells transfected with plasmids expressing WT RSV F or the RSV F P27 mutants were metabolically labeled for 3 hours and surface proteins were biotinylated to analyze the surface and total populations. Using band densitometry, percent F<sub>0</sub> (B), F<sub>1</sub> (C), and F<sub>1+</sub> (D) product formation was measured for both surface and total populations. E) A549 cells were infected with rgRSV-A2

at MOI of 1.0. Flow cytometry was used to determine the MFI of palivizumab and P27 on the cell surface. Measurements are normalized to palivizumab MFI. F) Vero cells transfected with plasmids expressing RSV F A2-KKKKKK and RSV F WT A2 were labeled with a P27 monoclonal antibody (red), dapi (blue), and WGA 488 (green). RSV F A2-KKKKKK samples imaged on Nikon CSU-W1 SORA 100X and deconvolved. RSV F WT A2 samples imaged on Axiovert 200M 100x. All measurements represent the average of three independent experiments  $\pm$  SD. Significance was determined by two-way ANOVA \* =  $p < 0.05$ , \*\* =  $p < 0.01$ , \*\*\*\* =  $p < 0.001$ . Flow cytometry was performed by Chase Heim and immunofluorescence was done by Kearstin Edmonds.

## CHAPTER 6. DISCUSSION AND FUTURE DIRECTIONS

### Overview

The work presented in this dissertation further characterizes specific regions of three class I fusion proteins. As the global pandemic brought focus to SARS-CoV-2 S, we discovered regions of the protein that may play a role in the fusion mechanism. We also analyzed key residues in proteolytic processing of the protein at the S1/S2 border, which appears to regulate trimer stability (Chapter 3). Using the HeV fusion protein, we discovered that residues M491/L492 within the TMD strongly affect membrane fusion, indicating they play a role in the overall fusion mechanism of the HeV F protein (Chapter 4) and further presenting this region as more than simply a membrane anchor. Lastly, we explored the mechanisms and cleavage patterns of RSV fusion proteins from different lineages, providing better understanding of how the fusion processes may differ between the RSV subtypes. The post-cleavage location and potential function of the conserved Pep27 region was also characterized (Chapter 5). Taken together, this work provides novel information on critical residues and regions within these fusion proteins; however, several questions surrounding these important therapeutic targets remain.

### SARS-CoV-2 spike protein mutations

The COVID-19 pandemic quickly became an international public health emergency. At the time of publication, the circulating mutations mentioned in Chapter 3 were the only circulating mutations identified. However, as the virus continued to spread, the spike protein continued to mutate. By late 2022, the WHO recognized five strains of SARS-CoV-2, each with varying mutations within S [34, 242, 243]. Interestingly, in the variants identified, fifteen mutations reduced virus neutralization in post-vaccination patient sera, with seven falling within the S1 subunit receptor binding domain (RBD) [243]. The strain of SARS-CoV-2 S initially identified in late 2019 exhibits stronger binding to the ACE2 receptor compared to SARS [41, 244]. Alternative receptors may be targeted by SARS-CoV-2 S variants,

potentially the dipeptidyl peptidase 4 receptor used by the closely related MERS [43, 245]. To determine if this is the case, plasmids expressing the newly identified mutations can be transfected into cell lines deficient in ACE2 and another cell line deficient in the dipeptidyl peptidase 4. Comparing cell-cell fusion between the two deficient cell lines would be indicative of impacts on viral spread. Additionally, the insertion of twelve residues upstream of the S1/S2 cleavage site set SARS-CoV-2 apart from other  $\beta$ -coronaviruses. Two recently identified mutations fall within that region. Evaluating the cleavage dynamics and stability impacts through surface expression assays and pulse chase analysis of these variants could illuminate how this insertion is giving SARS-CoV-2 a biological advantage over other coronaviruses.

Understanding the structural impacts of each of the currently circulating variants will help design more effective therapeutics. One potential antiviral therapeutic that has been used to target HIV is synthetic peptides [246–248]. Designing synthetic peptides to target the S1 subunit RBD, preventing receptor binding would effectively halt fusion. However, with the rapidly mutating S protein, designing long-term peptides targeting the S1 RBD presents a challenge.

#### HeV F TM stability

Our understanding of TM interactions in henipaviruses has grown substantially in the last decade. Importantly, previous work has shown that class I fusion protein TMs can trimerize in the absence of the remainder of the protein. This suggests that trimeric TM interactions are important factors mediating F folding and conformational stability. Interestingly, these interactions keep HRB in place in the prefusion conformation, indicating that TM-TM interactions prevent the early triggering of the HeV F [60, 62]. Using synthetic peptides targeting the HRB region in henipaviruses has been shown to prevent infection *in vitro* [249], making this a prominent candidate for antiviral therapeutics. However, disrupting the TM-TM interactions may also be an effective antiviral target, as this could result in

premature triggering of the F protein to its post-fusion state. Using synthetic peptides to disrupt TM-TM associations in combination with synthetic peptides targeting HRB may provide additional infection prevention.

### RSV F cleavage dynamics

RSV F has been a prominent vaccine target for nearly 60 years, though many questions remain regarding F cleavage and entry. The results of my work are in contrast to a very influential publication that suggested that RSV F is cleaved once in the secretory pathway and again after viral entry by macropinocytosis. The authors measured the RSV F<sub>1</sub> subunit size at viral binding and after internalization, finding that upon internalization, F<sub>1</sub> is smaller. They attributed this to cleavage at FCS2 after viral entry, effectively separating P27 from F<sub>1</sub> [98]. However, no further publications have supported this finding, and attempts to repeat this experiment within our lab have been unsuccessful. Using a pulse chase experiment, we determined that cleavage is nonsequential with both FCS1 and FCS2 being cleaved within the secretory pathway before budding of a new virus. The straightforward reasons why our data differs from the previous publication such as differences in cell lines or infection versus transfection models have been closely examined and ultimately ruled out. Cleavage dynamics in a transfection and infection model system remain consistent. The same RSV A2-Long strain used in this previous publication was used for infection, again yielding consistent results. We currently do not have an explanation for the difference in results between the work. However, my work is consistent with earlier studies [83, 250]. Moving forward, cleavage of the cytoplasmically-exposed C-terminal tail of the F protein might account for the decrease in band size observed in the 2013 study, but this has not been explored. Using a P27 monoclonal antibody to confirm that the size change seen is in fact due to the loss of P27 would be the first step in uncovering the cleavage dynamics they observed.

## P27 and conformational stability

Several of our findings suggest that the N-linked glycosylation sites within P27 may impact RSV F protein conformational stability or receptor binding. Deletion of the P27 region resulted in a mutant with decreased cell-cell fusion, suggesting a role for P27 in F function. In contrast, the RSV F A2 randomized P27 mutant which conserves the two N-linked glycosylation sites produced syncytia similar to WT F, suggesting that the presence of these sites was sufficient for the critical function of P27. This effect of the P27 glycans could be due to the impact glycosylation has on RSV F conformational stability, even though the glycans appear to be removed upon cleavage in the trans-Golgi. RSV F trimer stability was previously evaluated using an antibody specific for pre-fusion F trimers [109]. It was concluded that on the cell surface, the trimer of F<sub>1</sub>+F<sub>2</sub> heterodimers exists in a dynamic equilibrium between associated-dissociated trimers. This indicates a “breathing” mechanism in that trimerized F exhibits conformational flexibility, existing in two states on the cell surface, one more compact than the other. The HIV-1 envelope protein exhibits a similar mechanism [110–112]. The more open trimeric state permits a conformational change to facilitate receptor binding. It is possible that the cell-cell fusion seen in the RSV F A2 P27 randomized mutation is due to the conservation of the N-linked glycosylation sites in P27 maintaining the proper prefusion conformational flexibility in the early folding events to then permit receptor binding, while the deletion of P27 made for a more rigid prefusion protein unable to bind properly. Structural studies to determine how the removal of P27 impacts conformational stability have yet to be completed. The breathing mechanism is a working theory for RSV F. Understanding the oligomer equilibrium using cross-linking assays would gain further insight into which regions are crucial for proper oligomerization to generate cell-cell fusion competent F. The work presented in this dissertation has specifically highlighted the importance of P27 and the two N-linked glycosylation sites in terms of cell-cell fusion capability. Using plasmid constructs designed to delete P27 and disrupt N-linked glycosylation motifs to perform a cross-linking experiment would further confirm the reliance of F on these residues for conformational stability.

Interestingly, the same cell-cell fusion patterns were not seen in cells transfected with plasmids containing the RSV F B9320 clade mutations. Though the RSV F A2 P27 and RSV F B9320 P27 fragments share a homology of 68%, the randomization of RSV F B9320 P27 resulted in little to no syncytia formation, even with the glycan sites retained. This indicates that in the case of RSV F B9320, there may be increased importance of residue specificity within P27. The alteration of the P27 sequence may have disrupted early protein folding events which then trigger downstream impacts like a decrease in cell-cell fusion. The randomization could also be altering the ability of sites 116 and 126 to be glycosylated, therefore disrupting receptor binding and diminishing cell-cell fusion function.

The RSV A2 and RSV B9320 fusion proteins have often been grouped together due to their 89% sequence homology. However, recent work including ours suggests there may be important functional differences between the F proteins of the two clades. A recent study evaluated the differences between clades in terms of pre-fusion stability [251]. Under reducing and denaturing conditions, the authors detected higher levels of P27 in RSV A2 infected cells compared to RSV B9320, suggesting a different cleavage efficiency between subtypes. Additionally, when subjected to temperature stress tests, RSV F A2 was able to better sustain the pre-fusion F conformation, potentially due to the increased levels of P27. The impact of P27 on pre-fusion conformational stability has yet to be evaluated, though the pre-fusion conformation of F has become a prominent therapeutic target. Ultimately, the lack of understanding of RSV F conformational stability is universal to all clades. Notably, the two N-linked glycosylation sites within RSV F A2 P27 are conserved, but RSV F B9320 P27 has a third N-linked glycosylation site at residue 120. Using mass-spec analysis to uncover potential differences in post-translational modifications could expose why P27 detection and cell-cell fusion activity differ between subtypes. Identifying which specific residues or modifications impact RSV F A2 and RSV F B9320 differently in terms of stability may bring the field closer to uncovering what separates these clades.



### Pre-fusion F as a vaccine target

In 1966, a formalin inactivated vaccine was developed for RSV [252–254]. In the later stages of clinical trials, it was found that the vaccine stimulated high levels of serum antibodies but there was markedly little resistance to infection [253, 254]. Unfortunately, the vaccine induced a severe, and in two cases lethal, response to RSV infection [253, 254]. This failure resulted in vaccine development hesitancy and increased safety concerns, despite the major push to develop an effective vaccine continuing over the coming decades. With promising clinical results, almost sixty years later in March of 2022, Pfizer was granted breakthrough status by the FDA for their pre-fusion F vaccine, calling for the vaccine development process to be expedited. The vaccine is 81% effective in preventing hospitalization in the child's first 90 days after birth if given to mothers in their third trimester. There are currently five additional late-stage vaccine candidates, four of which target the pre-fusion conformation of F [255]. The pre-fusion F structural model does not include P27 as its intrinsically disordered nature precludes structural analyses. Interestingly, recent studies have found an increased immune response specifically to the P27 region of F after infection [217]. Regardless of the role P27 may play in fusion or stability, the immune recognition studies suggest there may be a large missing piece with the exclusion of P27 from therapeutic models. My work in combination with others [97] has shown some level of P27 on the surface of infected and transfected cells. However, it remains to be determined whether newly synthesized virions display P27 on the viral surface. Using flow virometry to potentially identify P27 on the viral surface would give insight into the role P27 plays in prefusion stability [256]. If P27 could be detected on the viral surface, it would indicate that pre-fusion F, or another viral surface protein, is interacting with the fragment as a newly synthesized virion.

### Protein triggering

One of the most prominent unanswered questions surrounding RSV F is what triggers the conformational change from the pre-fusion to post-fusion form.

The F protein from some strains of the closely related pneumovirus, human metapneumovirus, is triggered through a drop in pH, but RSV is pH-independent. Ebola virus is also pH independent, but is endocytosed and proteolytically processed by endosomal proteases. The active fusion protein is then triggered by endocytic receptor binding [257]. Understanding what triggers RSV F to change conformations is important for therapeutic development. The conformational change to insert the fusion peptide into the target membrane is absolutely crucial for viral entry. Understanding, and thereby preventing, that change would prevent viral entry. Recent publications have suggested potential receptors for RSV F and the RSV attachment protein (G) [258–260]. One proposed signaling cascade for RSV prefusion F begins with binding to insulin-like growth factor 1 (IGF1R) on the cell surface, activating protein kinase C zeta to recruit nucleolin to the surface which also binds to RSV F [259]. Meanwhile, RSV G has been suggested to bind to CX3C chemokine receptor 1, potentially calling more nucleolin to the surface while tethering the virus to the host cell during fusion [259, 260]. Though vaccine development is at the forefront of the RSV field, the interactions between prefusion RSV F and nucleolin have recently been characterized as potential targets for RSV drug development [258]. There is little consensus regarding the receptor binding activity and downstream signaling cascade for RSV. Because RSV is fusion competent in cell culture without G, transfecting plasmids containing RSV F into cell lines deficient in targeted receptors would uncover if binding to the respective receptors is facilitated by F. Re-introducing G using co-transfections would determine how receptor binding and thus fusion activity is impacted by the presence of both surface glycoproteins.

### P27 potential biological functions

Although no other human paramyxovirus or pneumovirus fusion protein uses two cleavage sites and generates a fragment similar to P27, the closely related bovine RSV (BRSV) does. BRSV and human RSV fusion proteins are strikingly similar with a homology of 82% [261]. After initial synthesis as inactive F<sub>0</sub>, BRSV is cleaved into disulfide linked subunits, F<sub>1</sub> and F<sub>2</sub>, releasing BRSV P27

[261]. In BRSV, P27 is metabolized into virokinin, a peptide hormone [262, 263]. Virokinin is a member of the tachykinin family, known to be proinflammatory and have immunomodulatory properties. After cleavage at FCS1 and FCS2, BRSV P27 is converted into virokinin through post translational modifications. Virokinin is then secreted by infected cells and desensitizes tachykinin receptor 1, while acting on tachykinin receptor 3 to induce a pulmonary inflammatory response [263]. Tachykinin receptors are prominent immunomodulators, so the constant secretion of virokinin suppresses the immune response. BRSV P27 contains a tachykinin motif that is not shared with human RSV P27 [262]. However, the direct impact of P27 on the immune response to BRSV suggests there could be a similar fate for human P27. Though not a tachykinin peptide hormone, human P27 may be metabolized into a bioactive peptide after cleavage. BRSV P27 is converted to virokinin through posttranslational modifications after release from F. To evaluate human RSV for a similar mechanism, the P27 monoclonal antibody could be used to immunoprecipitate P27 from infected cells. Posttranslational modifications could be identified through mass spec analysis, revealing potential modification patterns consistent with other bioactive peptides. Identifying the potential biological function of P27 would help characterize a seemingly overlooked fragment within the RSV fusion protein, which has remained at the forefront of vaccine and antiviral development for nearly six decades.

Elucidating the structure and function of these infection critical viral fusion proteins may present opportunities for more specific treatments and antivirals. As seen in SARS-CoV-2, vaccines targeting the fusion protein have been successful in preventing severe illness. As we continue to learn about viral fusion and entry, similar vaccines may be on the horizon for other viruses that continue to be a worldwide burden.

## APPENDIX: ABBREVIATIONS

|              |   |
|--------------|---|
| ACE2         | Human angiotensin converting enzyme 2           |
| BRSV         | Bovine respiratory syncytial virus              |
| Cath L       | Cathepsin L                                     |
| CoV          | Coronavirus                                     |
| COVID-19     | Coronavirus disease of 2019                     |
| CT           | Cytoplasmic tail domain                         |
| ER           | Endoplasmic reticulum                           |
| F            | Fusion protein                                  |
| FCS1         | Furin cleavage site 1                           |
| FCS2         | Furin cleavage site 2                           |
| FP           | Fusion peptide                                  |
| G            | Attachment protein                              |
| HeV          | Hendra Virus                                    |
| HIV-1        | Human immunodeficiency virus type 1             |
| HMPV         | Human metapneumovirus                           |
| Hpt          | Hours post transfection                         |
| HR           | Heptad repeat                                   |
| L-I Zipper   | Leucine-Isoleucine zipper                       |
| MERS         | Middle eastern respiratory syndrome coronavirus |
| Pep27 or P27 | Peptide 27                                      |
| RSV          | Respiratory syncytial virus                     |
| S            | Spike protein                                   |
| SARS         | Severe acute respiratory syndrome coronavirus   |
| SARS-CoV-2   | Severe acute respiratory syndrome coronavirus 2 |
| TM           | Transmembrane                                   |
| TMD          | Transmembrane domain                            |
| TMPRSS2      | Transmembrane serine protease 2                 |
| WT           | Wild-type                                       |

## REFERENCES:

1. Amarasinghe, G.K., Aréchiga Ceballos, N.G., Banyard, A.C., Basler, C.F., Bavari, S., Bennett, A.J., Blasdel, K.R., Briese, T., Bukreyev, A., Cai, Y., Calisher, C.H., Campos Lawson, C., Chandran, K., Chapman, C.A., Chiu, C.Y., Choi, K.S., Collins, P.L., Dietzgen, R.G., Dolja, V. v., Dolnik, O., Domier, L.L., Dürrwald, R., Dye, J.M., Easton, A.J., Ebihara, H., Echevarría, J.E., Fooks, A.R., Formenty, P.B.H., Fouchier, R.A.M., Freuling, C.M., Ghedin, E., Goldberg, T.L., Hewson, R., Horie, M., Hyndman, T.H., Jiāng, D., Kityo, R., Kobinger, G.P., Kondō, H., Koonin, E. v., Krupovic, M., Kurath, G., Lamb, R.A., Lee, B., Leroy, E.M., Maes, P., Maisner, A., Marston, D.A., Mor, S.K., Müller, T., Mühlberger, E., Ramírez, V.M.N., Netesov, S. v., Ng, T.F.F., Nowotny, N., Palacios, G., Patterson, J.L., Pawęska, J.T., Payne, S.L., Prieto, K., Rima, B.K., Rota, P., Rubbenstroth, D., Schwemmle, M., Siddell, S., Smither, S.J., Song, Q., Song, T., Stenglein, M.D., Stone, D.M., Takada, A., Tesh, R.B., Thomazelli, L.M., Tomonaga, K., Tordo, N., Towner, J.S., Vasilakis, N., Vázquez-Morón, S., Verdugo, C., Volchkov, V.E., Wahl, V., Walker, P.J., Wang, D., Wang, L.F., Wellehan, J.F.X., Wiley, M.R., Whitfield, A.E., Wolf, Y.I., Yè, G., Zhāng, Y.Z., Kuhn, J.H.: Taxonomy of the order Mononegavirales: update 2018. *Arch Virol.* 163, 2283–2294 (2018). <https://doi.org/10.1007/s00705-018-3814-x>
2. Husby, M.L., Stahelin, R. v.: Negative-sense rna viruses: An underexplored platform for examining virus-host lipid interactions, (2021)
3. Latorre, V., Mattenberger, F., Geller, R.: Chaperoning the mononegavirales: Current knowledge and future directions, (2018)
4. Ortega, V., Stone, J.A., Contreras, E.M., Iorio, R.M., Aguilar, H.C.: Addicted to sugar: Roles of glycans in the order Mononegavirales, (2019)
5. Ebel, H., Benecke, T., Vollmer, B.: Stabilisation of Viral Membrane Fusion Proteins in Prefusion Conformation by Structure-Based Design for Structure Determination and Vaccine Development, (2022)
6. White, J.M., Delos, S.E., Brecher, M., Schornberg, K.: Structures and mechanisms of viral membrane fusion proteins: Multiple variations on a common theme, (2008)
7. Harrison, S.C.: Viral membrane fusion, (2008)
8. Harrison, S.C.: Viral membrane fusion, (2015)
9. Wormald, M.R., Dwek, R.A.: Glycoproteins: glycan presentation and protein-fold stability. *Structure.* 7, 155–160 (1999)

10. Bradel-Tretheway, B.G., Liu, Q., Stone, J.A., McInally, S., Aguilar, H.C.: Novel Functions of Hendra Virus G N-Glycans and Comparisons to Nipah Virus. *J Virol.* 89, 7235–7247 (2015). <https://doi.org/10.1128/jvi.00773-15>
11. Watanabe, Y., Bowden, T.A., Wilson, I.A., Crispin, M.: Exploitation of glycosylation in enveloped virus pathobiology, (2019)
12. Fischer, K., Topallar, S., Kraatz, F., Groschup, M.H., Diederich, S.: The role of N-linked glycosylation in proteolytic processing and cell surface transport of the Cedar virus fusion protein. *Virol J.* 19, (2022). <https://doi.org/10.1186/s12985-022-01864-5>
13. Bagdonaite, I., Wandall, H.H.: Global aspects of viral glycosylation, (2018)
14. Li, Y., Liu, D., Wang, Y., Su, W., Liu, G., Dong, W.: The Importance of Glycans of Viral and Host Proteins in Enveloped Virus Infection, (2021)
15. Fischer, K., Topallar, S., Kraatz, F., Groschup, M.H., Diederich, S.: The role of N-linked glycosylation in proteolytic processing and cell surface transport of the Cedar virus fusion protein. *Virol J.* 19, (2022). <https://doi.org/10.1186/s12985-022-01864-5>
16. Kohli, E., Causse, S., Baverel, V., Dubrez, L., Borges-Bonan, N., Demidov, O., Garrido, C.: Endoplasmic Reticulum Chaperones in Viral Infection: Therapeutic Perspectives. (2021)
17. Klenk, H.-D., Wagner, R., Heuer, D., Wolff, T.: Importance of hemagglutinin glycosylation for the biological functions of influenza virus. (2002)
18. Gallagher, P.J., Henneberry, J.M., Sambrook, J.F., Gething, M.-J.H.: Glycosylation Requirements for Intracellular Transport and Function of the Hemagglutinin of Influenza Virus. (1992)
19. Wanzeck, K., Boyd, K.L., McCullers, J.A.: Glycan shielding of the influenza virus hemagglutinin contributes to immunopathology in mice. *Am J Respir Crit Care Med.* 183, 767–773 (2011). <https://doi.org/10.1164/rccm.201007-1184OC>
20. Stone, J.A., Nicola, A. V., Baum, L.G., Aguilar, H.C.: Multiple Novel Functions of Henipavirus O-glycans: The First O-glycan Functions Identified in the Paramyxovirus Family. *PLoS Pathog.* 12, (2016). <https://doi.org/10.1371/journal.ppat.1005445>
21. Düzgüneş, N., Fernandez-Fuentes, N., Konopka, K.: Inhibition of viral membrane fusion by peptides and approaches to peptide design, (2021)
22. Wild, C.T., Shugars, D.C., Greenwell, T.K., Mcdanal, C.B., Matthews, T.J.: Peptides corresponding to a predictive  $\alpha$ -helical domain of human

immunodeficiency virus type 1 gp41 are potent inhibitors of virus infection. (1994)

23. Outlaw, V.K., Bovier, F.T., Mears, M.C., Cajimat, M.N., Zhu, Y., Lin, M.J., Addetia, A., Lieberman, N.A.P., Peddu, V., Xie, X., Shi, P.Y., Greninger, A.L., Gellman, S.H., Bente, D.A., Moscona, A., Porotto, M.: Inhibition of coronavirus entry in vitro and ex vivo by a lipid-conjugated peptide derived from the sars-cov-2 spike glycoprotein hrc domain. *mBio*. 11, 1–14 (2020). <https://doi.org/10.1128/mBio.01935-20>
24. Vigant, F., Santos, N.C., Lee, B.: Broad-spectrum antivirals against viral fusion, (2015)
25. Zimmerberg, J., Kozlov, M.M.: How proteins produce cellular membrane curvature, (2006)
26. Porotto, M., Rockx, B., Yokoyama, C.C., Talekar, A., DeVito, I., Palermo, L.M., Liu, J., Cortese, R., Lu, M., Feldmann, H., Pessi, A., Moscona, A.: Inhibition of Nipah Virus Infection In Vivo: Targeting an early stage of paramyxovirus fusion activation during viral entry. *PLoS Pathog*. 6, (2010). <https://doi.org/10.1371/journal.ppat.1001168>
27. Porotto, M., Yokoyama, C.C., Palermo, L.M., Mungall, B., Aljofan, M., Cortese, R., Pessi, A., Moscona, A.: Viral Entry Inhibitors Targeted to the Membrane Site of Action. *J Virol*. 84, 6760–6768 (2010). <https://doi.org/10.1128/jvi.00135-10>
28. San-Juan-Vergara, H., Sampayo-Escobar, V., Reyes, N., Cha, B., Pacheco-Lugo, L., Wong, T., Peeples, M.E., Collins, P.L., Castaño, M.E., Mohapatra, S.S.: Cholesterol-Rich Microdomains as Docking Platforms for Respiratory Syncytial Virus in Normal Human Bronchial Epithelial Cells. *J Virol*. 86, 1832–1843 (2012). <https://doi.org/10.1128/jvi.06274-11>
29. Van Der Gucht, W., Leemans, A., De Schryver, M., Heykers, A., Caljon, G., Maes, L., Cos, P., Delputte, P.L.: Respiratory syncytial virus (RSV) entry is inhibited by serine protease inhibitor AEBSF when present during an early stage of infection. *Virol J*. 14, (2017). <https://doi.org/10.1186/s12985-017-0824-3>
30. De Wit, E., Van Doremalen, N., Falzarano, D., Munster, V.J.: SARS and MERS: Recent insights into emerging coronaviruses, (2016)
31. Song, Z., Xu, Y., Bao, L., Zhang, L., Yu, P., Qu, Y., Zhu, H., Zhao, W., Han, Y., Qin, C.: From SARS to MERS, thrusting coronaviruses into the spotlight, (2019)
32. Lu, G., Wang, Q., Gao, G.F.: Bat-to-human: Spike features determining “host jump” of coronaviruses SARS-CoV, MERS-CoV, and beyond, (2015)

33. Masters, P.S.: *The Molecular Biology of Coronaviruses*, (2006)
34. World Health Organization: WHO Coronavirus Disease (COVID-19) Dashboard. <https://covid19.who.int/> . (2020)
35. Shang, J., Wan, Y., Luo, C., Ye, G., Geng, Q., Auerbach, A., Li, F.: Cell entry mechanisms of SARS-CoV-2. <https://doi.org/10.1073/pnas.2003138117/-/DCSupplemental>
36. Li, F.: *Structure, Function, and Evolution of Coronavirus Spike Proteins*, (2016)
37. Li, W., Moore, M., Vasilieva, N., Sui, J., Wong, S., Berne, M., Somasundaran, M., Sullivan, J., Luzuriaga, K., Greenough, T., Choe, H., Farzan, M.: Angiotensin-converting enzyme 2 is a functional receptor for the SARS coronavirus. *Nature*. 426, 450–454 (2003)
38. Matsuyama, S., Ujike, M., Morikawa, S., Tashiro, M., Taguchi, F.: Protease-mediated enhancement of severe acute respiratory syndrome coronavirus infection. (2005)
39. Gallagher, T.M., Buchmeier, M.J.: Coronavirus spike proteins in viral entry and pathogenesis. *Virology*. 279, 371–374 (2001). <https://doi.org/10.1006/viro.2000.0757>
40. Coutard, B., Valle, C., de Lamballerie, X., Canard, B., Seidah, N.G., Decroly, E.: The spike glycoprotein of the new coronavirus 2019-nCoV contains a furin-like cleavage site absent in CoV of the same clade. *Antiviral Res.* 176, (2020). <https://doi.org/10.1016/j.antiviral.2020.104742>
41. Hatmal, M.M., Alshaer, W., Al-Hatamleh, M.A.I., Hatmal, M., Smadi, O., Taha, M.O., Oweida, A.J., Boer, J.C., Mohamud, R., Plebanski, M.: Comprehensive Structural and Molecular Comparison of Spike Proteins of SARS-CoV-2, SARS-CoV and MERS-CoV, and Their Interactions with ACE2, (2020)
42. Zhu, Z., Lian, X., Su, X., Wu, W., Marraro, G.A., Zeng, Y.: From SARS and MERS to COVID-19: A brief summary and comparison of severe acute respiratory infections caused by three highly pathogenic human coronaviruses, (2020)
43. Du, L., Yang, Y., Zhou, Y., Lu, L., Li, F., Jiang, S.: MERS-CoV spike protein: a key target for antivirals, (2017)
44. Ledford, H.: Moderna COVID vaccine becomes second to get US authorization. *Nature*. (2020). <https://doi.org/10.1038/d41586-020-03593-7>
45. Dooling, K., McClung, N., Chamberland, M., Marin, M., Wallace, M., Bell, B.P., Lee, G.M., Talbot, H.K., Romero, J.R., Oliver, S.E.: The Advisory



Committee on Immunization Practices' Interim Recommendation for Allocating Initial Supplies of COVID-19 Vaccine — United States, 2020. *MMWR Morb Mortal Wkly Rep.* 69, 1857–1859 (2020). <https://doi.org/10.15585/mmwr.mm6949e1>

46. Chang, A., Dutch, R.E.: Paramyxovirus fusion and entry: Multiple Paths to a common end, (2012)
47. Dutch, R.E.: Entry and fusion of emerging paramyxoviruses. *PLoS Pathog.* 6, (2010). <https://doi.org/10.1371/journal.ppat.1000881>
48. Smith, E.C., Popa, A., Chang, A., Masante, C., Dutch, R.E.: Viral entry mechanisms: The increasing diversity of paramyxovirus entry, (2009)
49. Meulendyke, K.A., Wurth, M.A., McCann, R.O., Dutch, R.E.: Endocytosis Plays a Critical Role in Proteolytic Processing of the Hendra Virus Fusion Protein. *J Virol.* 79, 12643–12649 (2005). <https://doi.org/10.1128/jvi.79.20.12643-12649.2005>
50. Bonaparte, M.I., Dimitrov, A.S., Bossart, K.N., Crameri, G., Mungall, B.A., Bishop, K.A., Choudhry, V., Dimitrov, D.S., Wang, L.-F., Eaton, B.T., Broder, C.C.: Ephrin-B2 ligand is a functional receptor for Hendra virus and Nipah virus. (2005)
51. Langosch, D., Arkin, I.T.: Interaction and conformational dynamics of membrane-spanning protein helices, (2009)
52. Moore, D.T., Berger, B.W., DeGrado, W.F.: Protein-Protein Interactions in the Membrane: Sequence, Structural, and Biological Motifs, (2008)
53. Mühlebach, M.D., Leonard, V.H.J., Cattaneo, R.: The Measles Virus Fusion Protein Transmembrane Region Modulates Availability of an Active Glycoprotein Complex and Fusion Efficiency. *J Virol.* 82, 11437–11445 (2008). <https://doi.org/10.1128/jvi.00779-08>
54. Talbert-Slagle, K., Marlatt, S., Barrera, F.N., Khurana, E., Oates, J., Gerstein, M., Engelman, D.M., Dixon, A.M., DiMaio, D.: Artificial Transmembrane Oncoproteins Smaller than the Bovine Papillomavirus E5 Protein Redefine Sequence Requirements for Activation of the Platelet-Derived Growth Factor  $\beta$  Receptor. *J Virol.* 83, 9773–9785 (2009). <https://doi.org/10.1128/jvi.00946-09>
55. Talbert-Slagle, K., DiMaio, D.: The bovine papillomavirus E5 protein and the PDGF  $\beta$  receptor: It takes two to tango, (2009)
56. Miyauchi, K., Curran, A.R., Long, Y., Kondo, N., Iwamoto, A., Engelman, D.M., Matsuda, Z.: The membrane-spanning domain of gp41 plays a

- critical role in intracellular trafficking of the HIV envelope protein. *Retrovirology*. 7, (2010). <https://doi.org/10.1186/1742-4690-7-95>
57. Yin, H.S., Wen, X., Paterson, R.G., Lamb, R.A., Jardetzky, T.S.: Structure of the parainfluenza virus 5 F protein in its metastable, prefusion conformation. *Nature*. 439, 38–44 (2006). <https://doi.org/10.1038/nature04322>
  58. Webb, S., Nagy, T., Moseley, H., Fried, M., Dutch, R.: Hendra virus fusion protein transmembrane domain contributes to pre-fusion protein stability. *Journal of Biological Chemistry*. 292, 5685–5694 (2017). <https://doi.org/10.1074/jbc.M117.777235>
  59. Bissonnette, M.L.Z., Donald, J.E., DeGrado, W.F., Jardetzky, T.S., Lamb, R.A.: Functional Analysis of the Transmembrane Domain in Paramyxovirus F Protein-Mediated Membrane Fusion. *J Mol Biol*. 386, 14–36 (2009). <https://doi.org/10.1016/j.jmb.2008.12.029>
  60. Smith, E.C., Culler, M.R., Hellman, L.M., Fried, M.G., Creamer, T.P., Dutch, R.E.: Beyond Anchoring: the Expanding Role of the Hendra Virus Fusion Protein Transmembrane Domain in Protein Folding, Stability, and Function. *J Virol*. 86, 3003–3013 (2012). <https://doi.org/10.1128/jvi.05762-11>
  61. Popa, A., Carter, J.R., Smith, S.E., Hellman, L., Fried, M.G., Dutch, R.E.: Residues in the Hendra Virus Fusion Protein Transmembrane Domain Are Critical for Endocytic Recycling. *J Virol*. 86, 3014–3026 (2012). <https://doi.org/10.1128/jvi.05826-11>
  62. Smith, E.C., Smith, S.E., Carter, J.R., Webb, S.R., Gibson, K.M., Hellman, L.M., Fried, M.G., Dutch, R.E.: Trimeric transmembrane domain interactions in paramyxovirus fusion proteins: Roles in protein folding, stability, and function. *Journal of Biological Chemistry*. 288, 35726–35735 (2013). <https://doi.org/10.1074/jbc.M113.514554>
  63. Amarasinghe, G.K., Ayllón, M.A., Bào, Y., Basler, C.F., Bavari, S., Blasdel, K.R., Briese, T., Brown, P.A., Bukreyev, A., Balkema-Buschmann, A., Buchholz, U.J., Chabi-Jesus, C., Chandran, K., Chiapponi, C., Crozier, I., de Swart, R.L., Dietzgen, R.G., Dolnik, O., Drexler, J.F., Dürrwald, R., Dundon, W.G., Duprex, W.P., Dye, J.M., Easton, A.J., Fooks, A.R., Formenty, P.B.H., Fouchier, R.A.M., Freitas-Astúa, J., Griffiths, A., Hewson, R., Horie, M., Hyndman, T.H., Jiāng, D., Kitajima, E.W., Kobinger, G.P., Kondō, H., Kurath, G., Kuzmin, I. v., Lamb, R.A., Lavazza, A., Lee, B., Lelli, D., Leroy, E.M., Lǐ, J., Maes, P., Marzano, S.Y.L., Moreno, A., Mühlberger, E., Netesov, S. v., Nowotny, N., Nylund, A., Økland, A.L., Palacios, G., Pályi, B., Pawęska, J.T., Payne, S.L., Prospero, A., Ramos-

- González, P.L., Rima, B.K., Rota, P., Rubbenstroth, D., Shī, M., Simmonds, P., Smither, S.J., Sozzi, E., Spann, K., Stenglein, M.D., Stone, D.M., Takada, A., Tesh, R.B., Tomonaga, K., Tordo, N., Towner, J.S., van den Hoogen, B., Vasilakis, N., Wahl, V., Walker, P.J., Wang, L.F., Whitfield, A.E., Williams, J. v., Zerbini, F.M., Zhāng, T., Zhang, Y.Z., Kuhn, J.H.: Taxonomy of the order Mononegavirales: update 2019. *Arch Virol.* 164, 1967–1980 (2019). <https://doi.org/10.1007/s00705-019-04247-4>
64. King, A., Adams, M., Carstens, E., Lefkowitz, E.: Part II-The Negative Sense Single Stranded RNA Viruses *Virus Taxonomy: Ninth Report of the International Committee on Taxonomy of Viruses Family Paramyxoviridae.* (2012)
  65. Masante, C., el Najjar, F., Chang, A., Jones, A., Moncman, C.L., Dutch, R.E.: The Human Metapneumovirus Small Hydrophobic Protein Has Properties Consistent with Those of a Viroporin and Can Modulate Viral Fusogenic Activity. *J Virol.* 88, 6423–6433 (2014). <https://doi.org/10.1128/JVI.02848-13/ASSET/2A4D7D4C-1E7E-44AB-8F19-7FD7277B1B33/ASSETS/GRAPHIC/ZJV9990990830007.JPEG>
  66. Gan, S.-W., Tan, E., Lin, X., Yu, D., Wang, J., Ming-Yeong Tan, G., Vararattanavech, A., Ying Yeo, C., Huang Soon, C., Wah Soong, T., Pervushin, K., Torres, J.: The Small Hydrophobic Protein of the Human Respiratory Syncytial Virus Forms Pentameric Ion Channels \* □ S. (2012). <https://doi.org/10.1074/jbc.M111.332791>
  67. Fuentes, S., Tran, K.C., Luthra, P., Teng, M.N., He, B.: Function of the Respiratory Syncytial Virus Small Hydrophobic Protein. *J Virol.* 81, 8361–8366 (2007). <https://doi.org/10.1128/JVI.02717-06>
  68. Anderson, L.J., Hierholzer, J.C., Tsou, C., Hendry, R.M., Fernie, B.F., Stone, Y., McIntosh, K.: Antigenic Characterization of Respiratory Syncytial Virus Strains with Monoclonal Antibodies. (1985)
  69. Maurice Mufson, B.A., Orvell, C., Rafnar, B., Norrby, E.: Two Distinct Subtypes of Human Respiratory Syncytial Virus. (1985)
  70. Moore, M.L., Stokes, K.L., Hartert, T. V: The Impact of Viral Genotype on Pathogenesis and Disease Severity: Respiratory Syncytial Virus and Human Rhinoviruses. (2013)
  71. Otieno, J.R., Kamau, E.M., Agoti, C.N., Lewa, C., Otieno, G., Bett, A., Ngama, M., Cane, P.A., Nokes, D.J.: Spread and evolution of respiratory syncytial virus a genotype ON1, coastal Kenya, 2010-2015. *Emerg Infect Dis.* 23, 264–271 (2017). <https://doi.org/10.3201/eid2302.161149>

72. Esposito, S., Piralla, A., Zampiero, A., Bianchini, S., Di Pietro, G., Scala, A., Pinzani, R., Fossali, E., Baldanti, F., Principi, N.: Characteristics and their clinical relevance of respiratory syncytial virus types and genotypes circulating in Northern Italy in five consecutive winter seasons. *PLoS One*. 10, (2015). <https://doi.org/10.1371/journal.pone.0129369>
73. Pandya, M.C., Callahan, S.M., Savchenko, K.G., Stobart, C.C.: A contemporary view of respiratory syncytial virus (RSV) biology and strain-specific differences, (2019)
74. Zlateva, K.T., Lemey, P., Moës, E., Vandamme, A.-M., Van Ranst, M.: Genetic Variability and Molecular Evolution of the Human Respiratory Syncytial Virus Subgroup B Attachment G Protein. *J Virol*. 79, 9157–9167 (2005). <https://doi.org/10.1128/jvi.79.14.9157-9167.2005>
75. Arnott, A., Vong, S., Mardy, S., Chu, S., Naughtin, M., Sovann, L., Buecher, C., Beauté, J., Rith, S., Borand, L., Asgari, N., Frutos, R., Guillard, B., Touch, S., Deubel, V., Buchy, P.: A study of the genetic variability of human respiratory syncytial virus (HRSV) in Cambodia reveals the existence of a new HRSV group B genotype. *J Clin Microbiol*. 49, 3504–3513 (2011). <https://doi.org/10.1128/JCM.01131-11>
76. Trento, A., Viegas, M., Galiano, M., Videla, C., Carballal, G., Mistchenko, A.S., Melero, J.A.: Natural History of Human Respiratory Syncytial Virus Inferred from Phylogenetic Analysis of the Attachment (G) Glycoprotein with a 60-Nucleotide Duplication. *J Virol*. 80, 975–984 (2006). <https://doi.org/10.1128/jvi.80.2.975-984.2006>
77. Collins, P.L., Mottett, G.: Post-translational processing and oligomerization of the fusion glycoprotein of human respiratory syncytial virus. (1991)
78. Smith, E.C., Popa, A., Chang, A., Masante, C., Dutch, R.E.: Viral entry mechanisms: The increasing diversity of paramyxovirus entry, (2009)
79. Elango, N., Satake, M., Coligan, J.E., Norrby, E., Camargo, E., Venkatesan, S.: Nucleic Acids Research Respiratory syncytial virus fusion glycoprotein: nucleotide sequence of mRNA, identification of cleavage activation site and amino acid sequence of N-terminus of F1 subunit.
80. Collins, P.L., Huang, Y.T., Wertz, G.W.: Nucleotide Sequence of the Gene Encoding the Fusion (F) Glycoprotein of Human Respiratory Syncytial Virus. (1984)
81. Basak, A., Zhong, M., Munzer, J.S., Chre, M., Tien, I., Seidah, N.G.: Implication of the proprotein convertases furin, PC5 and PC7 in the cleavage of surface glycoproteins of Hong Kong, Ebola and respiratory syncytial viruses : a comparative analysis with fluorogenic peptides. (2001)

82. Bolt, G., Pedersen, L.Ø., Birkeslund, H.H.: Cleavage of the respiratory syncytial virus fusion protein is required for its surface expression: role of furin. *Virus Res.* 68, 25–33 (2000). [https://doi.org/10.1016/S0168-1702\(00\)00149-0](https://doi.org/10.1016/S0168-1702(00)00149-0)
83. Zimmer, G., Budz, L., Herrler, G.: Proteolytic Activation of Respiratory Syncytial Virus Fusion Protein. *Journal of Biological Chemistry.* 276, 31642–31650 (2001). <https://doi.org/10.1074/jbc.M102633200>
84. Gonzá Lez-Reyes, L., Begoñ A Ruiz-Argü Ello, M., García-Barreno, B., Calder, L., Ló Pez §, J.A., Albar, J.P., Skehel, J.J., Wiley, D.C., Melero, J.A.: Cleavage of the human respiratory syncytial virus fusion protein at two distinct sites is required for activation of membrane fusion.
85. Zimmer, G., Conzelmann, K.-K., Herrler, G.: Cleavage at the Furin Consensus Sequence RAR/KR 109 and Presence of the Intervening Peptide of the Respiratory Syncytial Virus Fusion Protein Are Dispensable for Virus Replication in Cell Culture. *J Virol.* 76, 9218–9224 (2002). <https://doi.org/10.1128/JVI.76.18.9218-9224.2002>
86. Rawling, J., Cano, O., Garcin, D., Kolakofsky, D., Melero, J.A.: Recombinant Sendai Viruses Expressing Fusion Proteins with Two Furin Cleavage Sites Mimic the Syncytial and Receptor-Independent Infection Properties of Respiratory Syncytial Virus. *J Virol.* 85, 2771–2780 (2011). <https://doi.org/10.1128/JVI.02065-10>
87. Techaarpornkul, S., Barretto, N., Peeples, M.E.: Functional Analysis of Recombinant Respiratory Syncytial Virus Deletion Mutants Lacking the Small Hydrophobic and/or Attachment Glycoprotein Gene. *J Virol.* 75, 6825–6834 (2001). <https://doi.org/10.1128/jvi.75.15.6825-6834.2001>
88. Hause, A.M., Henke, D.M., Avadhanula, V., Shaw, C.A., Tapia, L.I., Piedra, P.A.: Sequence variability of the respiratory syncytial virus (RSV) fusion gene among contemporary and historical genotypes of RSV/A and RSV/B. *PLoS One.* 12, 1–21 (2017). <https://doi.org/10.1371/journal.pone.0175792>
89. Beyene, A., Basu, A., Meyer, K., Ray, R.: Influence of N-linked glycans on intracellular transport of hepatitis C virus E1 chimeric glycoprotein and its role in pseudotype virus infectivity. *Virology.* 324, 273–285 (2004). <https://doi.org/10.1016/j.virol.2004.03.039>
90. Vigerust, D.J., Shepherd, V.L.: Virus glycosylation: role in virulence and immune interactions, (2007)
91. Ellgaard, L., McCaul, N., Chatsisvili, A., Braakman, I.: Co- and Post-Translational Protein Folding in the ER, (2016)

92. Kimura, H., Nagasawa, K., Kimura, R., Tsukagoshi, H., Matsushima, Y., Fujita, K., Hirano, E., Ishiwada, N., Misaki, T., Oishi, K., Kuroda, M., Ryo, A.: Molecular evolution of the fusion protein (F) gene in human respiratory syncytial virus subgroup B. *Infection, Genetics and Evolution*. 52, 1–9 (2017). <https://doi.org/10.1016/J.MEEGID.2017.04.015>
93. Tan, L., Lemey, P., Houspie, L., Viveen, M.C., Jansen, N.J.G.: Genetic Variability among Complete Human Respiratory Syncytial Virus Subgroup A Genomes: Bridging Molecular Evolutionary Dynamics and Epidemiology. *PLoS One*. 7, 51439 (2012). <https://doi.org/10.1371/journal.pone.0051439>
94. Leemans, A., Boeren, M., Van der Gucht, W., Pintelon, I., Roose, K., Schepens, B., Saelens, X., Bailey, D., Martinet, W., Caljon, G., Maes, L., Cos, P., Delputte, P.: Removal of the N-glycosylation sequon at position N116 located in p27 of the respiratory syncytial virus fusion protein elicits enhanced antibody responses after DNA immunization. *Viruses*. 10, (2018). <https://doi.org/10.3390/v10080426>
95. Klink, H.A., Brady, R.P., Topliff, C.L., Eskridge, K.M., Srikumaran, S., Kelling, C.L.: Influence of bovine respiratory syncytial virus F glycoprotein N-linked glycans on in vitro expression and on antibody responses in BALB/c mice. *Vaccine*. 24, 3388–3395 (2006). <https://doi.org/10.1016/j.vaccine.2005.12.067>
96. Leemans, A., Boeren, M., Van der Gucht, W., Martinet, W., Caljon, G., Maes, L., Cos, P., Delputte, P.: Characterization of the role of N-glycosylation sites in the respiratory syncytial virus fusion protein in virus replication, syncytium formation and antigenicity. *Virus Res*. 266, 58–68 (2019). <https://doi.org/10.1016/j.virusres.2019.04.006>
97. Lee, J., Lee, Y., Klenow, L., Coyle, E.M., Tang, J., Ravichandran, S., Golding, H., Khurana, S.: Protective antigenic sites identified in respiratory syncytial virus fusion protein reveals importance of p27 domain. *EMBO Mol Med*. 14, 1–14 (2022). <https://doi.org/10.15252/emmm.202013847>
98. Krzyzaniak, M.A., Zumstein, M.T., Gerez, J.A., Picotti, P., Helenius, A.: Host Cell Entry of Respiratory Syncytial Virus Involves Macropinocytosis Followed by Proteolytic Activation of the F Protein. *PLoS Pathog*. 9, (2013). <https://doi.org/10.1371/journal.ppat.1003309>
99. Srinivasakumar, N., Ogra, P.L., Flanagan, T.D.: Characteristics of Fusion of Respiratory Syncytial Virus with HEp-2 Cells As Measured by R18 Fluorescence Dequenching Assay. (1991)
100. Smith, E.C., Popa, A., Chang, A., Masante, C., Dutch, R.E.: Viral entry mechanisms: The increasing diversity of paramyxovirus entry, (2009)

101. Smith, E.C., Popa, A., Chang, A., Masante, C., Dutch, R.E.: Viral entry mechanisms: the increasing diversity of paramyxovirus entry. *FEBS J.* 276, 7217–7227 (2009). <https://doi.org/10.1111/J.1742-4658.2009.07401.X>
102. Schowalter, R.M., Chang, A., Robach, J.G., Buchholz, U.J., Dutch, R.E.: Low-pH Triggering of Human Metapneumovirus Fusion: Essential Residues and Importance in Entry. *J Virol.* 83, 1511–1522 (2009). <https://doi.org/10.1128/JVI.01381-08/ASSET/2B7276EC-3671-4B89-8ECC-619C335DBB29/ASSETS/GRAPHIC/ZJV0030914910009.JPEG>
103. Schowalter, R.M., Smith, S.E., Dutch, R.E.: Characterization of Human Metapneumovirus F Protein-Promoted Membrane Fusion: Critical Roles for Proteolytic Processing and Low pH. *J Virol.* 80, 10931–10941 (2006). <https://doi.org/10.1128/JVI.01287-06/ASSET/C5369958-5900-406F-AA99-E37A4950016D/ASSETS/GRAPHIC/ZJV0220684030007.JPEG>
104. McLaughlin, J.M., Khan, F., Schmitt, H.J., Agosti, Y., Jodar, L., Simoes, E.A.F., Swerdlow, D.L.: Respiratory Syncytial Virus-Associated Hospitalization Rates among US Infants: A Systematic Review and Meta-Analysis, (2022)
105. Kolokoltsov, A.A., Deniger, D., Fleming, E.H., Roberts, N.J., Karpilow, J.M., Davey, R.A.: Small Interfering RNA Profiling Reveals Key Role of Clathrin-Mediated Endocytosis and Early Endosome Formation for Infection by Respiratory Syncytial Virus. *J Virol.* 81, 7786–7800 (2007). <https://doi.org/10.1128/jvi.02780-06>
106. Gilman, M.S.A., Moin, S.M., Mas, V., Chen, M., Patel, N.K., Kramer, K., Zhu, Q., Kabeche, S.C., Kumar, A., Palomo, C., Beaumont, T., Baxa, U., Ulbrandt, N.D., Melero, J.A., Graham, B.S., McLellan, J.S.: Characterization of a Prefusion-Specific Antibody That Recognizes a Quaternary, Cleavage-Dependent Epitope on the RSV Fusion Glycoprotein. *PLoS Pathog.* 11, (2015). <https://doi.org/10.1371/journal.ppat.1005035>
107. Krarup, A., Truan, D., Furmanova-Hollenstein, P., Bogaert, L., Bouchier, P., Bisschop, I.J.M., Widjojatmodjo, M.N., Zahn, R., Schuitemaker, H., McLellan, J.S., Langedijk, J.P.M.: A highly stable prefusion RSV F vaccine derived from structural analysis of the fusion mechanism. *Nat Commun.* 6, 8143 (2015). <https://doi.org/10.1038/ncomms9143>
108. McLellan, J.S., Ray, W.C., Peeples, M.E.: Structure and Function of Respiratory Syncytial Virus Surface Glycoproteins. In: *Current Topics in Microbiology and Immunology*. pp. 83–104 (2013)
109. Gilman, M.S.A., Furmanova-Hollenstein, P., Pascual, G., B. van 't Wout, A., Langedijk, J.P.M., McLellan, J.S.: Transient opening of trimeric

- prefusion RSV F proteins. *Nat Commun.* 10, 2105 (2019).  
<https://doi.org/10.1038/s41467-019-09807-5>
110. Liu, J., Bartesaghi, A., Borgnia, M.J., Sapiro, G., Subramaniam, S.: Molecular architecture of native HIV-1 gp120 trimers. *Nature.* 455, 109–113 (2008). <https://doi.org/10.1038/nature07159>
  111. Rutten, L., Lai, Y.T., Blokland, S., Truan, D., Bisschop, I.J.M., Strokappe, N.M., Koornneef, A., van Manen, D., Chuang, G.Y., Farney, S.K., Schuitemaker, H., Kwong, P.D., Langedijk, J.P.M.: A Universal Approach to Optimize the Folding and Stability of Prefusion-Closed HIV-1 Envelope Trimers. *Cell Rep.* 23, 584–595 (2018).  
<https://doi.org/10.1016/j.celrep.2018.03.061>
  112. Munro, J.B., Gorman, J., Ma, X., Zhou, Z., Arthos, J., Burton, D.R., Koff, W.C., Courter, J.R., Smith, A.B., Kwong, P.D., Blanchard, S.C., Mothes, W.: Conformational dynamics of single HIV-1 envelope trimers on the surface of native virions. *Science* (1979). 346, 759–763 (2014).  
<https://doi.org/10.1126/science.1254426>
  113. Tortorici, M.A., Veesler, D.: Structural insights into coronavirus entry. In: *Advances in Virus Research* (2019)
  114. Benton, D.J., Gamblin, S.J., Rosenthal, P.B.: Structural transitions in influenza haemagglutinin at membrane fusion pH. (2020).  
<https://doi.org/10.1038/s41586-020-2333-6>
  115. Hoffmann, M., Kleine-Weber, H., Schroeder, S., Krüger, N., Herrler, T., Erichsen, S., Schiergens, T.S., Herrler, G., Wu, N.H., Nitsche, A., Müller, M.A., Drosten, C., Pöhlmann, S.: SARS-CoV-2 Cell Entry Depends on ACE2 and TMPRSS2 and Is Blocked by a Clinically Proven Protease Inhibitor. *Cell.* 181, (2020). <https://doi.org/10.1016/j.cell.2020.02.052>
  116. Lan, J., Ge, J., Yu, J., Shan, S., Zhou, H., Fan, S., Zhang, Q., Shi, X., Wang, Q., Zhang, L., Wang, X.: Structure of the SARS-CoV-2 spike receptor-binding domain bound to the ACE2 receptor. *Nature.* 581, (2020).  
<https://doi.org/10.1038/s41586-020-2180-5>
  117. Luan, J., Lu, Y., Jin, X., Zhang, L.: Spike protein recognition of mammalian ACE2 predicts the host range and an optimized ACE2 for SARS-CoV-2 infection. *Biochem Biophys Res Commun.* 526, (2020).  
<https://doi.org/10.1016/j.bbrc.2020.03.047>
  118. Shang, J., Ye, G., Shi, K., Wan, Y., Luo, C., Aihara, H., Geng, Q., Auerbach, A., Li, F.: Structural basis of receptor recognition by SARS-CoV-2. *Nature.* 581, (2020). <https://doi.org/10.1038/s41586-020-2179-y>



119. Walls, A.C., Park, Y.J., Tortorici, M.A., Wall, A., McGuire, A.T., Veesler, D.: Structure, Function, and Antigenicity of the SARS-CoV-2 Spike Glycoprotein. *Cell*. 181, (2020). <https://doi.org/10.1016/j.cell.2020.02.058>
120. Wang, Q., Zhang, Y., Wu, L., Niu, S., Song, C., Zhang, Z., Lu, G., Qiao, C., Hu, Y., Yuen, K.Y., Wang, Q., Zhou, H., Yan, J., Qi, J.: Structural and Functional Basis of SARS-CoV-2 Entry by Using Human ACE2. *Cell*. 181, (2020). <https://doi.org/10.1016/j.cell.2020.03.045>
121. Zhou, P., Yang, X. Lou, Wang, X.G., Hu, B., Zhang, L., Zhang, W., Si, H.R., Zhu, Y., Li, B., Huang, C.L., Chen, H.D., Chen, J., Luo, Y., Guo, H., Jiang, R. Di, Liu, M.Q., Chen, Y., Shen, X.R., Wang, X., Zheng, X.S., Zhao, K., Chen, Q.J., Deng, F., Liu, L.L., Yan, B., Zhan, F.X., Wang, Y.Y., Xiao, G.F., Shi, Z.L.: A pneumonia outbreak associated with a new coronavirus of probable bat origin. *Nature*. 579, (2020). <https://doi.org/10.1038/s41586-020-2012-7>
122. Yan, R., Zhang, Y., Li, Y., Xia, L., Guo, Y., Zhou, Q.: Structural basis for the recognition of SARS-CoV-2 by full-length human ACE2. *Science* (1979). 367, (2020). <https://doi.org/10.1126/science.abb2762>
123. Harrison, S.C.: Viral Membrane Fusion. *Virology*. 479, 498–507 (2015). <https://doi.org/10.1016/j.virol.2015.03.043>
124. Belouzard, S., Millet, J.K., Licitra, B.N., Whittaker, G.R.: Mechanisms of coronavirus cell entry mediated by the viral spike protein., (2012)
125. Millet, J.K., Whittaker, G.R.: Host cell proteases: Critical determinants of coronavirus tropism and pathogenesis. *Virus Res*. 202, (2015). <https://doi.org/10.1016/j.virusres.2014.11.021>
126. Millet, J.K., Whittaker, G.R.: Physiological and molecular triggers for SARS-CoV membrane fusion and entry into host cells. *Virology*. 517, (2018). <https://doi.org/10.1016/j.virol.2017.12.015>
127. Hulswit, R.J.G., de Haan, C.A.M., Bosch, B.J.: Coronavirus Spike Protein and Tropism Changes. In: *Advances in Virus Research* (2016)
128. Benton, D.J., Wrobel, A.G., Xu, P., Roustan, C., Martin, S.R., Rosenthal, P.B., Skehel, J.J., Gamblin, S.J.: Receptor binding and priming of the spike protein of SARS-CoV-2 for membrane fusion. *Nature*. 588, (2020). <https://doi.org/10.1038/s41586-020-2772-0>
129. Zheng, Y., Shang, J., Yang, Y., Liu, C., Wan, Y., Geng, Q., Wang, M., Baric, R., Li, F.: Lysosomal Proteases Are a Determinant of Coronavirus Tropism. *J Virol*. 92, (2018). <https://doi.org/10.1128/jvi.01504-18>

130. Boni, M.F., Lemey, P., Jiang, X., Lam, T.T.Y., Perry, B.W., Castoe, T.A., Rambaut, A., Robertson, D.L.: Evolutionary origins of the SARS-CoV-2 sarbecovirus lineage responsible for the COVID-19 pandemic. *Nat Microbiol.* 5, (2020). <https://doi.org/10.1038/s41564-020-0771-4>
131. Menachery, V.D., Dinnon, K.H., Yount, B.L., McAnarney, E.T., Gralinski, L.E., Hale, A., Graham, R.L., Scobey, T., Anthony, S.J., Wang, L., Graham, B., Randell, S.H., Lipkin, W.I., Baric, R.S.: Trypsin Treatment Unlocks Barrier for Zoonotic Bat Coronavirus Infection. *J Virol.* 94, (2020). <https://doi.org/10.1128/jvi.01774-19>
132. Zhou, H., Chen, X., Hu, T., Li, J., Song, H., Liu, Y., Wang, P., Liu, D., Yang, J., Holmes, E.C., Hughes, A.C., Bi, Y., Shi, W.: A Novel Bat Coronavirus Closely Related to SARS-CoV-2 Contains Natural Insertions at the S1/S2 Cleavage Site of the Spike Protein. *Current Biology.* 30, (2020). <https://doi.org/10.1016/j.cub.2020.05.023>
133. Seidah, N.G., Prat, A.: *The biology and therapeutic targeting of the proprotein convertases*, (2012)
134. Braun, E., Sauter, D.: *Furin-mediated protein processing in infectious diseases and cancer*, (2019)
135. Izaguirre, G.: *The Proteolytic Regulation of Virus Cell Entry by Furin and Other Proprotein Convertases*, (2019)
136. Chan, C.M., Woo, P.C.Y., Lau, S.K.P., Tse, H., Chen, H.L., Li, F., Zheng, B.J., Chen, L., Huang, J.D., Yuen, K.Y.: Spike protein, S, of human coronavirus HKU1: Role in viral life cycle and application in antibody detection. *Exp Biol Med.* 233, (2008). <https://doi.org/10.3181/0806-RM-197>
137. Le Coupanec, A., Desforges, M., Meessen-Pinard, M., Dubé, M., Day, R., Seidah, N.G., Talbot, P.J.: Cleavage of a Neuroinvasive Human Respiratory Virus Spike Glycoprotein by Proprotein Convertases Modulates Neurovirulence and Virus Spread within the Central Nervous System. *PLoS Pathog.* 11, (2015). <https://doi.org/10.1371/journal.ppat.1005261>
138. Mille, J.K., Whittaker, G.R.: Host cell entry of Middle East respiratory syndrome coronavirus after two-step, furin-mediated activation of the spike protein. *Proc Natl Acad Sci U S A.* 111, (2014). <https://doi.org/10.1073/pnas.1407087111>
139. Claas, E.C.J., Osterhaus, A.D.M.E., Van Beek, R., De Jong, J.C., Rimmelzwaan, G.F., Senne, D.A., Krauss, S., Shortridge, K.F., Webster, R.G.: Human influenza A H5N1 virus related to a highly pathogenic avian

- influenza virus. *Lancet*. 351, (1998). [https://doi.org/10.1016/S0140-6736\(97\)11212-0](https://doi.org/10.1016/S0140-6736(97)11212-0)
140. Kido, H., Okumura, Y., Takahashi, E., Pan, H.Y., Wang, S., Yao, D., Yao, M., Chida, J., Yano, M.: Role of host cellular proteases in the pathogenesis of influenza and influenza-induced multiple organ failure, (2012)
  141. Sun, X., Tse, L. V., Ferguson, A.D., Whittaker, G.R.: Modifications to the Hemagglutinin Cleavage Site Control the Virulence of a Neurotropic H1N1 Influenza Virus. *J Virol*. 84, (2010). <https://doi.org/10.1128/jvi.00797-10>
  142. Johnson, B.A., Xie, X., Kalveram, B., Lokugamage, K.G., Muruato, A., Zou, J., Zhang, X., Juelich, T., Smith, J.K., Zhang, L., Bopp, N., Schindewolf, C., Vu, M., Vanderheiden, A., Swetnam, D., Plante, J.A., Aguilar, P., Plante, K.S., Lee, B., Weaver, S.C., Suthar, M.S., Routh, A.L., Ren, P., Ku, Z., An, Z., Debbink, K., Shi, P.Y., Freiberg, A.N., Menachery, V.D.: Furin Cleavage Site Is Key to SARS-CoV-2 Pathogenesis. *bioRxiv*. (2020). <https://doi.org/10.1101/2020.08.26.268854>
  143. Matsuyama, S., Ujike, M., Morikawa, S., Tashiro, M., Taguchi, F.: Protease-mediated enhancement of severe acute respiratory syndrome coronavirus infection. *Proc Natl Acad Sci U S A*. 102, (2005). <https://doi.org/10.1073/pnas.0503203102>
  144. Hoffmann, M., Kleine-Weber, H., Pöhlmann, S.: A Multibasic Cleavage Site in the Spike Protein of SARS-CoV-2 Is Essential for Infection of Human Lung Cells. *Mol Cell*. 78, (2020). <https://doi.org/10.1016/j.molcel.2020.04.022>
  145. Zhu, Y., Feng, F., Hu, G., Wang, Y., Yu, Y., Zhu, Y., Xu, W., Cai, X., Sun, Z., Han, W., Ye, R., Chen, H., Ding, Q., Qu, D., Xie, Y., Yuan, Z., Zhang, R.: The S1/S2 boundary of SARS-CoV-2 spike protein modulates cell 1 entry pathways and transmission 2 3. *bioRxiv*. (2020)
  146. Ou, T., Mou, H., Zhang, L., Ojha, A., Choe, H., Farzan, M.: Hydroxychloroquine-mediated inhibition of SARS-CoV-2 entry is attenuated by TMPRSS2. *PLoS Pathog*. 17, (2021). <https://doi.org/10.1371/journal.ppat.1009212>
  147. Buchrieser, J., Dufloo, J., Hubert, M., Monel, B., Planas, D., Rajah, M.M., Planchais, C., Porrot, F., Guivel-Benhassine, F., Van der Werf, S., Casartelli, N., Mouquet, H., Bruel, T., Schwartz, O.: Syncytia formation by SARS-CoV-2-infected cells. *EMBO J*. 39, (2020). <https://doi.org/10.15252/emboj.2020106267>
  148. Bussani, R., Schneider, E., Zentilin, L., Collesi, C., Ali, H., Braga, L., Volpe, M.C., Colliva, A., Zanconati, F., Berlot, G., Silvestri, F., Zacchigna, S.,

- Giacca, M.: Persistence of viral RNA, pneumocyte syncytia and thrombosis are hallmarks of advanced COVID-19 pathology. *EBioMedicine*. 61, (2020). <https://doi.org/10.1016/j.ebiom.2020.103104>
149. Oprinca, G.C., Muja, L.A.: Postmortem examination of three SARS-CoV-2-positive autopsies including histopathologic and immunohistochemical analysis. *Int J Legal Med*. 135, (2021). <https://doi.org/10.1007/s00414-020-02406-w>
  150. Stadlmann, S., Hein-Kuhnt, R., Singer, G.: Viropathic multinuclear syncytial giant cells in bronchial fluid from a patient with COVID-19, (2020)
  151. Tian, S., Hu, W., Niu, L., Liu, H., Xu, H., Xiao, S.Y.: Pulmonary Pathology of Early-Phase 2019 Novel Coronavirus (COVID-19) Pneumonia in Two Patients With Lung Cancer. *Journal of Thoracic Oncology*. 15, (2020). <https://doi.org/10.1016/j.jtho.2020.02.010>
  152. Correction to *Lancet Respir Med* 2021; published online Feb 26. [https://doi.org/10.1016/S2213-2600\(20\)30448-3](https://doi.org/10.1016/S2213-2600(20)30448-3). *Lancet Respir Med*. 9, (2021). [https://doi.org/10.1016/s2213-2600\(21\)00204-6](https://doi.org/10.1016/s2213-2600(21)00204-6)
  153. Hörnich, B.F., Großkopf, A.K., Schlagowski, S., Tenbusch, M., Kleine-Weber, H., Neipel, F., Stahl-Hennig, C., Hahn, A.S.: SARS-CoV-2 and SARS-CoV Spike-Mediated Cell-Cell Fusion Differ in Their Requirements for Receptor Expression and Proteolytic Activation. *J Virol*. 95, (2021). <https://doi.org/10.1128/jvi.00002-21>
  154. Papa, G., Mallery, D.L., Albecka, A., Welch, L.G., Cattin-Ortolá, J., Luptak, J., Paul, D., McMahan, H.T., Goodfellow, I.G., Carter, A., Munro, S., James, L.C.: Furin cleavage of SARS-CoV-2 Spike promotes but is not essential for infection and cell-cell fusion. *PLoS Pathog*. 17, (2021). <https://doi.org/10.1371/journal.ppat.1009246>
  155. Korber, B., Fischer, W.M., Gnanakaran, S., Yoon, H., Theiler, J., Abfalterer, W., Foley, B., Giorgi, E.E., Bhattacharya, T., Parker, M.D., Partridge, D.G., Evans, C.M., Freeman, T.M., de Silva, T.I., LaBranche, C.C., Montefiori, D.C.: Spike mutation pipeline reveals the emergence of a more transmissible form of SARS-CoV-2. *bioRxiv*. (2020)
  156. Korber, B., Fischer, W.M., Gnanakaran, S., Yoon, H., Theiler, J., Abfalterer, W., Hengartner, N., Giorgi, E.E., Bhattacharya, T., Foley, B., Hastie, K.M., Parker, M.D., Partridge, D.G., Evans, C.M., Freeman, T.M., de Silva, T.I., Angyal, A., Brown, R.L., Carrilero, L., Green, L.R., Groves, D.C., Johnson, K.J., Keeley, A.J., Lindsey, B.B., Parsons, P.J., Raza, M., Rowland-Jones, S., Smith, N., Tucker, R.M., Wang, D., Wyles, M.D., McDanal, C., Perez, L.G., Tang, H., Moon-Walker, A., Whelan, S.P., LaBranche, C.C., Saphire, E.O., Montefiori, D.C.: Tracking Changes in

- SARS-CoV-2 Spike: Evidence that D614G Increases Infectivity of the COVID-19 Virus. *Cell*. 182, (2020).  
<https://doi.org/10.1016/j.cell.2020.06.043>
157. Biswas, N., Majumder, P.: Analysis of RNA sequences of 3636 SARS-CoV-2 collected from 55 countries reveals selective sweep of one virus type. *Indian Journal of Medical Research*. 151, (2020).  
[https://doi.org/10.4103/ijmr.IJMR\\_1125\\_20](https://doi.org/10.4103/ijmr.IJMR_1125_20)
158. Gong, Y.N., Tsao, K.C., Hsiao, M.J., Huang, C.G., Huang, P.N., Huang, P.W., Lee, K.M., Liu, Y.C., Yang, S.L., Kuo, R.L., Chen, K.F., Liu, Y.C., Huang, S.Y., Huang, H.I., Liu, M.T., Yang, J.R., Chiu, C.H., Yang, C.T., Chen, G.W., Shih, S.R.: SARS-CoV-2 genomic surveillance in Taiwan revealed novel ORF8-deletion mutant and clade possibly associated with infections in Middle East. *Emerg Microbes Infect.* 9, (2020).  
<https://doi.org/10.1080/22221751.2020.1782271>
159. Isabel, S., Graña-Miraglia, L., Gutierrez, J.M., Bundalovic-Torma, C., Groves, H.E., Isabel, M.R., Eshaghi, A.R., Patel, S.N., Gubbay, J.B., Poutanen, T., Guttman, D.S., Poutanen, S.M.: Evolutionary and structural analyses of SARS-CoV-2 D614G spike protein mutation now documented worldwide. *Sci Rep*. 10, (2020). <https://doi.org/10.1038/s41598-020-70827-z>
160. Islam, O.K., Al-Emran, H.M., Hasan, M.S., Anwar, A., Jahid, M.I.K., Hossain, M.A.: Emergence of European and North American mutant variants of SARS-CoV-2 in South-East Asia. *Transbound Emerg Dis*. 68, (2021). <https://doi.org/10.1111/tbed.13748>
161. Koyama, T., Platt, D., Parida, L.: Variant analysis of SARS-cov-2 genomes. *Bull World Health Organ*. 98, (2020).  
<https://doi.org/10.2471/BLT.20.253591>
162. Koyama, T., Weeraratne, D., Snowdon, J.L., Parida, L.: Emergence of drift variants that may affect covid-19 vaccine development and antibody treatment. *Pathogens*. 9, (2020).  
<https://doi.org/10.3390/pathogens9050324>
163. Mercatelli, D., Giorgi, F.M.: Geographic and Genomic Distribution of SARS-CoV-2 Mutations. *Front Microbiol*. 11, (2020).  
<https://doi.org/10.3389/fmicb.2020.01800>
164. Caldas, L.A., Carneiro, F.A., Higa, L.M., Monteiro, F.L., da Silva, G.P., da Costa, L.J., Durigon, E.L., Tanuri, A., de Souza, W.: Ultrastructural analysis of SARS-CoV-2 interactions with the host cell via high resolution scanning electron microscopy. *Sci Rep*. 10, (2020). <https://doi.org/10.1038/s41598-020-73162-5>

165. Cheng, Y.W., Chao, T.L., Li, C.L., Chiu, M.F., Kao, H.C., Wang, S.H., Pang, Y.H., Lin, C.H., Tsai, Y.M., Lee, W.H., Tao, M.H., Ho, T.C., Wu, P.Y., Jang, L.T., Chen, P.J., Chang, S.Y., Yeh, S.H.: Furin Inhibitors Block SARS-CoV-2 Spike Protein Cleavage to Suppress Virus Production and Cytopathic Effects. *Cell Rep.* 33, (2020).  
<https://doi.org/10.1016/j.celrep.2020.108254>
166. Li, W.: Delving deep into the structural aspects of a furin cleavage site inserted into the spike protein of SARS-CoV-2: A structural biophysical perspective. *Biophys Chem.* 264, (2020).  
<https://doi.org/10.1016/j.bpc.2020.106420>
167. Örd, M., Faustova, I., Loog, M.: The sequence at Spike S1/S2 site enables cleavage by furin and phospho-regulation in SARS-CoV2 but not in SARS-CoV1 or MERS-CoV. *Sci Rep.* 10, (2020). <https://doi.org/10.1038/s41598-020-74101-0>
168. Glowacka, I., Bertram, S., Müller, M.A., Allen, P., Soilleux, E., Pfefferle, S., Steffen, I., Tsegaye, T.S., He, Y., Gnirss, K., Niemeyer, D., Schneider, H., Drosten, C., Pöhlmann, S.: Evidence that TMPRSS2 Activates the Severe Acute Respiratory Syndrome Coronavirus Spike Protein for Membrane Fusion and Reduces Viral Control by the Humoral Immune Response. *J Virol.* 85, (2011). <https://doi.org/10.1128/jvi.02232-10>
169. Simmons, G., Bertram, S., Glowacka, I., Steffen, I., Chaipan, C., Agudelo, J., Lu, K., Rennekamp, A.J., Hofmann, H., Bates, P., Pöhlmann, S.: Different host cell proteases activate the SARS-coronavirus spike-protein for cell-cell and virus-cell fusion. *Virology.* 413, (2011).  
<https://doi.org/10.1016/j.virol.2011.02.020>
170. Simmons, G., Reeves, J.D., Rennekamp, A.J., Amberg, S.M., Piefer, A.J., Bates, P.: Characterization of severe acute respiratory syndrome-associated coronavirus (SARS-CoV) spike glycoprotein-mediated viral entry. *Proc Natl Acad Sci U S A.* 101, (2004).  
<https://doi.org/10.1073/pnas.0306446101>
171. Simmons, G., Gosalia, D.N., Rennekamp, A.J., Reeves, J.D., Diamond, S.L., Bates, P.: Inhibitors of cathepsin L prevent severe acute respiratory syndrome coronavirus entry. *Proc Natl Acad Sci U S A.* 102, (2005).  
<https://doi.org/10.1073/pnas.0505577102>
172. Huang, I.C., Bosch, B.J., Li, F., Li, W., Kyoung, H.L., Ghiran, S., Vasilieva, N., Dermody, T.S., Harrison, S.C., Dormitzer, P.R., Farzan, M., Rottier, P.J.M., Choe, H.: SARS coronavirus, but not human coronavirus NL63, utilizes cathepsin L to infect ACE2-expressing cells. *Journal of Biological Chemistry.* 281, (2006). <https://doi.org/10.1074/jbc.M508381200>

173. Qian, Z., Dominguez, S.R., Holmes, K. V.: Role of the Spike Glycoprotein of Human Middle East Respiratory Syndrome Coronavirus (MERS-CoV) in Virus Entry and Syncytia Formation. *PLoS One*. 8, (2013). <https://doi.org/10.1371/journal.pone.0076469>
174. Kam, Y.W., Okumura, Y., Kido, H., Ng, L.F.P., Bruzzone, R., Altmeyer, R.: Cleavage of the SARS coronavirus spike glycoprotein by airway proteases enhances virus entry into human bronchial epithelial cells in vitro. *PLoS One*. 4, (2009). <https://doi.org/10.1371/journal.pone.0007870>
175. Bertram, S., Glowacka, I., Müller, M.A., Lavender, H., Gnirss, K., Nehlmeier, I., Niemeyer, D., He, Y., Simmons, G., Drosten, C., Soilleux, E.J., Jahn, O., Steffen, I., Pöhlmann, S.: Cleavage and Activation of the Severe Acute Respiratory Syndrome Coronavirus Spike Protein by Human Airway Trypsin-Like Protease. *J Virol*. 85, (2011). <https://doi.org/10.1128/jvi.05300-11>
176. Shirato, K., Kawase, M., Matsuyama, S.: Middle East Respiratory Syndrome Coronavirus Infection Mediated by the Transmembrane Serine Protease TMPRSS2. *J Virol*. 87, (2013). <https://doi.org/10.1128/jvi.01890-13>
177. Gierer, S., Müller, M.A., Heurich, A., Ritz, D., Springstein, B.L., Karsten, C.B., Schendzielorz, A., Gnirß, K., Drosten, C., Pöhlmann, S.: Inhibition of proprotein convertases abrogates processing of the middle eastern respiratory syndrome coronavirus spike protein in infected cells but does not reduce viral infectivity. *Journal of Infectious Diseases*. 211, (2015). <https://doi.org/10.1093/infdis/jiu407>
178. Shulla, A., Heald-Sargent, T., Subramanya, G., Zhao, J., Perlman, S., Gallagher, T.: A Transmembrane Serine Protease Is Linked to the Severe Acute Respiratory Syndrome Coronavirus Receptor and Activates Virus Entry. *J Virol*. 85, (2011). <https://doi.org/10.1128/jvi.02062-10>
179. Follis, K.E., York, J., Nunberg, J.H.: Furin cleavage of the SARS coronavirus spike glycoprotein enhances cell-cell fusion but does not affect virion entry. *Virology*. 350, (2006). <https://doi.org/10.1016/j.virol.2006.02.003>
180. Belouzard, S., Chu, V.C., Whittaker, G.R.: Activation of the SARS coronavirus spike protein via sequential proteolytic cleavage at two distinct sites. *Proc Natl Acad Sci U S A*. 106, (2009). <https://doi.org/10.1073/pnas.0809524106>
181. Belouzard, S., Madu, I., Whittaker, G.R.: Elastase-mediated activation of the severe acute respiratory syndrome coronavirus spike protein at

- discrete sites within the S2 domain. *Journal of Biological Chemistry*. 285, (2010). <https://doi.org/10.1074/jbc.M110.103275>
182. Heald-Sargent, T., Gallagher, T.: Ready, set, fuse! the coronavirus spike protein and acquisition of fusion competence, (2012)
  183. Bosch, B.J., Bartelink, W., Rottier, P.J.M.: Cathepsin L Functionally Cleaves the Severe Acute Respiratory Syndrome Coronavirus Class I Fusion Protein Upstream of Rather than Adjacent to the Fusion Peptide. *J Virol*. 82, (2008). <https://doi.org/10.1128/jvi.00415-08>
  184. Matsuyama, S., Nagata, N., Shirato, K., Kawase, M., Takeda, M., Taguchi, F.: Efficient Activation of the Severe Acute Respiratory Syndrome Coronavirus Spike Protein by the Transmembrane Protease TMPRSS2. *J Virol*. 84, (2010). <https://doi.org/10.1128/jvi.01542-10>
  185. Nguyen, H.T., Zhang, S., Wang, Q., Anang, S., Wang, J., Ding, H., Kappes, J.C., Sodroski, J.: Spike Glycoprotein and Host Cell Determinants of SARS-CoV-2 Entry and Cytopathic Effects. *J Virol*. 95, (2021). <https://doi.org/10.1128/jvi.02304-20>
  186. Lemmin, T., Kalbermatter, D., Harder, D., Plattet, P., Fotiadis, D.: Structures and dynamics of the novel S1/S2 protease cleavage site loop of the SARS-CoV-2 spike glycoprotein. *J Struct Biol X*. 4, (2020). <https://doi.org/10.1016/j.yjsbx.2020.100038>
  187. Wrapp, D., Wang, N., Corbett, K.S., Goldsmith, J.A., Hsieh, C.-L., Abiona, O., Graham, B.S., McLellan, J.S.: Cryo-EM structure of the 2019-nCoV spike in the prefusion conformation. (2019)
  188. Li, F., Berardi, M., Li, W., Farzan, M., Dormitzer, P.R., Harrison, S.C.: Conformational States of the Severe Acute Respiratory Syndrome Coronavirus Spike Protein Ectodomain. *J Virol*. 80, (2006). <https://doi.org/10.1128/jvi.02744-05>
  189. Beniac, D.R., de Varennes, S.L., Andonov, A., He, R., Booth, T.F.: Conformational reorganization of the SARS coronavirus spike following receptor binding: Implications for membrane fusion. *PLoS One*. 2, (2007). <https://doi.org/10.1371/journal.pone.0001082>
  190. Zhang, L., Jackson, C.B., Mou, H., Ojha, A., Peng, H., Quinlan, B.D., Rangarajan, E.S., Pan, A., Vanderheiden, A., Suthar, M.S., Li, W., IZard, T., Rader, C., Farzan, M., Choe, H.: SARS-CoV-2 spike-protein D614G mutation increases virion spike density and infectivity. *Nat Commun*. 11, (2020). <https://doi.org/10.1038/s41467-020-19808-4>
  191. Ogawa, J., Zhu, W., Tonnu, N., Singer, O., Hunter, T., Ryan, A.L., Pao, G.M.: The D614G mutation in the SARS-CoV2 Spike protein increases



infectivity in an ACE2 receptor dependent manner. *bioRxiv*. (2020).  
<https://doi.org/10.1101/2020.07.21.214932>

192. Yurkovetskiy, L., Wang, X., Pascal, K.E., Tomkins-Tinch, C., Nyalile, T.P., Wang, Y., Baum, A., Diehl, W.E., Dauphin, A., Carbone, C., Veinotte, K., Egri, S.B., Schaffner, S.F., Lemieux, J.E., Munro, J.B., Rafique, A., Barve, A., Sabeti, P.C., Kyratsous, C.A., Dudkina, N. V., Shen, K., Luban, J.: Structural and Functional Analysis of the D614G SARS-CoV-2 Spike Protein Variant. *Cell*. 183, (2020). <https://doi.org/10.1016/j.cell.2020.09.032>
193. Zhang, L., Jackson, C., Mou, H., Ojha, A., Rangarajan, E., Izard, T., Farzan, M., Choe, H.: The D614G mutation in the SARS-CoV-2 spike protein reduces S1 shedding and increases infectivity. *bioRxiv*. (2020). <https://doi.org/10.1101/2020.06.12.148726>
194. Mansbach, R.A., Chakraborty, S., Nguyen, K., Montefiori, D.C., Korber, B., Gnanakaran, S.: The SARS-CoV-2 Spike variant D614G favors an open conformational state. *Sci Adv*. 7, (2021). <https://doi.org/10.1126/sciadv.abf3671>
195. Shi, P.-Y., Plante, J., Liu, Y., Liu, J., Xia, H., Johnson, B., Lokugamage, K., Zhang, X., Muruato, A., Zou, J., Fontes-Garfias, C., Mirchandani, D., Scharton, D., Kalveram, B., Bilello, J., Ku, Z., An, Z., Freiberg, A., Menachery, V., Xie, X., Plante, K., Weaver, S.: Spike mutation D614G alters SARS-CoV-2 fitness and neutralization susceptibility. *Res Sq*. (2020). <https://doi.org/10.21203/rs.3.rs-70482/v1>
196. Jiang, X., Zhang, Z., Wang, C., Ren, H., Gao, L., Peng, H., Niu, Z., Ren, H., Huang, H., Sun, Q.: Bimodular effects of D614G mutation on the spike glycoprotein of SARS-CoV-2 enhance protein processing, membrane fusion, and viral infectivity, (2020)
197. Buonvino, S., Melino, S.: New Consensus pattern in Spike CoV-2: potential implications in coagulation process and cell–cell fusion, (2020)
198. Branttie, J.M., Dutch, R.E.: Parainfluenza virus 5 fusion protein maintains pre-fusion stability but not fusogenic activity following mutation of a transmembrane leucine/isoleucine domain. *J Gen Virol*. (2020). <https://doi.org/10.1099/jgv.0.001399>
199. Webb, S., Nagy, T., Moseley, H., Fried, M., Dutch, R.: Hendra virus fusion protein transmembrane domain contributes to pre-fusion protein stability. *Journal of Biological Chemistry*. 292, 5685–5694 (2017). <https://doi.org/10.1074/jbc.M117.777235>

200. Slaughter, K.B., Dutch, R.E.: Transmembrane Domain Dissociation Is Required for Hendra Virus F Protein Fusogenic Activity. *J Virol.* 93, (2019). <https://doi.org/10.1128/jvi.01069-19>
201. White, J.M., Delos, S.E., Brecher, M., Schornberg, K.: Structures and mechanisms of viral membrane fusion proteins: Multiple variations on a common theme, (2008)
202. Harrison, S.C.: *Viral membrane fusion*, (2015)
203. Smith, E.C., Dutch, R.E.: Side Chain Packing below the Fusion Peptide Strongly Modulates Triggering of the Hendra Virus F Protein. *J Virol.* 84, (2010). <https://doi.org/10.1128/jvi.01108-10>
204. Barrett, C.T., Dutch, R.E.: *Viral membrane fusion and the transmembrane domain*, (2020)
205. Lamb RA, Parks GD: *Paramyxoviridae: the viruses and their replication*,. *Fields virology*. (2007)
206. Pager, C.T., Wurth, M.A., Dutch, R.E.: Subcellular Localization and Calcium and pH Requirements for Proteolytic Processing of the Hendra Virus Fusion Protein. *J Virol.* 78, (2004). <https://doi.org/10.1128/jvi.78.17.9154-9163.2004>
207. Pager, C.T., Dutch, R.E.: Cathepsin L Is Involved in Proteolytic Processing of the Hendra Virus Fusion Protein. *J Virol.* 79, (2005). <https://doi.org/10.1128/jvi.79.20.12714-12720.2005>
208. Cifuentes-Muñoz, N., Sun, W., Ray, G., Schmitt, P.T., Webb, S., Gibson, K., Dutch, R.E., Schmitt, A.P.: Mutations in the Transmembrane Domain and Cytoplasmic Tail of Hendra Virus Fusion Protein Disrupt Virus-Like-Particle Assembly. *J Virol.* 91, (2017). <https://doi.org/10.1128/jvi.00152-17>
209. Slaughter, K.B., Dutch, R.E.: Transmembrane Domain Dissociation Is Required for Hendra Virus F Protein Fusogenic Activity. *J Virol.* 93, (2019). <https://doi.org/10.1128/jvi.01069-19>
210. Rha, B., Curns, A.T., Lively, J.Y., Campbell, A.P., Englund, J.A., Boom, J.A., Azimi, P.H., Weinberg, G.A., Staat, M.A., Selvarangan, R., Halasa, N.B., Mcneal, M.M., Klein, E.J., Harrison, C.J., Williams, J. v, Szilagyi, P.G., Singer, M.N., Sahni, L.C., Figueroa-Downing, D., Mcdaniel, D., Prill, M.M., Whitaker, B.L., Stewart, L.S., Schuster, J.E., Pahud, B.A., Weddle, G., Pc, C.-A./, Avadhanula, V., Munoz, F.M., Piedra, P.A., Payne, D.C., Langley, G., Gerber, S.I.: Respiratory Syncytial Virus-Associated Hospitalizations Among Young Children: 2015-2016.

211. McLaughlin, J.M., Khan, F., Schmitt, H.J., Agosti, Y., Jodar, L., Simoes, E.A.F., Swerdlow, D.L.: Respiratory Syncytial Virus-Associated Hospitalization Rates among US Infants: A Systematic Review and Meta-Analysis, (2022)
212. Boyoglu-Barnum, S., Chirkova, T., Anderson, L.J.: Biology of Infection and Disease Pathogenesis to Guide RSV Vaccine Development, (2019)
213. Gonzá Lez-Reyes, L., Begoñ A Ruiz-Argü Ello, M., García-Barreno, B., Calder, L., Ló Pez §, J.A., Albar, J.P., Skehel, J.J., Wiley, D.C., Melero, J.A.: Cleavage of the human respiratory syncytial virus fusion protein at two distinct sites is required for activation of membrane fusion.
214. Lamb, R.: 1-s2.0-S0042682283715618-main (1). *Virology*. 197, 1–11 (1993)
215. Lamb, R.A., Paterson, R.G., Jardetzky, T.S.: Paramyxovirus membrane fusion: Lessons from the F and HN atomic structures, (2006)
216. Lamb, R.A., Jardetzky, T.S.: Structural basis of viral invasion: lessons from paramyxovirus F.
217. Fuentes, S., Coyle, E.M., Beeler, J., Golding, H., Khurana, S.: Antigenic Fingerprinting following Primary RSV Infection in Young Children Identifies Novel Antigenic Sites and Reveals Unlinked Evolution of Human Antibody Repertoires to Fusion and Attachment Glycoproteins. *PLoS Pathog.* 12, 1–24 (2016). <https://doi.org/10.1371/journal.ppat.1005554>
218. Blunck, B.N., Aideyan, L., Ye, X., Avadhanula, V., Ferlic-Stark, L., Zechiedrich, L., Gilbert, B.E., Piedra, P.A.: Antibody responses of healthy adults to the p27 peptide of respiratory syncytial virus fusion protein. *Vaccine*. 40, 536–543 (2022). <https://doi.org/10.1016/J.VACCINE.2021.11.087>
219. Vigerust, D.J., Shepherd, V.L.: Virus glycosylation: role in virulence and immune interactions, (2007)
220. Wagner, R., Wolff, T., Herwig, † Astrid, Pleschka, S., Klenk, H.-D.: Interdependence of Hemagglutinin Glycosylation and Neuraminidase as Regulators of Influenza Virus Growth: a Study by Reverse Genetics. (2000)
221. Beyene, A., Basu, A., Meyer, K., Ray, R.: Influence of N-linked glycans on intracellular transport of hepatitis C virus E1 chimeric glycoprotein and its role in pseudotype virus infectivity. *Virology*. 324, 273–285 (2004). <https://doi.org/10.1016/j.virol.2004.03.039>
222. Chu, F. lu, Wen, H. ling, Hou, G. hua, Lin, B., Zhang, W. qiang, Song, Y. yan, Ren, G. jie, Sun, C. xi, Li, Z. mei, Wang, Z.: Role of N-linked

- glycosylation of the human parainfluenza virus type 3 hemagglutinin-neuraminidase protein. *Virus Res.* 174, 137–147 (2013).  
<https://doi.org/10.1016/j.virusres.2013.03.012>
223. Hanna, S.L., Pierson, T.C., Sanchez, M.D., Ahmed, A.A., Murtadha, M.M., Doms, R.W.: N-Linked Glycosylation of West Nile Virus Envelope Proteins Influences Particle Assembly and Infectivity. *J Virol.* 79, 13262–13274 (2005). <https://doi.org/10.1128/jvi.79.21.13262-13274.2005>
224. Machamers, C.E., Rose, J.K.: THE JOURNAL 0 1988 by The American Society for Biochemistry OF BIOLOGICAL CHEMISTRY and Molecular Biology Vesicular Stomatitis Virus G Proteins with Altered Glycosylation Sites Display Temperature-sensitive Intracellular Transport and Are Subject to Aberrant Intermolecular Disulfide Bonding\*. (1988)
225. Gallagher, P.J., Henneberry, J.M., Sambrook, J.F., Gething, M.-J.H.: Glycosylation Requirements for Intracellular Transport and Function of the Hemagglutinin of Influenza Virus. (1992)
226. Zimmer, G., Trotz, I., Herrler, G.: N-Glycans of F Protein Differentially Affect Fusion Activity of Human Respiratory Syncytial Virus. *J Virol.* 75, 4744–4751 (2001). <https://doi.org/10.1128/jvi.75.10.4744-4751.2001>
227. König, P., Giesow, K., Schuldt, K., Buchholz, U.J., Keil, G.M.: A novel protein expression strategy using recombinant bovine respiratory syncytial virus (BRSV): Modifications of the peptide sequence between the two furin cleavage sites of the BRSV fusion protein yield secreted proteins, but affect processing and function of the BSRV fusion protein. *Journal of General Virology.* 85, 1815–1824 (2004).  
<https://doi.org/10.1099/vir.0.80010-0>
228. Sugrue, R.J., Brown, C., Brown, G., Aitken, J., McL Rixon, H.W.: Furin cleavage of the respiratory syncytial virus fusion protein is not a requirement for its transport to the surface of virus-infected cells. (2001)
229. Grishin, A.M., Dolgova, N. V., Landreth, S., Fiset, O., Pickering, I.J., George, G.N., Falzarano, D., Cygler, M.: Disulfide Bonds Play a Critical Role in the Structure and Function of the Receptor-binding Domain of the SARS-CoV-2 Spike Antigen. *J Mol Biol.* 434, (2022).  
<https://doi.org/10.1016/j.jmb.2021.167357>
230. Barrett, C.T., Neal, H.E., Edmonds, K., Moncman, C.L., Thompson, R., Brantje, J.M., Boggs, K.B., Wu, C.Y., Leung, D.W., Dutch, R.E.: Effect of clinical isolate or cleavage site mutations in the SARS-CoV-2 spike protein on protein stability, cleavage, and cell–cell fusion. *Journal of Biological Chemistry.* 297, (2021). <https://doi.org/10.1016/j.jbc.2021.100902>

231. Snijder, J., Benevento, M., Moyer, C.L., Reddy, V., Nemerow, G.R., Heck, A.J.R.: The cleaved N-Terminus of pVI binds peripentonal hexons in mature adenovirus. *J Mol Biol.* 426, 1971–1979 (2014). <https://doi.org/10.1016/j.jmb.2014.02.022>
232. Snijder, J., Benevento, M., Moyer, C.L., Reddy, V., Nemerow, G.R., Heck, A.J.R.: The cleaved N-Terminus of pVI binds peripentonal hexons in mature adenovirus. *J Mol Biol.* 426, 1971–1979 (2014). <https://doi.org/10.1016/j.jmb.2014.02.022>
233. Kulanayake, S., Tikoo, S.K.: Adenovirus core proteins: Structure and function, (2021)
234. Dai, X., Wu, L., Sun, R., Zhou, Z.H.: Atomic Structures of Minor Proteins VI and VII in Human Adenovirus. *J Virol.* 91, (2017). <https://doi.org/10.1128/jvi.00850-17>
235. Hernando-Pérez, M., Martín-González, N., Pérez-Illana, M., Suomalainen, M., Condezo, G.N., Ostapchuk, P., Gallardo, J., Menéndez, M., Greber, U.F., Hearing, P., de Pablo, P.J., Martín, C.S.: Dynamic competition for hexon binding between core protein VII and lytic protein VI promotes adenovirus maturation and entry. *Prog Nucl Energy 6 Biol Sci.* 117, 13699–13707 (2020). <https://doi.org/10.1073/pnas.1920896117/-/DCSupplemental>
236. McLellan, J.S., Chen, M., Joyce, M.G., Sastry, M., Stewart-Jones, G.B.E., Yang, Y., Zhang, B., Chen, L., Srivatsan, S., Zheng, A., Zhou, T., Graepel, K.W., Kumar, A., Moin, S., Boyington, J.C., Chuang, G.Y., Soto, C., Baxa, U., Bakker, A.Q., Spits, H., Beaumont, T., Zheng, Z., Xia, N., Ko, S.Y., Todd, J.P., Rao, S., Graham, B.S., Kwong, P.D.: Structure-based design of a fusion glycoprotein vaccine for respiratory syncytial virus. *Science* (1979). 342, 592–598 (2013). <https://doi.org/10.1126/science.1243283>
237. Alkhatib, G., Shen, S.-H., Briedis, D., Richardson, C., Massie, B., Weinberg, R., Smith, D., Taylor, J., Paoletti, E., Roder, J.: Functional Analysis of N-Linked Glycosylation Mutants of the Measles Virus Fusion Protein Synthesized by Recombinant Vaccinia Virus Vectors. (1994)
238. Bernardi, A., Huang, Y., Harris, B., Xiong, Y., Nandi, S., McDonald, K.A., Faller, R.: Development and simulation of fully glycosylated molecular models of ace2-fc fusion proteins and their interaction with the sars-cov-2 spike protein binding domain. *PLoS One.* 15, (2020). <https://doi.org/10.1371/journal.pone.0237295>
239. Carter, J.R., Pager, C.T., Fowler, S.D., Dutch, R.E.: Role of N-Linked Glycosylation of the Hendra Virus Fusion Protein. *J Virol.* 79, 7922–7925 (2005). <https://doi.org/10.1128/jvi.79.12.7922-7925.2005>

240. Fischer, K., Topallar, S., Kraatz, F., Groschup, M.H., Diederich, S.: The role of N-linked glycosylation in proteolytic processing and cell surface transport of the Cedar virus fusion protein. *Virology* 19, (2022). <https://doi.org/10.1186/s12985-022-01864-5>
241. Zimmer, G., Rohn, M., McGregor, G.P., Schemann, M., Conzelmann, K.K., Herrler, G.: Virokinin, a Bioactive Peptide of the Tachykinin Family, Is Released from the Fusion Protein of Bovine Respiratory Syncytial Virus. *Journal of Biological Chemistry*. 278, 46854–46861 (2003). <https://doi.org/10.1074/jbc.M306949200>
242. Tegally, H., Moir, M., Everatt, J., Giovanetti, M., Scheepers, C., Wilkinson, E., Subramoney, K., Makatini, Z., Moyo, S., Amoako, D.G., Baxter, C., Althaus, C.L., Anyaneji, U.J., Kekana, D., Viana, R., Giandhari, J., Lessells, R.J., Mponga, T., Maruapula, D., Choga, W., Matshaba, M., Mbulawa, M.B., Msomi, N., Bester, A.P., Claassen, M., Doolabh, D., Mudau, I., Mbhele, N., Engelbrecht, S., Goedhals, D., Hardie, D., Hsiao, N.Y., Iranzadeh, A., Ismail, A., Joseph, R., Maharaj, A., Mahlangu, B., Mahlkwane, K., Davis, A., Marais, G., Mlisana, K., Mnguni, A., Mohale, T., Motsatsi, G., Mwangi, P., Ntuli, N., Nyaga, M., Olubayo, L., Radibe, B., Ramphal, Y., Ramphal, U., Strasheim, W., Tebeila, N., van Wyk, S., Wilson, S., Lucaci, A.G., Weaver, S., Maharaj, A., Pillay, Y., Davids, M., Mendes, A., Mayaphi, S., Naidoo, Y., Pillay, S., Sanko, T.J., San, J.E., Scott, L., Singh, L., Magini, N.A., Smith-Lawrence, P., Stevens, W., Dor, G., Tshiabuila, D., Wolter, N., Preiser, W., Treurnicht, F.K., Venter, M., Chiloane, G., McIntyre, C., O'Toole, A., Ruis, C., Peacock, T.P., Roemer, C., Kosakovsky Pond, S.L., Williamson, C., Pybus, O.G., Bhiman, J.N., Glass, A., Martin, D.P., Jackson, B., Rambaut, A., Laguda-Akingba, O., Gaseitsiwe, S., von Gottberg, A., de Oliveira, T.: Emergence of SARS-CoV-2 Omicron lineages BA.4 and BA.5 in South Africa. *Nat Med*. 28, 1785–1790 (2022). <https://doi.org/10.1038/s41591-022-01911-2>
243. Magazine, N., Zhang, T., Wu, Y., McGee, M.C., Veggiani, G., Huang, W.: Mutations and Evolution of the SARS-CoV-2 Spike Protein, (2022)
244. Du, L., He, Y., Zhou, Y., Liu, S., Zheng, B.J., Jiang, S.: The spike protein of SARS-CoV - A target for vaccine and therapeutic development, (2009)
245. Mou, H., Raj, V.S., van Kuppeveld, F.J.M., Rottier, P.J.M., Haagmans, B.L., Bosch, B.J.: The Receptor Binding Domain of the New Middle East Respiratory Syndrome Coronavirus Maps to a 231-Residue Region in the Spike Protein That Efficiently Elicits Neutralizing Antibodies. *J Virol*. 87, 9379–9383 (2013). <https://doi.org/10.1128/jvi.01277-13>
246. Judice, J.K., Tom, J.Y.K., Huang, W., Wrin, T., Vennari, J., Petropoulos, C.J., McDowell, R.S.: Inhibition of HIV type 1 infectivity by constrained a-

- helical peptides: implications for the viral fusion mechanism. *Proc. Natl. Acad. Sci. USA.* 94, 13426–13430 (1997)
247. Jiang, S., Lin, K., Strick, N., Neurath, A.R.: HIV-1 inhibition by a peptide. *Nature.* 365, 113 (1993)
  248. Jiang, S., Lin, K., Strick, N., Neurath, A.R.: Inhibition of HIV-1 infection by a fusion domain binding peptide from the HIV-1 envelope glycoprotein GP41. *Biochem. Biophys. Res. Commun.* 195, 533–538 (1993)
  249. Bossart, K.N., Mungall, B.A., Cramer, G., Wang, L.F., Eaton, B.T., Broder, C.C.: Inhibition of Henipavirus fusion and infection by heptad-derived peptides of the Nipah virus fusion glycoprotein. *Virology* 2, (2005).  
<https://doi.org/10.1186/1743-422X-2-57>
  250. Gonzalez-Reyes, L., Ruiz-Arguello, M.B., Garcia-Barreno, B., Calder, L., Lopez, J.A., Albar, J.P., Skehel, J.J., Wiley, D.C., Melero, J.A.: Cleavage of the human respiratory syncytial virus fusion protein at two distinct sites is required for activation of membrane fusion. *Proc Natl Acad Sci U S A.* 98, 9859–64. (2001)
  251. Rezende, W., Ye, X., Angelo, L.S., Carisey, A., Avadhanula, V., Piedra, P.A.: THE EFFICIENCY OF P27 PEPTIDE CLEAVAGE DURING IN VITRO RESPIRATORY SYNCYTIAL VIRUS (RSV) INFECTION IS CELL LINE AND RSV SUBTYPE 2 DEPENDENT 3.  
<https://doi.org/10.1101/2022.10.17.512554>
  252. Murphy, B.R., Walsh, E.E.: Formalin-Inactivated Respiratory Syncytial Virus Vaccine Induces Antibodies to the Fusion Glycoprotein That Are Deficient in Fusion-Inhibiting Activity. (1988)
  253. Kapikian, A.Z., Mitchell, R.H., Chanock, R.M., Shvedoff, R.A., Stewart, C.E., Kapikian, A.Z., Chanock, M., Shvedoff, R.A., Stewart, C.E.: AN EPIDEMIOLOGIC STUDY OF ALTERED CLINICAL REACTIVITY TO RESPIRATORY SYNCYTIAL (RS) VIRUS INFECTION IN CHILDREN PREVIOUSLY VACCINATED WITH AN INACTIVATED RS VIRUS VACCINE. (1968)
  254. Kim, H.W., Canchola, J.G., Brandt, C.D., Pyles, G., Chanock, R.M., Jensen, K., Parrott, R.H., Kim, H.W., Canchola, J.G., Brandt, C.D., Pyles, G., Chanock, R.M., Jensen, K., Parrott, R.H.: RESPIRATORY SYNCYTIAL VIRUS DISEASE IN INFANTS DESPITE PRIOR ADMINISTRATION OF ANTIGENIC INACTIVATED VACCINE 1-2. (1968)
  255. Jenkins, V.A., Hoet, B., Hochrein, H., De Moerloose, L.: The Quest for a Respiratory Syncytial Virus Vaccine for Older Adults: Thinking beyond the F Protein, (2023)

256. Zamora, J.L.R., Aguilar, H.C.: Flow virometry as a tool to study viruses, (2018)
257. Moller-Tank, S., Maury, W.: Ebola Virus Entry: A Curious and Complex Series of Events, (2015)
258. Mastrangelo, P., Chin, A.A., Tan, S., Jeon, A.H., Ackerley, C.A., Siu, K.K., Lee, J.E., Hegele, R.G.: Identification of rsv fusion protein interaction domains on the virus receptor, nucleolin. *Viruses*. 13, (2021). <https://doi.org/10.3390/v13020261>
259. Griffiths, C.D., Bilawchuk, L.M., McDonough, J.E., Jamieson, K.C., Elawar, F., Cen, Y., Duan, W., Lin, C., Song, H., Casanova, J.L., Ogg, S., Jensen, L.D., Thienpont, B., Kumar, A., Hobman, T.C., Proud, D., Moraes, T.J., Marchant, D.J.: IGF1R is an entry receptor for respiratory syncytial virus. *Nature*. 583, 615–619 (2020). <https://doi.org/10.1038/s41586-020-2369-7>
260. Feng, Z., Xu, L., Xie, Z.: Receptors for Respiratory Syncytial Virus Infection and Host Factors Regulating the Life Cycle of Respiratory Syncytial Virus, (2022)
261. Buchholz, U.J., Granzow, H., Schuldt, K., Whitehead, S.S., Murphy, B.R., Collins, P.L.: Chimeric Bovine Respiratory Syncytial Virus with Glycoprotein Gene Substitutions from Human Respiratory Syncytial Virus (HRSV): Effects on Host Range and Evaluation as a Live-Attenuated HRSV Vaccine. (2000)
262. Zimmer, G., Rohn, M., McGregor, G.P., Schemann, M., Conzelmann, K.K., Herrler, G.: Virokinin, a Bioactive Peptide of the Tachykinin Family, Is Released from the Fusion Protein of Bovine Respiratory Syncytial Virus. *Journal of Biological Chemistry*. 278, 46854–46861 (2003). <https://doi.org/10.1074/jbc.M306949200>
263. Valarcher, J.F., Furze, J., Wyld, S.G., Cook, R., Zimmer, G., Herrler, G., Taylor, G.: Bovine respiratory syncytial virus lacking the virokinin or with a mutation in furin cleavage site RA(R/K)R109 induces less pulmonary inflammation without impeding the induction of protective immunity in calves. *Journal of General Virology*. 87, 1659–1667 (2006). <https://doi.org/10.1099/vir.0.81755-0>



## VITA

Hadley Neal

Department of Molecular and Cellular Biochemistry, University of Kentucky

### EDUCATION

University of Kentucky  
PhD in Molecular and Cellular Biochemistry  
April 2023  
Advisor: Dr. Rebecca Dutch

Bellarmino University  
BS Biochemistry and Molecular Biology, Minor in Biology  
May 2019

### RESEARCH EXPERIENCE

*University of Kentucky* August 2019 – April 2023  
Department of Cellular and Molecular Biochemistry, Lexington, KY  
Principle Investigator: Dr. Rebecca Dutch

- Analyzing other highly pathogenic class I viral fusion proteins to better understand mechanisms, focusing on the transmembrane domain

*Kentucky Biomedical Research Infrastructure Network* June 2017 – August 2017  
Department of Biology, University of Kentucky, Lexington, KY  
Principle Investigator: Dr. Ann Morris

- Studied the effects of *Sox4* on vertebrate eye development in zebrafish

*Independent Biochemical Research* August 2016 – May 2019  
Department of Chemistry, Bellarmine University, Louisville KY  
Advisor: Dr. Amanda Krzysiak

- Evaluated the effects of different chalcone derivatives to hinder the growth of embryonic kidney (HEK-293) and breast cancer (MCF-7) cells

### INDUSTRY EXPERIENCE

*Proctor & Gamble | Microbiology PhD Intern* May 2022 – August 2022  
Fabric and Home Care R&D, Mason, OH

- Developed a high-throughput screening method to increase product throughput by 10X

### AWARDS

- Early Publication Award
  - 2022
  - Awarded by the University of Kentucky College of Medicine for publishing as a co-author within the first three years of graduate training

## PUBLICATIONS

- Barrett CT, **Neal HE**, Edmonds K, Moncman CL, Thompson R, Branttie JM, Boggs KB, Wu CY, Leung DW, Dutch RE. Effect of clinical isolate or cleavage site mutations in the SARS-CoV-2 spike protein on protein stability, cleavage, and cell-cell fusion. *J Biol Chem*. 2021 Jun 19:100902. doi: 10.1016/j.jbc.2021.100902. Epub ahead of print. PMID: 34157282; PMCID: PMC8214756.
- Barrett CT\*, **Neal HE\***, Edmonds K, Zamora JLR, Moncman CL, Popa A, Smith EC, Webb SR, Dutch RE. Analysis of Hendra Virus Fusion Protein N-Terminal Transmembrane Residues. *Viruses*. 2021 Nov 24;13(12):2353. doi: 10.3390/v13122353. PMID: 34960622; PMCID: PMC8707071.
- Neal Hadley E, Joann M. Lau, and David L. Robinson. Genomic DNA sequence for White Snakeroot (*Eupatorium rugosum*) glyceraldehyde-3-phosphate dehydrogenase (GAPC-1) gene, partial cds. 993 bp. (*in submission to the NIH-NCBI GenBank*).

## PRESENTATIONS

- “Factors that impact SARS-CoV-2 spike protein trimer stability and cleavage” American Society for Biochemistry and Molecular Biology Annual Meeting, April 2021
- “Effect of mutations in the SARS-CoV-2 spike protein on protein stability, cleavage, and cell-cell fusion function” American Society for Virology Annual Meeting, July 2021
- “Elucidating the role of the P27 fragment in RSV fusion protein function and stability” 12th International RSV Symposium, October 2022.

## LEADERSHIP EXPERIENCE

- American Society for Biochemistry and Molecular Biology Student Chapter
  - 2017- 2019
  - Co-President
- Biomedical Graduate Student Organization: Professional Development Committee
  - 2021-2023
  - Chair
- American Society for Microbiology Student Chapter

- 2021-2022
- Diversity Representative

## **OUTREACH**

- Bellarmine University American Society for Biochemistry and Molecular Biology
  - November 2017
  - Assisted high school students in learning basic lab techniques
- Morton Middle School Science Fair Judge
  - January 2022, 2022 & 2023
  - Judged middle school science fair posters and presentations
- University of Kentucky Curiosity Fair
  - October 2021
  - Organized interactive activities to teach the community about antibiotic resistance